Coupled parameterized reduced order modelling of thermomechanical phenomena arising in blast furnaces

Advisor:
Prof. Gianluigi Rozza (SISSA)
Prof. Peregrina Quintela (ITMATI)
Ing. Alejandro Lengomin (AMIII)
Co-advisor:
Asst. Prof. Michele Girfoglio (SISSA)
Asso. Prof. Patricia Barral (ITMATI)

Candidate:
Nirav Vasant Shah

Academic Year 2021-22

Coupled parameterized reduced order modelling of thermomechanical phenomena arising in blast furnaces

Nirav Vasant Shah, Early Stage Researcher, Reduced Order Modelling, Simulation and Optimization of Coupled Systems (ROMSOC) and Scuola Internazionale Superiore di Studi Avanzati (SISSA)

Advisors:
Asst. Prof. Michele Girfoglio and Prof. Gianluigi Rozza, Scuola Internazionale Superiore di Studi Avanzati (SISSA)
Asso. Prof. Patricia Barral and Prof. Peregrina Quintela, Instituto tecnológico de Matemática Industrial (ITMATI)
Ing. Alejandro Lengomin, ArcelorMittal Innovación Investigación e Inversion S.L. (AMIII)

Doctoral thesis
February 23, 2022

Acronyms

AMIII	ArcelorMittal Innovación Investigación e Inversion S.L.
ITMATI	Instituto Tecnolóxico de Matemática Industrial
ROMSOC	Reduced Order Modelling, Simulation and Optimization of Coupled Systems
SISSA	Scuola Internazionale Superiore di Studi Avanzati
TUB	Technische Universität Berlin
TU/e	Technische Universiteit Eindhoven
USC	Universidade de Santiago de Compostela

Acknowledgement

This contribution is the result of the work carried out between April 2018 - April 2022 at SISSA, ITMATI and AMIII. The outcomes presented here are possible due to support of a number of people to whom I would like to express my gratitude.

To my supervisors Prof. Gianluig Rozza, Prof. Peregrina Quintela and Ing. Alejandro Legomin: I express my deep gratitude to them for providing able supervision and sharing their expertise. I am also thankful for their personal support during my stay at SISSA, AMIII and during my visits at ITMATI.

To my co-advisors Asst. Prof. Michele Girfoglio and Asso. Prof. Patricia Barral: I am grateful to them for their continuous support and guidance throughout the project to develop relevant skills as pertaining to resolution of research challenges.

To my colleagues: I thank Asst. Prof. Francesco Ballarin, Dr. Federico Pichi and Dr. Luis Javier Pérez for their crucial support during the project. I also thank Asst. Prof. Andrea Mola, Asso. Prof. Giovanni Noselli, Dr. Martin Hess and Asst. Prof. Giovanni Stabile for their positive interest in my work.

To administration: It is very important to recognise support from SISSA mobility office: Ms. Gabriella Peressini, Ms. Francesca Gandolfo, Ms. Tatiana Usenich; SISSA Students' Secretariat: Mr. Marco Marin, Mr. Riccardo Iancer, Ms. Valeria Mirabella; and ROM-SOC coordinators: Prof. Volker Mehrmann, Dr. rer. nat. Lena Scholz for their support in matters relating to administration of the project.

To external referees: I am thankful to Prof. Volker Mehrmann (TUB) and Prof. Wil H.A. Schilders (TU/e) for their time and consideration for reviewing the thesis.

To my brother and his family, my parents: Last but most importantly, I would like to thank my family for their continuous encouragement, infusion of new energy and support during critical and difficult times.

Contents

Chapter 1

Conceptual model

Steelmaking is a very old process that has contributed to the development of technological societies since ancient times. The previous stage to steelmaking is the ironmaking process, which is performed inside a blast furnace, whose general layout is shown in Figure 1.1. It is a metallurgical reactor used to produce hot metal from iron ore. For further details the reader is referred, e.g., to [25, 37].

Blast furnace operates at a high temperature (up to 1500 °C). The associated thermal stresses significantly limit the overall blast furnace campaign period. In this context, thermomechanical modeling has been used extensively either to support experimental campaign or to design various components. Vázquez-Fernández et al. [101] simulated heat transfer in a trough of a blast furnace to ensure durability based on the location of critical isotherm. Numerical modeling of heat flows in the blast furnace hearth lining was used by Swartling M. et al. [97] for improving experimental assessment. Thermomechanical modeling of blast furnace hearth was also developed by Brulin et al. [24]: they used micro-macro approach with homogenization method for replacing bricks and mortars by an equivalent material. Finite element method [21, 23, 72] has been successfully applied in several practical applications involving thermomechanical modeling, such as flowform technology [89], stress analysis for VLSI devices [22], and additive manufacturing [39].
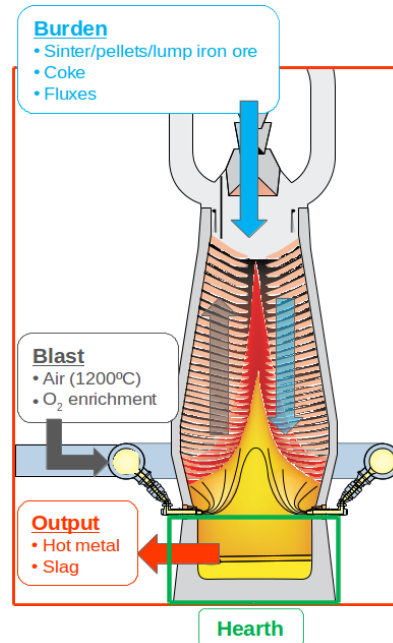
Figure 1.1: Blast furnace [Courtesy: ArcelorMittal]

Blast furnace operates under different conditions, each of which is governed by a different mathematical model. Considering objectives of the present work, following simplifications are considered:

(A1) Taphole operation [10] is not part of this study. The perforation action of the taphole and pressures in the draining of the hot metal and slag produce important mechanical stresses located in the area that requires a deeper analysis and that is out of the scope of this work.

(A2) Since the objective is to be able to calculate in real time the effects of wall design on blast furnace operation, we focus on the steady state operations.

(A3) We assume that the hearth is made up of elastic materials.

(A4) Heat transfer only by conduction within hearth walls will be considered. The temperature of the molten metal inside the hearth is assumed constant and known. Therefore, the fluid region will not be part of the problem.

Due to technological developments occurred in recent years, high-fidelity numerical computations, based on the so-called Full Order Models (FOM) (e.g., finite element or finite volume methods), are required to be performed for many configurations. This puts the computational resources under considerable stress. In this context, Model Order Reduction (MOR) or Reduced Basis (RB) approach has been introduced as an efficient tool to accelerate the computations with "affordable" and "controllable" loss of accuracy. For a comprehensive review on MOR, we refer to, e.g., [4, 14, 16, 17, 42, 46, 62, 73, 84]. In this work, we address the development of a MOR framework in a Finite Element (FE) environment for one-way coupled steady state thermomechanical problem as relevant to normal operating conditions inside blast furnace hearth walls. In the literature different MOR techniques have been proposed in the context of thermomechanical problems. Guérin et al. [41] developed Rational Craig-Hale methodology for the investigation of thermomechanical coupling effects in turbomachinery. Benner et al. [15] compared the performance of Proper Orthogonal Decomposition (POD), Balanced Truncation, Padé approach and iterative rational Krylov algorithm for the approximation of the transient thermal field concerning an optimal sensor placement problem for a thermo-elastic solid body model. Zhang et al. [105] introduced reduced order variational multiscale enrichment method and tested their approach on proper benchmark tests related to the thermomechanical loading applied to a 2D composite beam and a functionally graded composite beam. More recently, Hernández-Beccero et al. [44] used Krylov Modal Subspace method for thermomechanical models as applicable to machine tools. We highlight that all these works are focused on MOR for the efficient reconstruction of the time evolution of the thermomechanical field. Regarding steady state problems, such as those dealt with in this work, Hoang et al. [50] used a two-field reduced basis algorithm based on the greedy algorithm in a physical parametrization setting. However, here we consider not only physical parameters but also

geometrical parameters. There is a broad range of strategies for the development of new deep learning architectures for non-intrusive MOR approaches, i.e. without the need to access to FOM implementation: see, e.g., [3, 27, 30, 33, 45, 63, 69, 83, 100, 102].

In first part of the thesis, we make further assumption as compared to the assumptions (A1)-(A4): we assume that the blast furnace hearth is made up of single material with material properties independent of the temperature. Chapter 2 introduces thermomechanical model along with application of the axisymmetric hypothesis. In chapter 3, we introduce weighted Sobolev spaces and axisymmeric weak formulation. Next, we derive the finite element formulation corresponding to axisymmertic weak formulation (Chapter 4). In order to verify the numerical implementation of the finite element formulation, benchmark tests are discussed in chapter 5. Chapter 6 introduces relevant geometric and physical parameters, parametric formulation and model order reduction approach. Under model order reduction framework, we discuss intrusive projection based POD-Galerkin approach and non-intrusive data-driven POD-Artificial Neural Network (ANN) approach [86].

Blast furnace hearth is made up of several zones. Each zone has different design requirement depending on the type of environment to which a particular zone is exposed. Ceramic cup is required to withstand high temperature due to direct contact with the molten metal. Carbon blocks are expected to reduce accumulation of excess heat. Steel shell is required to have sufficient mechanical strength to sustain the weight of other blast furnace components. An optimum design increases hearth lifetime and consequently, the blast furnace campaign. In second part of the thesis, we deal with more complex model by taking into account temperature dependence of material properties, presence of different materials and orthotropy due to replacement of periodic assembly of isotropic materials with equivalent orthotopic material. Chapter 7 introduces axisymmetric thermomechanical model with complexities involving non-linearity due to temperature dependence of material properties, interface conditions due to presence of different materials (at which one could refer to as heterogeneous material) [87]. Further, homogenization to identify equivalent orthotropic material for replacement of periodic assembly of bricks and mortar is introduced. Further, axisymmetric weak formulation is introduced based on this complex thermomechanical model. Chapter 8 introduces corresponding finite element formulation and POD-ANN based model order reduction approach for this complex model.

Finally, concluding remarks and some directions for the future work are presented.

1.1   Project framework

This work has been carried out in collaboration with Asso. Prof. Patricia Barral and Prof. Peregrina Quintela, Instituto tecnológico de Matemática Industrial (ITMATI), Santiago de Compostela and Ing. Alejandro Lengomin, ArcelorMittal Innovación Investigación e Inversion S.L. (AMIII), Asturias under the framework of Reduced Order Modelling, Simulation and Optimization of Coupled Systems (ROMSOC).

ROMSOC is a European Industrial Doctorate (EID) project in the programme Innovative Training Networks (ITN) and part of Marie Sklodowska Curie Actions (Grant Agreement No. 765374) within the Horizon 2020 programme. The mathematical models differ strongly in different applications and industrial sectors. However, there is a common framework via an appropriate representation of the physical model. ROMSOC project brings together international academic institutions and industry partners to further develop this common framework driven by industrial applications. It consists of projects from diverse application domains such as Cardiac blood pump [61], Atmospheric tomography [78, 92], Financial risk analysis [19, 20], Electric circuits [5, 6] and Steel production [64, 86, 87]. In accordance with the ROMSOC objectives, this contribution was prepared at research facility of SISSA mathlab with secondment at industrial partner AMIII and in collaboration with ITMATI. Conceptual model presented in this contribution is aimed at understanding and improving the industrial process of ironmaking.

Prof. Gianluigi Rozza's group at SISSA mathlab has focused on efficient reduced basis methods for parametrized Partial Differential Equations (PDEs) [46, 81], computational fluid dynamics [54, 91] including application to environmental sciences [93, 96], Aero-Naval-Mechanical Engineering [32, 99], fluid structure interaction [38, 66] and open source software development for computational science and engineering. This contribution is mainly based on open source software RBniCS [79], which is developed at SISSA mathlab. The application areas of RBniCS include Stokes equation [1, 47], optimal control problem [94, 95], cardiovascular applications [98], environmental science [26]. This contribution extends the application of RBniCS to thermomechanical model as relevant to the industrial process of ironmaking. Additionally, RBniCS was combined with pytorch [71], an open source machine learning framework. Our work is a part of ongoing developments in the direction of data-driven deep learning based model order reduction methods for various problems such as: Non-linear Reduction of Hyperbolic Equations [67], extension of physics informed supervised learning strategies [31], bifurcating phenomena in computational fluid dynamics [70], hybrid neural network [103], deep learning with dimensionality reduction [63] and hemodynamic [88].

ITMATI is a public consortium in which the three Galician universities participate. It provides advanced solutions for businesses, industries and the public administration. Prof. Peregrina Quintela, director of ITMATI and full professor of applied mathematics at USC, has focused primarily on mathematical modelling of thermomechanical issues including industrial problems [8, 9, 11, 12, 64, 101]. Our work is further contribution to the thermomechanical problem as relevant to an industrial project.

ArcelorMittal is the largest steel manufacturer in North america, South america and Europe. AMIII, which belongs to ArcelorMittal group, specializes in the implementation of new technologies related to advanced process control and monitoring systems at industrial plants, energy, environment and recycling research in order to improve steelmaking process. This contribution is the result of closer collaboration with Ing. Alejandro Lengomin including secondment of the early stage researcher at AMIII and adaptation of mathematical

modelling in an industrial environment.

As can be expected, this contribution is supervised by experts in engineering, applied mathematics, and scientific computing. Accordingly, this contribution utilises knowledge from diverse fields such as weighted Sobolev spaces to scientific machine learning. From practical point of view, key contributions of this work are the usage of open source software and the application of scientific machine learning to an industrial problem.

- Open source software facilitate the dissemination of knowledge and ensure greater control over the computational tools.

- In many industrial processes, commercial software are used for performing high-fidelity computations. Usually, source code of a commercial software is not readily available. Since, scientific machine learning is data-driven non-intrusive technique, it does not necessarily require access to source code.

We expect this work to serve as a benchmark for facilitating the collaboration between academia and industry.

Part I

Linear isotropic homogeneous model

Chapter 2

Thermomechanical model

We now discuss the mathematical formulation corresponding to the conceptual model discussed in Chapter 1. The governing equations for thermomechanical problems are linear momentum conservation and energy conservation from continuum mechanics [18, 40]. We first briefly discuss the conservation equations in section 2.1. In section 2.2, we introduce the domain and the boundary conditions. We then motivate the application of the axisymmetric hypothesis and derive the axisymmetry thermomechanical model (Section 2.3).

2.1 Conservation laws

2.1.1 Linear momentum conservation

In order to investigate the deformation of a body $\mathcal{B}$, it is necessary to quantify the change in its shape as it is transformed from the undeformed state $\mathcal{B}$ (typically taken as reference configuration), $\mathcal{B} \subset \mathbb{R}^3$, into its deformed configuration $\mathcal{B}_t$ at time $t \in \mathbb{R}$. For that, let us introduce the notion of a motion of $\mathcal{B}$. It is an application $X : \mathcal{B} \times \mathbb{R} \mapsto \mathcal{E}$, defined as,

$$X(p,t) = p + \overrightarrow{u}(p,t) \ , \ p \in \mathcal{B} \ , \ t \in \mathbb{R} \ ,$$

being $\overrightarrow{u}$ the displacement, and $\mathcal{E}$ the Euclidean space. We refer to $x = X(p,t)$ as the place occupied by the material point p at time t, while $\mathcal{B}_t = X(\mathcal{B}, t)$ is the region occupied by the body $\mathcal{B}$ at time t. The gradient of the motion is the tensor,

$$\boldsymbol{F} : \mathcal{B} \times \mathbb{R} \mapsto Lin^+ \ , \tag{2.1}$$

where Lin^+ denotes the subset of second order tensors with positive determinant. $\boldsymbol{F}$ is related to displacement $\overrightarrow{u}$ as,

$$\boldsymbol{F} = \boldsymbol{I} + \nabla \overrightarrow{u} \ , \tag{2.2}$$

where $\boldsymbol{I}$ refers to the identity tensor.

By applying D'Alembert's principle, we obtain,

$$\rho \ddot{\vec{u}} - div\boldsymbol{T} = \vec{f} \ , \ \forall x \in \mathcal{B}_t, \ \forall t \in \mathbb{R} \ , \tag{2.3}$$

where $\vec{f}$ and $\boldsymbol{T}$ are the external force density and the Cauchy stress tensor, respectively. In this equation ρ represents the density in the motion X. By the mass conservation, ρ must satisfy,

$$\rho(x,t) \det(\boldsymbol{F}(p,t)) = \rho_0(p) \ , \ x = X(p,t) \ , \tag{2.4}$$

ρ_0 being the density of the body at the reference configuration. From equation (2.3), it can be verified, for each part $\mathcal{P} \subset \mathcal{B}$,

$$\int_{\mathcal{P}_t} \rho \ddot{\vec{u}} \ dV_x - \int_{\mathcal{P}_t} div\boldsymbol{T} \ dV_x = \int_{\mathcal{P}_t} \vec{f} \ dV_x, \ \forall \mathcal{P}_t \subset \mathcal{B}_t \ , \tag{2.5}$$

where $\mathcal{P}_t = X(\mathcal{P},t)$ and $x = X(p,t)$.

It is important to note that the configuration $\mathcal{B}_t$ is not known in advance. Therefore, it is crucial to represent all relevant measurements with respect to the reference configuration $\mathcal{B}$. For this purpose, we now introduce the notion of material field. The material description T_m of spatial variable T is defined as,

$$T_m(p,t) = T(x,t) \ , \tag{2.6}$$

for $p \in \mathcal{B}, t \in \mathbb{R}$ and $x \in \mathcal{B}_t$, such that $x = X(p,t)$.

We will express each term of the equation (2.5) by making use of the corresponding material field of each spatial field, so that it can be rewritten in the reference configuration. Indeed, by applying the Gauss divergence theorem and taking into account the change of variable theorem on tensors (see Gurtin [40]),

$$\int_{\mathcal{P}_t} div\boldsymbol{T} \ dV_x = \int_{\partial \mathcal{P}_t} \boldsymbol{T}\vec{m} \ dA_x =$$
$$\int_{\partial \mathcal{P}} (\det(\boldsymbol{F})\boldsymbol{T}_m \boldsymbol{F}^{-T}) \cdot \vec{n} \ dA_p \ = \int_{\partial \mathcal{P}} \boldsymbol{S} \cdot \vec{n} \ dA_p \ , \tag{2.7}$$

where $P_t = X(P,t)$, $\vec{n}(\vec{m})$ is the outward pointing unit normal vector to $\partial \mathcal{P}$ $(\partial \mathcal{P}_t)$, which denotes the boundary of $\mathcal{P}$ $(\mathcal{P}_t)$, and $\boldsymbol{S}$ is the first Piola Kirchhoff stress tensor defined by:

$$\boldsymbol{S}(p,t) = \det(\boldsymbol{F}(p,t))\boldsymbol{T}_m(p,t)\boldsymbol{F}^{-T}(p,t) \ .$$

If the material is elastic, there exists a response function $\hat{\boldsymbol{S}}$, so the first Piola Kirchhoff tensor can also be expressed in terms of deformation:

$$\boldsymbol{S}(p,t) = \hat{\boldsymbol{S}}(\boldsymbol{F}(p,t),p) \ . \tag{2.8}$$

The linear approximation of the first Piola Kirchoff stress tensor, $\boldsymbol{\sigma}(p,t)$, provides a good estimate of the stress tensor for small displacements:

$$\boldsymbol{\sigma}(p,t) = \hat{\boldsymbol{S}}(\boldsymbol{I},p) + \frac{\partial \hat{\boldsymbol{S}}}{\partial \boldsymbol{F}}(\boldsymbol{I},p)[\boldsymbol{F}(p,t) - \boldsymbol{I}] \ . \tag{2.9}$$

If the reference configuration is a natural state, $\hat{\boldsymbol{S}}(\boldsymbol{I},p) = \boldsymbol{0}$, and the expression of the linearized stress is reduced to:

$$\boldsymbol{\sigma} = \frac{\partial \hat{\boldsymbol{S}}}{\partial \boldsymbol{F}}(\boldsymbol{I},p)[\nabla \overrightarrow{u}] \ . \tag{2.10}$$

The other terms of equation (2.5), by using the theorem of change of variable, can be rewritten as:

$$\int_{\mathcal{P}_t} \overrightarrow{f} \ dV_x = \int_{\mathcal{P}} \det(\boldsymbol{F}) \overrightarrow{f_m} \ dV_p \ , \tag{2.11}$$

$$\int_{\mathcal{P}_t} \rho \overset{..}{\overrightarrow{u}} \ dV_x = \int_{\mathcal{P}} \det(\boldsymbol{F}) \rho_m \overset{..}{\overrightarrow{u}} \ dV_p \ . \tag{2.12}$$

Therefore, the material formulation of equation (2.5) is given by:

$$\int_{\mathcal{P}} \det(\boldsymbol{F}) \rho_m \overset{..}{\overrightarrow{u}} \ dV_p - \int_{\partial \mathcal{P}} \boldsymbol{S} \overrightarrow{n} \ dA_p = \int_{\mathcal{P}} \det(\boldsymbol{F}) \overrightarrow{f_m} \ dV_p, \ \forall \mathcal{P} \subset \mathcal{B}, \ \forall t \in \mathbb{R} \ . \tag{2.13}$$

If $\overrightarrow{f_0}$ is defined as the volume force density in the reference configuration,

$$\overrightarrow{f_0} = \det(\boldsymbol{F}) \ \overrightarrow{f_m} \ ,$$

the mass conservation (2.4) is taken into account, and using the Gauss divergence theorem, equation (2.13) can be written as:

$$\int_{\mathcal{P}} \rho_0 \overset{..}{\overrightarrow{u}} \ dV_p - \int_{\mathcal{P}} Div(\boldsymbol{S}) \ dV_p = \int_{\mathcal{P}} \overrightarrow{f_0} \ dV_p, \ \forall \mathcal{P} \subset \mathcal{B}, \forall t \in \mathbb{R} \ . \tag{2.14}$$

Thanks to the localization theorem (see Bermúdez [18]), the following local formulation of the linear momentum conservation can be written:

$$\rho_0 \overset{..}{\overrightarrow{u}} - Div(\boldsymbol{S}) = \overrightarrow{f_0}, \ \forall p \in \mathcal{B}, \ \forall t \in \mathbb{R} \ . \tag{2.15}$$

In case of steady state, equation (2.15) can be stated as:

$$-Div(\boldsymbol{S}) = \overrightarrow{f_0}, \ \forall p \in \mathcal{B} \ . \tag{2.16}$$

Under linearization hypotheses (equations (2.8) - (2.10)), equation (2.16) can be rewritten as:

$$-Div(\boldsymbol{\sigma}) = \overrightarrow{f_0}, \ \forall p \in \mathcal{B} \ . \tag{2.17}$$

Hereinafter, when not necessary, the subscript m will be omitted for notation simplification.

2.1.2 Energy conservation

According to the first law of thermodynamics, the increase in internal energy of the system, at any time, is the sum of work done on the system by external forces and heat supplied. The work is done on the system either by boundary forces, $\overrightarrow{s}$, or body forces, $\overrightarrow{f}$. The heat is supplied to the system either by body source, Q, or heat flux, $\overrightarrow{q}$, at system boundary. Now, for all subset $\mathcal{P}$ of $\mathcal{B}$, the energy conservation equation is stated as (see Bermúdez [18]),

$$\frac{d}{dt} \int_{\mathcal{P}_t} \rho U \ dV_x = \int_{\partial \mathcal{P}_t} \overrightarrow{s} \cdot \dot{\overrightarrow{u}} \ dA_x + \int_{\mathcal{P}_t} \overrightarrow{f} \cdot \dot{\overrightarrow{u}} \ dV_x - \int_{\partial \mathcal{P}_t} \overrightarrow{q} \cdot \overrightarrow{m} \ dA_x$$
$$+ \int_{\mathcal{P}_t} Q \ dV_x \ , \ \forall \mathcal{P} \subset \mathcal{B} \ , \quad (2.18)$$

where, U is the specific total energy of the system, $\mathcal{P}_t = X(\mathcal{P}, t)$ and $x = X(p, t)$. Under steady condition, the above equation reduces to,

$$\int_{\partial \mathcal{P}_t} \overrightarrow{q} \cdot \overrightarrow{m} \ dA_x = \int_{\mathcal{P}_t} Q \ dV_x \ , \ \forall \mathcal{P} \subset \mathcal{B} \ . \quad (2.19)$$

By using the Gauss divergence theorem,

$$\int_{\mathcal{P}_t} div \overrightarrow{q} \ dV_x = \int_{\mathcal{P}_t} Q \ dV_x \ , \ \forall \mathcal{P} \subset \mathcal{B} \ , \quad (2.20)$$

and by using the theorem of change of variable,

$$\int_{\mathcal{P}} \det(\boldsymbol{F}) Div \overrightarrow{q}_m \ dA_p = \int_{\mathcal{P}} \det(\boldsymbol{F}) Q_m \ dV_p \ , \ \forall \mathcal{P} \subset \mathcal{B} \ . \quad (2.21)$$

Therefore, the localization theorem (see [18]) can be applied again to obtain:

$$Div \overrightarrow{q} = Q \ , \ \forall p \in \mathcal{B} \ , \quad (2.22)$$

where to simplify the notation the subscript m is omitted.

Since the body $\mathcal{B}$ is a solid, the heat flux considered in energy equation (2.22) is the one produced by conduction, which is the dominant mode of heat transfer in solids. In particular, we consider the Fourier law, so the heat flux $\overrightarrow{q}$ is proportional to the gradient of temperature T. Therefore, if $\boldsymbol{K}$ denotes thermal conductivity tensor, then:

$$\overrightarrow{q} = -\boldsymbol{K} \nabla T \ . \quad (2.23)$$

In the case of isotropic material the thermal conductivity $\boldsymbol{K}$ is expressed as:

$$\boldsymbol{K} = k \boldsymbol{I} \ , \ k > 0 \ . \quad (2.24)$$
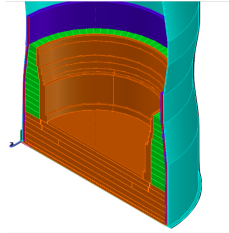
(a) 3-dimensional hearth geometry
[Courtesy : ArcelorMittal]
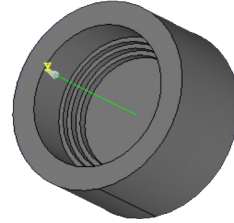
(b) Hearth 3-dimensional simplified domain
Ω
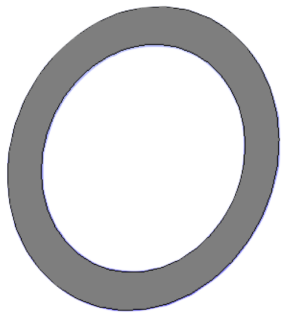
(c) Top boundary Γ_+
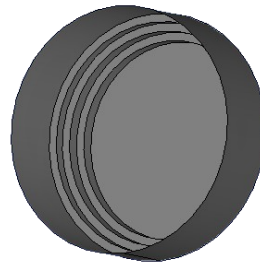
(d) Inner boundary Γ_{sf}
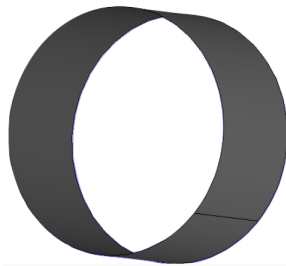
(e) Outer boundary Γ_{out}
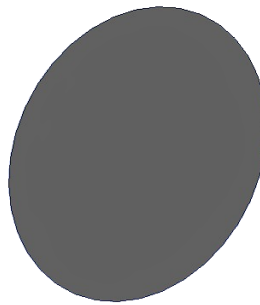
(f) Bottom boundary Γ_-

Figure 2.1: Hearth geometry : 3-dimensional domains, the real one and its simplification, as well as the boundaries of the latter

(a) Computational domain ω (b) Boundaries $\partial\omega$
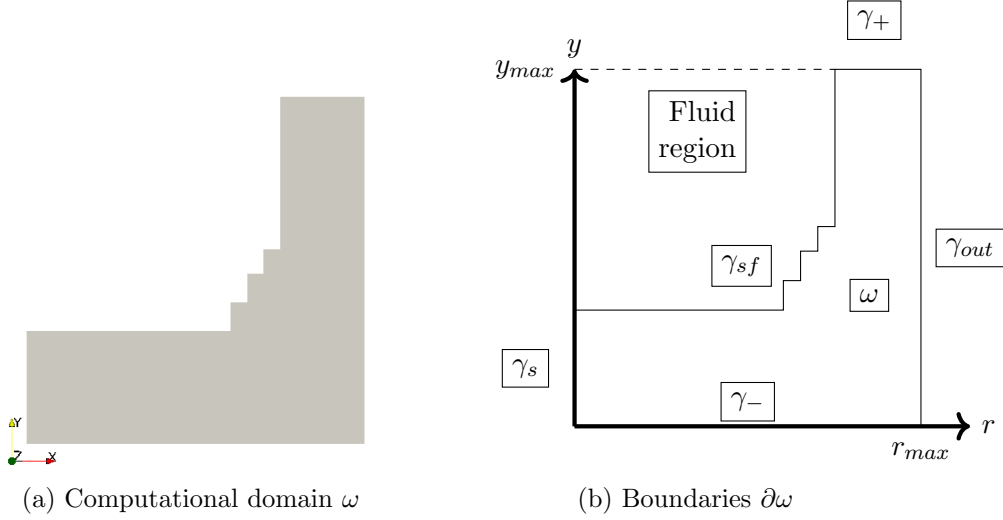
Figure 2.2: Computational domain and its boundaries

2.2 Thermomechanical model for blast furnace walls

In this section, we introduce the strong formulation of the mathematical model, based on the physical problem and simplifications described in Chapter 1, associated with the thermomechanical behaviour of blast furnace walls.

We consider the three dimensional domain Ω as in Figure 2.1. Ω represents a simplified hearth geometry of the lower part of the blast furnace. The hearth refractory materials are in direct contact with liquid iron and slag, so they are exposed to very high temperature environment. Hence, the hearth walls are subjected to severe erosion, chemical attack and high thermal stresses. Based on the simplifications listed in Chapter 1 , the momentum conservation for small displacements, and the energy conservation can be written as (see equations (2.17), (2.22) and (2.23)):

$$-Div(\boldsymbol{\sigma}) = \overrightarrow{f_0} \text{ in } \Omega \ , \tag{2.25}$$

$$-Div(\boldsymbol{K}\nabla T) = Q \text{ in } \Omega \ . \tag{2.26}$$

The thermomechanical stress tensor $\boldsymbol{\sigma}$ is related to the strain tensor through the Hooke's law:

$$\boldsymbol{\sigma}(\overrightarrow{u})[T] = \lambda \operatorname{Tr}(\boldsymbol{\varepsilon}(\overrightarrow{u}))\boldsymbol{I} + 2\mu\boldsymbol{\varepsilon}(\overrightarrow{u}) - (2\mu + 3\lambda)\alpha(T - T_0)\boldsymbol{I} \ , \tag{2.27}$$

where $\boldsymbol{I}$ refers to the identity tensor, $\boldsymbol{\varepsilon}(\overrightarrow{u})$ is the strain tensor defined as:

$$\boldsymbol{\varepsilon}(\overrightarrow{u}) = \frac{1}{2}(\nabla\overrightarrow{u} + \nabla\overrightarrow{u}^T) \ . \tag{2.28}$$

In addition in (2.27), T_0 is the reference temperature, α is the thermal expansion coefficient, and λ and μ are the Lamé parameters of the material. These latter can be expressed in terms of Young's modulus, E, and the Poisson's ratio, ν, as:

$$\mu = \frac{E}{2(1+\nu)} \ , \ \lambda = \frac{E\nu}{(1-2\nu)(1+\nu)} \ . \tag{2.29}$$

Since the simplifications assumed allow us to consider that Ω has axial symmetry, the equations ((2.25)-(2.27)) will be solved on its vertical section, ω (Figure 2.2).

2.2.1 Boundary conditions

In the following, we introduce the notations for the boundaries of the domain Ω, and its vertical cross section in $r - y$ plane, ω (see Figure 2.1 and 2.2). On Ω, and therefore on ω, the following boundaries need to be identified,

$$\begin{aligned}
\Gamma_{out} &= \partial\Omega \cap (r \equiv r_{max}) \ = \gamma_{out} \times [0, 2\pi) \ , \\
\Gamma_{+} &= \partial\Omega \cap (y \equiv y_{max}) \ = \gamma_{+} \times [0, 2\pi) \ , \\
\Gamma_{-} &= \partial\Omega \cap (y \equiv 0) \ = \gamma_{-} \times [0, 2\pi) \ , \\
\Gamma_{sf} &= \partial\Omega \backslash (\Gamma_{out} \cup \Gamma_{+} \cup \Gamma_{-}) \ = \gamma_{sf} \times [0, 2\pi) \ , \\
\gamma_{s} &= \partial\omega \cap (r \equiv 0) \ ,
\end{aligned}$$

where, $r_{max} \in \mathbb{R}^{+}$ and $y_{max} \in \mathbb{R}^{+}$. In further analysis, we use the terms normal force σ_n and tangential force $\overrightarrow{\sigma_t}$ defined by:

$$\sigma_n = (\boldsymbol{\sigma}\overrightarrow{n}) \cdot \overrightarrow{n} \ , \ \overrightarrow{\sigma_t} = \boldsymbol{\sigma}\overrightarrow{n} - \sigma_n \overrightarrow{n} \ . \tag{2.30}$$

- On the upper boundary, Γ_{+}, the applied force, $\overrightarrow{g}_{+}$, and the density of heat flux, q_{+}, are known. Therefore, on Γ_{+}, the following boundary conditions are considered:

$$(-\boldsymbol{K}\nabla T) \cdot \overrightarrow{n} = q_{+} \ , \ \boldsymbol{\sigma}\overrightarrow{n} = \overrightarrow{g}_{+} \ . \tag{2.31}$$

  Here, q_{+} is the heat flux flowing from the upper boundary. The applied force $\overrightarrow{g}_{+}$ refers to force due to weight of the components and fixtures at the top boundary.

- On the bottom boundary, Γ_{-}, the convection heat transfer with heat exchanger at temperature T_{-} and heat transfer coefficient $h_{c,-}$ occurs. The normal displacement is null and shear forces are assumed to be $\overrightarrow{g}_{-}$. Therefore, on Γ_{-}, it is verified,

$$(-\boldsymbol{K}\nabla T) \cdot \overrightarrow{n} = h_{c,-}(T - T_{-}) \ , \ \overrightarrow{u} \cdot \overrightarrow{n} = 0 \ , \ \overrightarrow{\sigma_t} = \overrightarrow{g}_{-} \ , \tag{2.32}$$

  where the data $\overrightarrow{g}_{-}$ is assumed to have zero normal component, i.e. $\overrightarrow{g}_{-} \cdot \overrightarrow{n} = 0$. The shear force $\overrightarrow{g}_{-}$ refers to friction at the bottom surface. In case of frictionless surface, the shear force $\overrightarrow{g}_{-}$ becomes zero.

- On the inner boundary, Γ_{sf}, convection heat transfer with the fluid phase occurs and hydrostatic pressure is acting. So, on this boundary the following boundary conditions are considered.

$$(-\boldsymbol{K}\nabla T) \cdot \overrightarrow{n} = h_{c,f}(T - T_f) \ , \ \boldsymbol{\sigma}\overrightarrow{n} = \overrightarrow{g}_{sf} \ , \tag{2.33}$$

  where T_f is the fluid temperature, assumed to be known and constant at the steady state, $h_{c,f}$ the convective heat transfer coefficient on Γ_{sf}, and $\overrightarrow{g}_{sf}$ is the applied force. In the blast furnace, $\overrightarrow{g}_{sf}$ is related to the hydrostatic pressure by the expression: $\overrightarrow{g}_{sf} = -p_h \overrightarrow{n}$, p_h being the hydrostatic pressure.

- On the outer boundary, Γ_{out}, a convective heat flux and known applied force $\overrightarrow{g}_{out}$ are assumed,

$$(-\boldsymbol{K}\nabla T) \cdot \overrightarrow{n} = h_{c,out}(T - T_{out}) \ , \ \boldsymbol{\sigma}\overrightarrow{n} = \overrightarrow{g}_{out} \ , \tag{2.34}$$

  $h_{c,out}$ being the convective heat transfer coefficient on Γ_{out}, and T_{out} the ambient temperature.

2.2.2 Thermomechanical model in cylindrical coordinates

We express now the governing equations (2.25), (2.26) and the boundary conditions (2.31)-(2.34) in cylindrical coordinate system (r, y, θ) having corresponding unit vectors $(\overrightarrow{e_r}, \overrightarrow{e_y}, \overrightarrow{e_\theta})$. As we will see in next section, this transformation leads to significant simplification. The operators introduced during the previous sections need to be transformed accordingly. The normal vector will now be represented as $\overrightarrow{n} = n_r \overrightarrow{e_r} + n_y \overrightarrow{e}_y + n_\theta \overrightarrow{e}_\theta$. The body force term $\overrightarrow{f_0}$ is expressed as:

$$\overrightarrow{f}_0 = f_{0,r} \overrightarrow{e}_r + f_{0,y} \overrightarrow{e}_y + f_{0,\theta} \overrightarrow{e}_\theta \ . \tag{2.35}$$

The boundary forces are expressed as:

$$\overrightarrow{g}_+ = g_{+,r} \overrightarrow{e}_r + g_{+,y} \overrightarrow{e}_y + g_{+,\theta} \overrightarrow{e}_\theta \ , \tag{2.36a}$$

$$\overrightarrow{g}_- = g_{-,r} \overrightarrow{e}_r + g_{-,y} \overrightarrow{e}_y + g_{-,\theta} \overrightarrow{e}_\theta \ , \tag{2.36b}$$

$$\overrightarrow{g}_{out} = g_{out,r} \overrightarrow{e}_r + g_{out,y} \overrightarrow{e}_y + g_{out,\theta} \overrightarrow{e}_\theta \ , \tag{2.36c}$$

$$\overrightarrow{g}_{sf} = g_{sf,r} \overrightarrow{e}_r + g_{sf,y} \overrightarrow{e}_y + g_{sf,\theta} \overrightarrow{e}_\theta \ . \tag{2.36d}$$

The displacement vector $\overrightarrow{u}$ is expressed as,

$$\overrightarrow{u} = u_r(r,y,\theta) \overrightarrow{e}_r + u_y(r,y,\theta) \overrightarrow{e}_y + u_\theta(r,y,\theta) \overrightarrow{e}_\theta \ , \tag{2.37}$$

the temperature scalar, T, is expressed as,

$$T = T(r,y,\theta) \ , \tag{2.38}$$

and the material point $p = (r, y, \theta)$, with $(r, y) \in \omega$ (see Figure 2.2), and $\theta \in [0, 2\pi)$. The divergence of displacement field $\overrightarrow{u}$ in cylindrical coordinate system is given by:

$$Div(u) = \frac{1}{r} \frac{\partial (u_r r)}{\partial r} + \frac{\partial u_y}{\partial y} + \frac{1}{r} \frac{\partial u_\theta}{\partial \theta} \ . \tag{2.39}$$

The gradient of temperature field, T, in cylindrical coordinate system, is given by:

$$\nabla T = \frac{\partial T}{\partial r} \overrightarrow{e}_r + \frac{\partial T}{\partial y} \overrightarrow{e}_y + \frac{1}{r} \frac{\partial T}{\partial \theta} \overrightarrow{e}_\theta \ . \tag{2.40}$$

The strain tensor in cylindrical coordinate system (r, y, θ) is given by:

$$\varepsilon(\overrightarrow{u}) = \begin{bmatrix} \frac{\partial u_r}{\partial r} & \frac{1}{2}\left(\frac{\partial u_r}{\partial y} + \frac{\partial u_y}{\partial r}\right) & \frac{1}{2}\left(\frac{\partial u_\theta}{\partial r} + \frac{1}{r}\frac{\partial u_r}{\partial \theta} - \frac{u_\theta}{r}\right) \\ \frac{1}{2}\left(\frac{\partial u_r}{\partial y} + \frac{\partial u_y}{\partial r}\right) & \frac{\partial u_y}{\partial y} & \frac{1}{2r}\left(\frac{\partial u_y}{\partial \theta} + r\frac{\partial u_\theta}{\partial y}\right) \\ \frac{1}{2}\left(\frac{\partial u_\theta}{\partial r} + \frac{1}{r}\frac{\partial u_r}{\partial \theta} - \frac{u_\theta}{r}\right) & \frac{1}{2r}\left(\frac{\partial u_y}{\partial \theta} + r\frac{\partial u_\theta}{\partial y}\right) & \frac{1}{r}\frac{\partial u_\theta}{\partial \theta} + \frac{u_r}{r} \end{bmatrix} . \tag{2.41}$$

If $\boldsymbol{A}$ denotes the fourth order tensor defined as,

$$\boldsymbol{A} = \frac{E}{(1 - 2\nu)(1 + \nu)} \begin{bmatrix} 1-\nu & \nu & \nu & 0 & 0 & 0 \\ \nu & 1-\nu & \nu & 0 & 0 & 0 \\ \nu & \nu & 1-\nu & 0 & 0 & 0 \\ 0 & 0 & 0 & \frac{1-2\nu}{2} & 0 & 0 \\ 0 & 0 & 0 & 0 & \frac{1-2\nu}{2} & 0 \\ 0 & 0 & 0 & 0 & 0 & \frac{1-2\nu}{2} \end{bmatrix} , \tag{2.42}$$

the stress-strain relationship can be expressed in vector formulation as,

$$\{\boldsymbol{\sigma}(\overrightarrow{u})[T]\} = \boldsymbol{A}\{\varepsilon(\overrightarrow{u})\} - (2\mu + 3\lambda)\alpha(T - T_0)\{\boldsymbol{I}\} \ , \tag{2.43}$$

where the following column vectors have been considered:

$$\begin{aligned} \{\boldsymbol{\sigma}\} &= \{\sigma_{rr} \quad \sigma_{yy} \quad \sigma_{\theta\theta} \quad \sigma_{y\theta} \quad \sigma_{r\theta} \quad \sigma_{ry}\}^T \ , \\ \{\boldsymbol{\varepsilon}\} &= \{\varepsilon_{rr} \quad \varepsilon_{yy} \quad \varepsilon_{\theta\theta} \quad 2\varepsilon_{y\theta} \quad 2\varepsilon_{r\theta} \quad 2\varepsilon_{ry}\}^T \ , \\ \{\boldsymbol{I}\} &= \{1 \quad 1 \quad 1 \quad 0 \quad 0 \quad 0\}^T \ . \end{aligned} \tag{2.44}$$

- Stationary thermal model:

  For the thermal model, we consider that the tensor of thermal conductivity is isotropic and no dependency on time is considered. Therefore, the energy conservation equation (2.26) can be rewritten as:

  $$-\frac{1}{r} \frac{\partial}{\partial r}\left(rk\frac{\partial T}{\partial r}\right) - \frac{\partial}{\partial y}\left(k\frac{\partial T}{\partial y}\right) - \frac{1}{r} \frac{\partial}{\partial \theta}\left(\frac{k}{r}\frac{\partial T}{\partial \theta}\right) = Q \ , \text{ in } \Omega \ . \tag{2.45}$$

The corresponding thermal boundary conditions in (2.31)-(2.34) are:

$$
\begin{aligned}
\text{on } \Gamma_+ &: (-k\nabla T) \cdot \overrightarrow{n} = q_+ \;, \\
\text{on } \Gamma_- &: (-k\nabla T) \cdot \overrightarrow{n} = h_{c,-}(T - T_-) \;, \\
\text{on } \Gamma_{sf} &: (-k\nabla T) \cdot \overrightarrow{n} = h_{c,f}(T - T_f) \;, \\
\text{on } \Gamma_{out} &: (-k\nabla T) \cdot \overrightarrow{n} = h_{c,out}(T - T_{out}) \;.
\end{aligned}
\tag{2.46}
$$

- Stationary mechanical model:

  Vectorial equation (2.25) in cylindrical coordinates corresponds to following three equations:

$$
\begin{aligned}
\frac{\partial \sigma_{rr}}{\partial r} + \frac{\partial \sigma_{ry}}{\partial y} + \frac{1}{r}\frac{\partial \sigma_{r\theta}}{\partial \theta} + \frac{\sigma_{rr} - \sigma_{\theta\theta}}{r} + f_{0,r} = 0 \;, \text{ in } \Omega \;, \\
\frac{\partial \sigma_{r\theta}}{\partial r} + \frac{\partial \sigma_{\theta y}}{\partial y} + \frac{1}{r}\frac{\partial \sigma_{\theta\theta}}{\partial \theta} + 2\frac{\sigma_{r\theta}}{r} + f_{0,\theta} = 0 \;, \text{ in } \Omega \;, \\
\frac{\partial \sigma_{ry}}{\partial r} + \frac{1}{r}\frac{\partial \sigma_{\theta y}}{\partial \theta} + \frac{\partial \sigma_{yy}}{\partial y} + \frac{\sigma_{ry}}{r} + f_{0,y} = 0 \;, \text{ in } \Omega \;.
\end{aligned}
\tag{2.47}
$$

The corresponding mechanical boundary conditions introduced in (2.31)-(2.34) are:

$$
\begin{aligned}
\text{on } \Gamma_+ &: \; \boldsymbol{\sigma}\overrightarrow{n} = \overrightarrow{g}_+ \;, \\
\text{on } \Gamma_- &: \; \overrightarrow{u} \cdot \overrightarrow{n} = 0 \;, \; \overrightarrow{\sigma_t} = \overrightarrow{g}_- \;, \\
\text{on } \Gamma_{sf} &: \; \boldsymbol{\sigma}\overrightarrow{n} = \overrightarrow{g}_{sf} \;, \\
\text{on } \Gamma_{out} &: \; \boldsymbol{\sigma}\overrightarrow{n} = \overrightarrow{g}_{out} \;.
\end{aligned}
\tag{2.48}
$$

2.3   Axisymmetric thermomechanical model

In the context of blast furnace application, the body force density term $\overrightarrow{f_0}$ can be expressed as,

$$
\overrightarrow{f}_0 = f_{0,r}\overrightarrow{e}_r + f_{0,y}\overrightarrow{e}_y \;,
\tag{2.49}
$$

and it depends only on (r,y) coordinates. Similarly, applied surface forces have zero component in $\overrightarrow{e}_\theta$ direction and they do not depend on θ. Besides, the heat source term, Q, the heat flux density, q_+, the heat transfer coefficients, $h_{c,-}, h_{c,f}, h_{c,out}$, and temperatures T_-, T_f, T_{out} are assumed to be only dependent on (r,y) coordinates.

Therefore, the introduced 3-dimensional model (equations (2.45) - (2.48)) is independent of θ, and hence a symmetry hypothesis is applicable. The axisymmetric model leads to significant computational savings as the 3-dimensional model defined in Ω (see Figure 2.1) is replaced by the corresponding 2-dimensional model defined in its vertical section,

ω (see Figure 2.2). The unit outer normal vector to the boundary of this section will now be represented as $\overrightarrow{n} = n_r \overrightarrow{e}_r + n_y \overrightarrow{e}_y$. In the axisymmetric system, we represent the displacement $\overrightarrow{u}$ and temperature T, both independent of θ, as:

$$\overrightarrow{u} = u_r(r,y)\overrightarrow{e}_r + u_y(r,y)\overrightarrow{e}_y \; , \; T = T(r,y) \; . \tag{2.50}$$

The associated axisymmetric model is reduced to consider conservation equations (2.45), (2.47) defined in ω and the boundary conditions (2.46), (2.48) replacing the Γ boundaries by γ such that $\Gamma = (\gamma \backslash \gamma_s) \times [0, 2\pi)$ (see figures 2.1c, 2.1d, 2.1e, 2.1f and 2.2b), adding the usual symmetry conditions on γ_s:

$$(-k\nabla T) \cdot \overrightarrow{n} = 0 \; , \; \overrightarrow{u} \cdot \overrightarrow{n} = 0 \; , \; \overrightarrow{\sigma_t} = \overrightarrow{0} \; . \tag{2.51}$$

Under the assumption of axisymmetry, the strain and stress tensors in cylindrical coordinate system (r, y, θ) given by (2.41) and (2.43), respectively, can be reduced to:

$$\varepsilon(\overrightarrow{u}) = \begin{bmatrix} \frac{\partial u_r}{\partial r} & \frac{1}{2}\left(\frac{\partial u_r}{\partial y} + \frac{\partial u_y}{\partial r}\right) & 0 \\ \frac{1}{2}\left(\frac{\partial u_r}{\partial y} + \frac{\partial u_y}{\partial r}\right) & \frac{\partial u_y}{\partial y} & 0 \\ 0 & 0 & \frac{u_r}{r} \end{bmatrix} \; , \tag{2.52}$$

$$\boldsymbol{\sigma}(\overrightarrow{u})[T] = \begin{bmatrix} \sigma_{rr} & \sigma_{ry} & 0 \\ \sigma_{ry} & \sigma_{yy} & 0 \\ 0 & 0 & \sigma_{\theta\theta} \end{bmatrix} \; . \tag{2.53}$$

Taking into account the expression of the unit normal vector at different boundaries as,

$$\begin{aligned} \text{on } \gamma_+ \; &: n_r = 0 \; , n_y = 1 \; , \overrightarrow{n} = \overrightarrow{e}_y \; , \\ \text{on } \gamma_- \; &: n_r = 0 \; , n_y = -1 \; , \overrightarrow{n} = -\overrightarrow{e}_y \; , \\ \text{on } \gamma_{sf} \; &: \overrightarrow{n} = n_r \overrightarrow{e}_r + n_y \overrightarrow{e}_y \; , \\ \text{on } \gamma_{out} \; &: n_r = 1 \; , n_y = 0 \; , \overrightarrow{n} = \overrightarrow{e}_r \; , \\ \text{on } \gamma_s \; &: n_r = -1 \; , n_y = 0 \; , \overrightarrow{n} = -\overrightarrow{e}_r \; , \end{aligned} \tag{2.54}$$

the axisymmetric thermomechanical model considered can be summarized as:

- Thermal model (T1):

$$-\frac{1}{r}\frac{\partial}{\partial r}\left(rk\frac{\partial T}{\partial r}\right) - \frac{\partial}{\partial y}\left(k\frac{\partial T}{\partial y}\right) = Q \; , \; \text{in } \omega \; . \tag{2.55}$$

Boundary conditions:

$$\text{on } \gamma_+ \ : -k\frac{\partial T}{\partial y} = q_+ \ ,$$

$$\text{on } \gamma_- \ : k\frac{\partial T}{\partial y} = h_{c,-}(T - T_-) \ ,$$

$$\text{on } \gamma_{sf} \ : -k\frac{\partial T}{\partial r}n_r - k\frac{\partial T}{\partial y}n_y = h_{c,f}(T - T_f) \ , \qquad (2.56)$$

$$\text{on } \gamma_{out} \ : -k\frac{\partial T}{\partial r} = h_{c,out}(T - T_{out}) \ ,$$

$$\text{on } \gamma_s \ : \frac{\partial T}{\partial r} = 0 \ .$$

- Mechanical model (M1):

$$\frac{\partial \sigma_{rr}}{\partial r} + \frac{\partial \sigma_{ry}}{\partial y} + \frac{\sigma_{rr} - \sigma_{\theta\theta}}{r} + f_{0,r} = 0 \ , \ \text{in } \omega \ ,$$
$$\frac{\partial \sigma_{ry}}{\partial r} + \frac{\partial \sigma_{yy}}{\partial y} + \frac{\sigma_{ry}}{r} + f_{0,y} = 0 \ , \ \text{in } \omega \ . \qquad (2.57)$$

In vector notation, axisymmetric stress-strain relationship can be expressed as,

$$\{\boldsymbol{\sigma}(\overrightarrow{u})[T]\} = \boldsymbol{A}\{\boldsymbol{\varepsilon}(\overrightarrow{u})\} - (2\mu + 3\lambda)\alpha(T - T_0)\{\boldsymbol{I}\} \ ,$$

$$\boldsymbol{A} = \frac{E}{(1 - 2\nu)(1 + \nu)}
\begin{bmatrix}
1 - \nu & \nu & \nu & 0 \\
\nu & 1 - \nu & \nu & 0 \\
\nu & \nu & 1 - \nu & 0 \\
0 & 0 & 0 & \frac{1-2\nu}{2}
\end{bmatrix} \ ,$$

$$\{\boldsymbol{\sigma}\} = \{\sigma_{rr} \quad \sigma_{yy} \quad \sigma_{\theta\theta} \quad \sigma_{ry}\}^T \ , \qquad (2.58)$$

$$\{\boldsymbol{\varepsilon}\} = \{\varepsilon_{rr} \quad \varepsilon_{yy} \quad \varepsilon_{\theta\theta} \quad 2\varepsilon_{ry}\}^T \ ,$$

$$\{\boldsymbol{I}\} = \{1 \quad 1 \quad 1 \quad 0\}^T \ .$$

Boundary conditions :

$$\text{on } \gamma_+ \ : \sigma_{ry} = g_{+,r} \ , \ \sigma_{yy} = g_{+,y} \ ,$$

$$\text{on } \gamma_- \ : \ u_y = 0, \ \sigma_{ry} = -g_{-,r} \ ,$$

$$\text{on } \gamma_{sf} \ : \ \sigma_{rr}n_r + \sigma_{ry}n_y = g_{sf,r} \ ,$$

$$\sigma_{ry}n_r + \sigma_{yy}n_y = g_{sf,y} \ , \qquad (2.59)$$

$$\text{on } \gamma_{out} \ : \ \sigma_{rr} = g_{out,r} \ , \ \sigma_{ry} = g_{out,y} \ ,$$

$$\text{on } \gamma_s \ : \ u_r = 0 \ , \ \sigma_{ry} = 0 \ .$$

In this chapter, we introduced a thermomechanical model as relevant to the blast furnace hearth walls and applied axisymmetric hypothesis. Subsequently, we introduced axisymmetric thermomechanical model, which will be the basis for the weak formulation discussed in the chapter 3.

Chapter 3

Weak formulation of axisymmetric thermomechanical model

We derive the weak formulation related to the axisymmetric thermomechanical model (2.55)-(2.59) introduced in the Chapter 2. We first introduce the relevant function spaces in section 3.1. In section 3.2, we discuss hypotheses on the data such that the weak formulation is well defined and investigate the well-posedness of the problem, i.e. the existence and uniqueness of the weak solution. We also introduce the variational principle, which provides an alternative interpretation of the weak formulation (Section 3.3).

3.1 Weighted Sobolev spaces and axisymmetric functions

We introduce weighted Sobolev spaces [48, 49, 57], $L_r^2(\omega)$ and $H_r^1(\omega)$ with respective norms $||\cdot||_{L_r^2(\omega)}$ and $||\cdot||_{H_r^1(\omega)}$ as:

$$L_r^2(\omega) = \left\{ \psi : \omega \mapsto \mathbb{R} \ , \ \int_\omega \psi^2 r dr dy < \infty \right\} ,$$

$$||\psi||_{L_r^2(\omega)}^2 = \int_\omega \psi^2 r dr dy ,$$

$$H_r^1(\omega) = \left\{ \psi : \omega \mapsto \mathbb{R} \ , \ \int_\omega \left(\psi^2 + \left(\frac{\partial \psi}{\partial r} \right)^2 + \left(\frac{\partial \psi}{\partial y} \right)^2 \right) r dr dy < \infty \right\} , \qquad (3.1)$$

$$||\psi||_{H_r^1(\omega)}^2 = \int_\omega \left(\psi^2 + \left(\frac{\partial \psi}{\partial r} \right)^2 + \left(\frac{\partial \psi}{\partial y} \right)^2 \right) r dr dy .$$

Analogously, given γ a subset of $\partial\omega$, the boundary of ω:

$$L_r^2(\gamma) = \left\{ g : \gamma \mapsto \mathbb{R}, \int_\gamma g^2 r d\gamma < \infty \right\} . \qquad (3.2)$$

Let $L^\infty(\omega)$ be the space:

$$L^\infty(\omega) = \{ f : \omega \mapsto \mathbb{R} \, , \sup_\omega |f| \leq C \, , \; C \geq 0 \, \} \, , \; ||f||_{L^\infty(\omega)} = \sup_\omega |f| \; . \tag{3.3}$$

Analogously, $L^\infty(\gamma)$ is defined.

Notice that $H_r^1(\omega)$ is closely related to the usual Sobolev space $H^1(\Omega)$. Indeed, if ψ belongs to $L_r^2(\omega)$, and we extend it to $\Omega = \omega \times [0, 2\pi)$ as an axisymmetric function $\bar{\psi}$ defined as: $\bar{\psi}(r, y, \theta) = \psi(r, y)$, then:

$$\begin{aligned}
||\bar{\psi}||_{L^2(\Omega)} &= \sqrt{2\pi} ||\psi||_{L_r^2(\omega)} \; , \\
||\bar{\psi}||_{H^1(\Omega)} &= \sqrt{2\pi} ||\psi||_{H_r^1(\omega)} \; .
\end{aligned} \tag{3.4}$$

The reciprocal is also true for all axisymmetric function $\bar{\psi}$ with respect to the cylindrical coordinates (r, y, θ). Let $\bar{H}^1(\Omega) \subset H^1(\Omega)$ be the subspace of all axisymmetric functions in $H^1(\Omega)$ with respect to $y-$axis. Then the following properties are verified (see [57]):

1. $\bar{H}^1(\Omega)$ is isometric to $H_r^1(\omega)$.

2. The space of smooth functions $C^\infty(\omega)$ is dense in $L_r^2(\omega)$ and in $H_r^1(\omega)$.

3. By isometry, it can be concluded that the embedding of $H_r^1(\omega)$ in $L_r^2(\omega)$ is compact.

3.2   Weak formulation

3.2.1   Thermal model

Before discussing the weak formulation of the thermal model (T1), we assume the following hypotheses on the data.

(TH1) The heat source term, Q, verifies:

$$Q \in L_r^2(\omega) \; .$$

(TH2) The convection temperatures belong to the spaces:

$$T_{sf} \in L_r^2(\gamma_{sf}) \, , \; T_- \in L_r^2(\gamma_-) \, , \; T_{out} \in L_r^2(\gamma_{out}) \; .$$

(TH3) The boundary heat flux verifies:

$$q_+ \in L_r^2(\gamma_+) \; .$$

(TH4) There exists a constant $k_0 > 0$, such that the thermal conductivity, $k(r, y)$ satisfies:

$$k(r,y) \in L^\infty(\omega) \ , \ \ k(r,y) > k_0 \ , \ \text{in } \omega \ .$$

Also, there exist constants $h_{c,f,0} > 0, h_{c,out,0} > 0, h_{c,-,0} > 0$ such that:

$$h_{c,f}(r,y) \in L^\infty(\gamma_{sf}) \ , \ \ h_{c,f}(r,y) > h_{c,f,0} \ , \ \text{on } \gamma_{sf} \ ,$$
$$h_{c,out}(r,y) \in L^\infty(\gamma_{out}) \ , \ \ h_{c,out}(r,y) > h_{c,out,0} \ \text{on } \gamma_{out} \ ,$$
$$h_{c,-}(r,y) \in L^\infty(\gamma_-) \ , \ \ h_{c,-}(r,y) > h_{c,-,0} \ , \ \text{on } \gamma_- \ .$$

In order to propose a weak formulation for the thermal model (2.55) and (2.56), in the following we assume sufficient regularity to perform the following calculations. We multiply the energy equation (2.55) by $r\psi(r, y)$ and integrate over the domain ω with respect to (r, y) variables, so we obtain:

$$- \int_\omega \frac{\psi}{r} \frac{\partial}{\partial r} \left(rk \frac{\partial T}{\partial r} \right) r dr dy - \int_\omega \psi \frac{\partial}{\partial y} \left(k \frac{\partial T}{\partial y} \right) r dr dy = \int_\omega \psi Q r dr dy \ . \qquad (3.5)$$

By applying Gauss divergence theorem, we deduce,

$$\int_\omega rk \left(\frac{\partial T}{\partial y} \frac{\partial \psi}{\partial y} + \frac{\partial T}{\partial r} \frac{\partial \psi}{\partial r} \right) dr dy = \int_\omega \psi Q r dr dy + \int_{\partial \omega} r \psi k \left(\frac{\partial T}{\partial y} n_y + \frac{\partial T}{\partial r} n_r \right) d\gamma \ , \qquad (3.6)$$

where $\overrightarrow{n} = (n_r, n_y)$ is the unit outer normal vector to the boundaries of ω. Using boundary conditions from equation (2.56), expression (3.6) can be written as:

$$\int_\omega rk \left(\frac{\partial T}{\partial y} \frac{\partial \psi}{\partial y} + \frac{\partial T}{\partial r} \frac{\partial \psi}{\partial r} \right) dr dy + \int_{\gamma_{sf}} \psi h_{c,f} T r d\gamma + \int_{\gamma_{out}} \psi h_{c,out} T r d\gamma +$$

$$\int_{\gamma_-} \psi h_{c,-} T r d\gamma = \int_\omega \psi Q r dr dy + \int_{\gamma_{sf}} \psi h_{c,f} T_f r d\gamma + \qquad (3.7)$$

$$\int_{\gamma_{out}} \psi h_{c,out} T_{out} r d\gamma + \int_{\gamma_-} \psi h_{c,-} T_- \ r d\gamma - \int_{\gamma_+} \psi q^+ r d\gamma \ .$$

Therefore, we propose the following weak formulation for thermal problem $(T1)$:

Problem 1 *Weak thermal formulation $(WT1)$: Under the assumptions $(TH1)$-$(TH4)$, find $T \in H_r^1(\omega)$, such that equality (3.7) is verified for all $\psi \in H_r^1(\omega)$.*

It is to be noted that under assumptions (TH1)-(TH4) all integrals of the proposed weak formulation are well defined. The left hand side of equation (3.7) is bilinear and symmetric. So, we define in $H_r^1(\omega) \times H_r^1(\omega)$ the operator:

$$a_T(T, \psi) = \int_\omega rk \left(\frac{\partial T}{\partial y} \frac{\partial \psi}{\partial y} + \frac{\partial T}{\partial r} \frac{\partial \psi}{\partial r} \right) dr dy + \int_{\gamma_{sf}} \psi h_{c,f} T r d\gamma$$

$$+ \int_{\gamma_{out}} \psi h_{c,out} T r d\gamma + \int_{\gamma_-} \psi h_{c,-} T r d\gamma \ . \qquad (3.8)$$

The right hand side of equation (3.7) is linear and the following linear operator defined on $H_r^1(\omega)$ is introduced:

$$l_T(\psi) = \int_\omega \psi Q r dr dy + \int_{\gamma_{sf}} \psi h_{c,f} T_f r d\gamma + \int_{\gamma_{out}} \psi h_{c,out} T_{out} r d\gamma +$$
$$\int_{\gamma_-} \psi h_{c,-} T_- \, r d\gamma - \int_{\gamma_+} \psi q^+ r d\gamma \ . \tag{3.9}$$

With the help of these operators the weak formulation $(WT1)$ can be rewritten more simply in the equivalent way:

Problem 2 *Weak thermal model $(WT2)$: Under the assumptions (TH1)-(TH4), find $T \in H_r^1(\omega)$ such that:*

$$a_T(T, \psi) = l_T(\psi) \ , \ \forall \ \psi \in H_r^1(\omega) \ . \tag{3.10}$$

By using Cauchy-Schwarz inequality and the trace operator properties [23], it can be shown that, under the assumptions (TH1)-(TH4), $a_T(T, \psi)$ and $l_T(\psi)$ are continuous on $H_r^1(\omega) \times H_r^1(\omega)$ and $H_r^1(\omega)$, respectively. In other words, there exists a constant, $C_T > 0$, referred as continuity constant of $a_T(\cdot, \cdot)$, such that:

$$a_T(T, \psi) \leq C_T \|T\|_{H_r^1(\omega)} \|\psi\|_{H_r^1(\omega)} \ , \ \forall T, \psi \in H_r^1(\omega) \ . \tag{3.11}$$

Besides, since $mes(\gamma_- \cup \gamma_{out} \cup \gamma_{sf}) > 0$, by Friedrich's inequality (see theorem 1.9 of [65]) as applied to $H^1(\Omega)$, using equation (3.4), and hypothesis $(TH4)$ on the data, there exists a constant, $c_T > 0$, referred as coercivity constant of $a_T(\cdot, \cdot)$, such that:

$$c_T \|\psi\|_{H_r^1(\omega)}^2 \leq a_T(\psi, \psi) \ , \ \forall \psi \in H_r^1(\omega) \ . \tag{3.12}$$

In other words, the bilinear form $a_T(\psi, \psi)$ is coercive on $H_r^1(\omega) \times H_r^1(\omega)$. Hence, the conditions of the Lax-Milgram theorem [23] are satisfied and accordingly, the weak thermal formulation $(WT2)$ has unique solution T. Given the equivalence between $(WT1)$ and $(WT2)$ formulations, T is the unique solution of weak thermal formulation $(WT1)$.

3.2.2   Thermomechanical model

Before discussing the weak formulation for the mechanical model $(M1)$, the following space $\mathbb{V}$ for the displacement is considered:

$$\mathbb{V} = (H_r^1(\omega) \cap L_{1/r}^2(\omega)) \times H_r^1(\omega) \ .$$

It will be equipped with the inner product,

$$< \overrightarrow{u}, \overrightarrow{\phi} >_{\mathbb{V}} = \int_\omega \left(\phi_r u_r + \phi_y u_y + \frac{\partial u_r}{\partial r} \frac{\partial \phi_r}{\partial r} + \frac{\partial u_r}{\partial y} \frac{\partial \phi_r}{\partial y} + \frac{u_r}{r} \frac{\phi_r}{r} + \right.$$
$$\left. \frac{\partial u_y}{\partial r} \frac{\partial \phi_y}{\partial r} + \frac{\partial u_y}{\partial y} \frac{\partial \phi_y}{\partial y} + \frac{\partial u_r}{\partial y} \frac{\partial \phi_y}{\partial r} + \frac{\partial u_y}{\partial r} \frac{\partial \phi_r}{\partial y} \right) r dr dy \ , \tag{3.13}$$

and the norm,

$$\| \overrightarrow{\phi} \|_{\mathbb{V}}^2 = < \overrightarrow{\phi}, \overrightarrow{\phi} >_{\mathbb{V}} . \tag{3.14}$$

Its closed and convex subspace

$$\mathbb{U} = \{ \overrightarrow{\phi} = (\phi_r \ \phi_y) \in \mathbb{V} , \ \phi_y = 0 \text{ on } \gamma_- , \ \phi_r = 0 \text{ on } \gamma_s \} ,$$

will be the set of admissible displacements. The subspace $\mathbb{U}$ is equipped with the same norm as spave $\mathbb{V}$ i.e. $\| \overrightarrow{\phi} \|_{\mathbb{U}} = \| \overrightarrow{\phi} \|_{\mathbb{V}}, \forall \overrightarrow{\phi} \in \mathbb{U}$.

The function space for the stress tensor is defined as:

$$\mathbb{S} = \{ \boldsymbol{\sigma} = [\sigma_{ij}] \in [L_r^2(\omega)]^{3\times3}, \sigma_{ij} = \sigma_{ji}, \sigma_{\alpha 3} = 0, \alpha = 1, 2 \} .$$

We assume the following hypotheses on the mechanical data:

(MH1) The body force density, $\overrightarrow{f_0}$, is such that:

$$\overrightarrow{f_0} \in [L_r^2(\omega)]^2 .$$

(MH2) The boundary forces verify the following regularity assumptions:

$$\overrightarrow{g}_+ \in [L_r^2(\gamma_+)]^2, \ \overrightarrow{g}_{sf} \in [L_r^2(\gamma_{sf})]^2, \ \overrightarrow{g}_{out} \in [L_r^2(\gamma_{out})]^2,$$
$$\overrightarrow{g}_- \in [L_r^2(\gamma_-)]^2, \text{ and } \overrightarrow{n} \cdot \overrightarrow{g}_- = 0 \text{ on } \gamma_-.$$

(MH3) There exist constants $E_0 > 0$ and $\alpha_0 > 0$ such that, the Young's modulus, $E(r, y)$, and the coefficient of thermal expansion, $\alpha(r, y)$ satisfy:

$$E(r, y) \in L^\infty(\omega) , \ E > E_0 , \ \alpha(r, y) \in L^\infty(\omega) , \ \alpha > \alpha_0 , \text{ in } \omega .$$

(MH4) There exist constants $\nu_0 > 0, \nu_1 < 0.5$ such that, the Poisson's ratio, $\nu(r, y)$, satisfies:

$$\nu(r, y) \in L^\infty(\omega) , \ \nu_0 < \nu < \nu_1 , \text{ in } \omega .$$

It can be seen that in case $T = T_0$ in equation (2.58), the stress tensor $\boldsymbol{\sigma}(\overrightarrow{\phi})$ belongs to the space $\mathbb{S}$. Besides, if T and T_0 belong to $H_r^1(\omega)$, the stresses generated belong to $\mathbb{S}$ too. In other words, the stresses generated due to mechanical effects lie also in the same space as that of stresses generated due to thermomechanical effects.

In order to propose a weak formulation of the mechanical model (2.57) - (2.59), we assume that all functions have sufficiently regularity as necessary for the following calculations. Given a function $\overrightarrow{\phi} = (\phi_r, \phi_y)$, we multiply the first equation of (2.57) by $r\phi_r(r, y)$, the second one by $r\phi_y(r, y)$, we sum both, and integrate over ω to obtain:

$$\int_\omega \left(\phi_r \frac{\partial \sigma_{rr}}{\partial r} + \phi_r \frac{\partial \sigma_{ry}}{\partial y} + \frac{\phi_r}{r}(\sigma_{rr} - \sigma_{\theta\theta}) + \phi_y \frac{\partial \sigma_{ry}}{\partial r} + \phi_y \frac{\partial \sigma_{yy}}{\partial y} + \phi_y \frac{\sigma_{ry}}{r} \right) r \, dr \, dy +$$

$$\int_\omega (\phi_r f_{0,r} + \phi_y f_{0,y}) \, r \, dr \, dy = 0 .$$

So,

$$\int_\omega \left(\phi_r \frac{\partial \sigma_{rr}}{\partial r} + \phi_y \frac{\partial \sigma_{ry}}{\partial r} \right) r dr dy + \int_\omega \left(\phi_r \frac{\partial \sigma_{ry}}{\partial y} + \phi_y \frac{\partial \sigma_{yy}}{\partial y} \right) r dr dy +$$

$$\int_\omega \left(\phi_r (\sigma_{rr} - \sigma_{\theta\theta}) + \phi_y \sigma_{ry} \right) dr dy + \int_\omega \left(\phi_r f_{0,r} + \phi_y f_{0,y} \right) r dr dy = 0 \ .$$

Then, applying Green formula we deduce,

$$- \int_\omega \frac{\partial (r\phi_r)}{\partial r} \sigma_{rr} dr dy - \int_\omega \frac{\partial (r\phi_y)}{\partial r} \sigma_{ry} dr dy - \int_\omega r \left[\left(\frac{\partial \phi_r}{\partial y} \right) \sigma_{ry} + \left(\frac{\partial \phi_y}{\partial y} \right) \sigma_{yy} \right] dr dy +$$

$$\int_\omega \left(\phi_r (\sigma_{rr} - \sigma_{\theta\theta}) + \phi_y \sigma_{ry} \right) dr dy + \int_{\partial\omega} r \phi_r \sigma_{rr} n_r d\gamma + \int_{\partial\omega} r \phi_y \sigma_{ry} n_r d\gamma$$

$$+ \int_{\partial\omega} r \left(\phi_r \sigma_{ry} + \phi_y \sigma_{yy} \right) n_y d\gamma + \int_\omega \left(\phi_r f_{0,r} + \phi_y f_{0,y} \right) r dr dy = 0 \ ,$$

from which we can write,

$$- \int_\omega r \frac{\partial \phi_r}{\partial r} \sigma_{rr} dr dy - \int_\omega r \frac{\partial \phi_y}{\partial r} \sigma_{ry} dr dy - \int_\omega r \left[\frac{\partial \phi_r}{\partial y} \sigma_{ry} + \frac{\partial \phi_y}{\partial y} \sigma_{yy} \right] dr dy$$

$$- \int_\omega \phi_r \sigma_{\theta\theta} dr dy + \int_{\partial\omega} r \phi_r \sigma_{rr} n_r d\gamma + \int_{\partial\omega} r \phi_y \sigma_{ry} n_r d\gamma$$

$$+ \int_{\partial\omega} r (\phi_r \sigma_{ry} + \phi_y \sigma_{yy}) n_y d\gamma + \int_\omega \left(\phi_r f_{0,r} + \phi_y f_{0,y} \right) r dr dy = 0 \ .$$

By using boundary conditions given by equations in (2.59), taking into account (2.52) and (2.53), assuming that the normal component of $\overrightarrow{\phi}$ is null on $\gamma_- \cup \gamma_s$, we have:

$$\int_\omega r (\varepsilon(\overrightarrow{\phi})) : (\boldsymbol{\sigma}(\overrightarrow{u})) dr dy = \int_\omega \left(\phi_r f_{0,r} + \phi_y f_{0,y} \right) r dr dy + \int_{\gamma_{sf}} \overrightarrow{\phi} \cdot \overrightarrow{g}_{sf} r d\gamma +$$

$$\int_{\gamma_{out}} \overrightarrow{\phi} \cdot \overrightarrow{g}_{out} r d\gamma + \int_{\gamma_-} \overrightarrow{\phi} \cdot \overrightarrow{g}_- r d\gamma + \int_{\gamma_+} \overrightarrow{\phi} \cdot \overrightarrow{g}_+ r d\gamma \ .$$

Writing the left hand side term in vector notation, and replacing in this expression $\boldsymbol{\sigma}(\overrightarrow{u})$ in terms of the strain given by relation (2.58), we obtain,

$$\int_\omega \boldsymbol{A} \{ \varepsilon(\overrightarrow{u}) \} \cdot \{ \varepsilon(\overrightarrow{\phi}) \} r dr dy = \int_\omega (2\mu + 3\lambda) \alpha (T - T_0) \{ \boldsymbol{I} \} \cdot \{ \varepsilon(\overrightarrow{\phi}) \} r dr dy +$$

$$\int_\omega \left(\phi_r f_{0,r} + \phi_y f_{0,y} \right) r dr dy + \int_{\gamma_{sf}} \overrightarrow{\phi} \cdot \overrightarrow{g}_{sf} r d\gamma + \int_{\gamma_{out}} \overrightarrow{\phi} \cdot \overrightarrow{g}_{out} r d\gamma + \qquad (3.15)$$

$$\int_{\gamma_-} \overrightarrow{\phi} \cdot \overrightarrow{g}_- r d\gamma + \int_{\gamma_+} \overrightarrow{\phi} \cdot \overrightarrow{g}_+ r d\gamma \ ,$$

where T is assumed to be the solution of the weak thermal model $(WT2)$.

Firstly, notice that under assumptions (MH1)-(MH4), and since $T \in H^1_r(\omega)$, all integrals in (3.15) are well defined. Therefore, we propose the following weak formulation for the mechanical model $(M1)$:

Problem 3 *Weak mechanical formulation $(WM1)$: Let $T \in H^1_r(\omega)$ be the solution of the weak thermal model $(WT2)$. Under assumptions (MH1)-(MH4), find $\overrightarrow{u} \in \mathbb{U}$, such that equality (3.15) is verified for all $\overrightarrow{\phi} \in \mathbb{U}$.*

The left hand side of equation (3.15) is bilinear in $\mathbb{V} \times \mathbb{V}$,

$$a_M(\overrightarrow{u}, \overrightarrow{\phi}) = \int_{\omega} \boldsymbol{A}\{\boldsymbol{\varepsilon}(\overrightarrow{u})\} \cdot \{\boldsymbol{\varepsilon}(\overrightarrow{\phi})\} r dr dy , \qquad (3.16)$$

while the right hand side of the equation is linear in $\mathbb{V}$,

$$l_M[T](\overrightarrow{\phi}) = \int_{\omega} (2\mu + 3\lambda)\alpha(T - T_0)\{\boldsymbol{I}\} \cdot \{\boldsymbol{\varepsilon}(\overrightarrow{\phi})\} r dr dy + \int_{\omega} (\phi_r f_{0,r} + \phi_y f_{0,y})\, r dr dy +$$

$$\int_{\gamma_{sf}} \overrightarrow{\phi} \cdot \overrightarrow{g}_{sf} r d\gamma + \int_{\gamma_{out}} \overrightarrow{\phi} \cdot \overrightarrow{g}_{out} r d\gamma + \int_{\gamma_-} \overrightarrow{\phi} \cdot \overrightarrow{g}_- r d\gamma + \int_{\gamma_+} \overrightarrow{\phi} \cdot \overrightarrow{g}_+ r d\gamma . \qquad (3.17)$$

With the help of these two operators, the weak formulation of the mechanical problem can be written in the simplified and equivalent form as:

Problem 4 *Weak mechanical problem $(WM2)$: Let $T \in H^1_r(\omega)$ be the solution of the weak thermal model $(WT2)$. Under the assumptions (MH1)-(MH4), find $\overrightarrow{u} \in \mathbb{U}$ such that:*

$$a_M(\overrightarrow{u}, \overrightarrow{\phi}) = l_M[T](\overrightarrow{\phi}) , \ \forall\, \overrightarrow{\phi} \in \mathbb{U} . \qquad (3.18)$$

Since the mechanical problem includes as parameter the temperature, which is the solution of the thermal model, a one way coupling between both models is considered.

Under the assumptions $(MH3)$ and $(MH4)$, Lemma 2.2 of [49] shows that $a_M(\overrightarrow{u}, \overrightarrow{\phi})$ is continuous in $\mathbb{V} \times \mathbb{V}$. Similarly, under assumptions $(MH1)$ and $(MH2)$, and assuming that $T \in H^1_r(\omega)$, Lemma 2.3 of [49] shows that $l_M[T](\overrightarrow{\phi})$ is continuous in $\mathbb{V}$ and it is bounded.

Besides, $a_M(\overrightarrow{\phi}, \overrightarrow{\phi})$ is a norm on $\mathbb{U}$ equivalent to the norm of $[H^1_r(\omega)]^2$ thanks to the hypothesis on the Young's modulus and the Poisson's ratio, and since the boundaries γ_s and γ_- have positive measure. Therefore, a_M is $\mathbb{U}$-coercive.

In other words, there exists a constant, $C_M > 0$, referred as continuity constant of $a_M(\cdot, \cdot)$, such that,

$$a_M(\overrightarrow{u}, \overrightarrow{\phi}) \leq C_M ||\overrightarrow{u}||_{\mathbb{U}} ||\overrightarrow{\phi}||_{\mathbb{U}} , \ \forall \overrightarrow{u}, \overrightarrow{\phi} \in \mathbb{U} , \qquad (3.19)$$

and there exists a constant $c_M > 0$, referred as coercivity constant of $a_M(\cdot, \cdot)$, such that,

$$c_M \|\overrightarrow{\phi}\|_{\mathbb{U}}^2 \leq a_M(\overrightarrow{\phi}, \overrightarrow{\phi}) \ , \ \forall \overrightarrow{\phi} \in \mathbb{U} \ .$$

It can be observed that,

$$a_M(\overrightarrow{\phi}, \overrightarrow{\phi}) \geq \lambda_{min} \int_\omega \boldsymbol{\varepsilon}(\overrightarrow{\phi}) : \boldsymbol{\varepsilon}(\overrightarrow{\phi}) r dr dy \ , \tag{3.20}$$

where, $\lambda_{min} > 0$ is the minimum eigenvalue of $\boldsymbol{A}$.

Hence, the conditions of the Lax-Milgram theorem [23] are satisfied and accordingly, the weak mechanical formulation $(WM2)$ has unique solution $\overrightarrow{u} \in \mathbb{U}$. Given the equivalence between $(WM1)$ and $(WM2)$ formulations, $\overrightarrow{u}$ is the unique solution of weak mechanical formulation $(WM1)$.

Notice that here we could use the principle of superposition: the net displacement at any point in the domain $\overrightarrow{u}$ is the sum of the displacement due to purely mechanical effects $\overrightarrow{u}_M \in \mathbb{U}$ and the displacement due to purely thermal effects $\overrightarrow{u}_T \in \mathbb{U}$:

$$\overrightarrow{u} = \overrightarrow{u}_M + \overrightarrow{u}_T \ . \tag{3.21}$$

Therefore, the problem $(WM2)$ could be split in two sub-problems:

Problem 5 *Problem $(WM2M)$: Under the assumptions (MH1)-(MH4), find $\overrightarrow{u}_M \in \mathbb{U}$ such that:*

$$a_M(\overrightarrow{u}_M, \overrightarrow{\phi}) = l_M[T_0](\overrightarrow{\phi}) \ , \ \forall \overrightarrow{\phi} \in \mathbb{U} \ . \tag{3.22}$$

Problem 6 *Problem $(WM2T)$: Let $T \in H_r^1(\omega)$ be the solution of the weak thermal model (WT). Under the assumptions (MH1)-(MH4), find $\overrightarrow{u}_T \in \mathbb{U}$ such that:*

$$a_M(\overrightarrow{u}_T, \overrightarrow{\phi}) = l_M[T](\overrightarrow{\phi}) - l_M[T_0](\overrightarrow{\phi}) \ , \ \forall \overrightarrow{\phi} \in \mathbb{U} \ . \tag{3.23}$$

3.3   Variational principle

It is known from physics that when a body is at equilibrium, the potential energy of the system is stationary and is minimum. Under this condition the body is said to be stable. This gives an alternate interpretation to the weak mechanical formulation. This interpretation introduces the concept of variational principle or energy functional.

The elastic strain energy of model $(WM2)$ is given by:

$$\frac{1}{2} a_M(\overrightarrow{u}, \overrightarrow{u}) = \frac{1}{2} \int_\omega \boldsymbol{A}\{\boldsymbol{\varepsilon}(\overrightarrow{u})\} \cdot \{\boldsymbol{\varepsilon}(\overrightarrow{u})\} r dr dy \ .$$

The work done on the system by external forces, which is stored in the system as potential energy due to external forces, is given by:

$$l_M[T](\overrightarrow{u}) = \int_\omega (2\mu + 3\lambda)\alpha(T - T_0)\{\boldsymbol{I}\} \cdot \{\boldsymbol{\varepsilon}(\overrightarrow{u})\}rdrdy + \int_\omega (u_r f_{0,r} + u_y f_{0,y})\,rdrdy +$$

$$\int_{\gamma_{sf}} \overrightarrow{u} \cdot \overrightarrow{g}_{sf} rd\gamma + \int_{\gamma_{out}} \overrightarrow{u} \cdot \overrightarrow{g}_{out} rd\gamma + \int_{\gamma_-} \overrightarrow{u} \cdot \overrightarrow{g}_- rd\gamma + \int_{\gamma_+} \overrightarrow{u} \cdot \overrightarrow{g}_+ rd\gamma \; .$$

It is to be noted that the work done due to the external forces also includes the work done on the system due to stress induced by thermal effects.

The total energy of the system is the sum of elastic strain energy of the system and potential energy due to external forces:

$$\mathcal{J}_M[T](\overrightarrow{u}) = \frac{1}{2}a_M(\overrightarrow{u}, \overrightarrow{u}) - l_M[T](\overrightarrow{u}) \; . \tag{3.24}$$

It can be verified that the solution $\overrightarrow{u}$ of equation (3.15) is the displacement field corresponding to which the energy of the system is minimum:

$$a_M(\overrightarrow{u}, \overrightarrow{\phi}) = l_M[T](\overrightarrow{\phi}) \; , \; \forall \overrightarrow{\phi} \in \mathbb{U} \implies \mathcal{J}_M[T](\overrightarrow{\phi}) \geq \mathcal{J}_M[T](\overrightarrow{u}) \; , \; \forall \overrightarrow{\phi} \in \mathbb{U} \; . \tag{3.25}$$

This interpretation that the displacement field, which satisfies the weak formulation, minimizes the energy functional defined over the space of admissible displacements is known as variational principle.

Since the space $\mathbb{V}$ is complete, the space of admissible displacements $\mathbb{U}$ is a closed convex subset of $\mathbb{V}$, and the bilinear form $a_M(\cdot, \cdot)$ is symmetric and coercive on $\mathbb{U} \times \mathbb{U}$, by theorem 1.1.1 of [28], the minimizer $\overrightarrow{u}$ of energy functional $\mathcal{J}_M$ exists and is unique.

Analogously, the solution of equation (3.7) can also be viewed as minimizer of functional $\mathcal{J}_T$ defined as:

$$\mathcal{J}_T(T) = \frac{1}{2}\left(\int_\omega rk\left(\left(\frac{\partial T}{\partial y}\right)^2 + \left(\frac{\partial T}{\partial r}\right)^2\right)drdy\right)$$

$$+ \frac{1}{2}\left(\int_{\gamma_{sf}} T^2 h_{c,f} rd\gamma + \int_{\gamma_{out}} T^2 h_{c,out} rdy + \int_{\gamma_-} T^2 h_{c,-} rdr\right) - \int_\omega \psi Q rdrdy$$

$$- \left(\int_{\gamma_{sf}} T h_{c,f} T_f rd\gamma + \int_{\gamma_{out}} T h_{c,out} T_{out} rdy + \int_{\gamma_-} T h_{c,-} T_- rdr - \int_{\gamma_+} \psi q^+ rdr\right) \; . \tag{3.26}$$

In other words, the solution T of the weak form defined by the equation (3.7) is the stationary point of variational principle defined by the equation (3.26):

$$a_T(T, \psi) = l_T(\psi) \; , \; \forall \psi \in H_r^1(\omega) \implies J_T(\psi) \geq J_T(T) \; , \; \forall \psi \in H_r^1(\omega) \; . \tag{3.27}$$

Since the space $H_r^1(\omega)$ is complete and convex, and the bilinear form $a_T(T, \psi)$ is symmetric and coercive on $H_r^1(\omega) \times H_r^1(\omega)$, there exists a unique minimizer of the functional $\mathcal{J}_T$ (see theorem 1.1.1 of [28]). As it can be noticed, the solution of weak formulation can be viewed as minimizer of a functional. Alternatively, finding solution of weak formulation is equivalent to minimizing the energy functional.

In the subsequent chapters, we will continue to work with the weak formulation introduced in the section 3.2. In chapter 4, we restrict the weak formulation to an adequate finite dimensional space and introduce finite element formulation.

Chapter 4

Finite element discretization of axisymmetric thermomechanical model

We now look at the weak forms $(WT2)$ and $(WM2), (WM2M), (WM2T)$ introduced in Chapter 3 to approach them in adequate finite dimensional subspaces in order to make suitable formulations for their numerical analysis and simulation. Since the final objective is to make the finite element resolution of both thermal and thermomechanical models in real time using model order reduction methods, we will make a discretization of the models taking full advantage of the type of geometry that defines the domain. Firstly, in Section 4.1, we introduce domain discretization and some discrete function spaces are defined in Section 4.2. Next, Section 4.3 is devoted to introduce and solve the finite element formulations, derived by restricting weak formulations to the considered finite dimensional subspaces, for both thermal and thermomechanical models, respectively. Finally, we also analyze whether the discrete solutions are good approximations of the corresponding weak solutions of corresponding discrete problems by performing some error analysis in Sections 4.4 and 4.5. Throughout the chapter, the assumptions $(TH1) - (TH4)$ and $(MH1) - (MH4)$ introduced in Chapter 3 are considered to be valid.

4.1   Reference domain discretization

In numerical analysis, the continuous problem is discretized using a finite number of degrees of freedom. To facilitate the introduction of model order reduction later, we take advantage of the characteristics of the computational domain, and before proceeding to its meshing,

we consider a decomposition of the domain ω into n_{su} triangular subdomains as:

$$\omega = \bigcup_{i=1}^{n_{su}} \omega_i \ , \ \ \omega_i \cap \omega_j = \emptyset \text{ for } i \neq j \ , \ \ 1 \leq i,j \leq n_{su} \ .$$

Each subdomain ω_i is further divided into $\mathcal{N}_{el,i}$ smaller triangular elements τ_k. The total number of triangular elements in ω is $\mathcal{N}_{el}$. Grid $\mathcal{T}$ is the set of all triangular elements of ω:

$$\omega = \bigcup_{k=1}^{\mathcal{N}_{el}} \tau_k \ , \ \ \mathcal{N}_{el} = \sum_{i=1}^{n_{su}} \mathcal{N}_{el,i} \ , \ \ \mathcal{T} = \{\tau_k\}_{k=1}^{\mathcal{N}_{el}} \ .$$

The edges of triangular element τ_k are denoted as $\partial \tau_k$. The end points of an edge are called vertices. The vertices serve as nodes in the case of "Lagrange" basis functions of degree 1. However, additional nodes are also required for higher degree basis functions. The unit normal vector pointing outwards to $\partial \tau_k$ is denoted as $\overrightarrow{n}_k$. The size of τ_k is denoted as h_k.

4.2   Function space in finite dimension

In the course of finite dimensional analysis, we seek the solutions $T_h \in H^1_{r,h}(\omega)$ and $\overrightarrow{u}_h \in \mathbb{U}_h$ of the discretized models corresponding to $(WT2)$ and $(WM2)$, respectively. It is to be noted that $T_h \in H^1_{r,h}(\omega)$ and $\overrightarrow{u}_h \in \mathbb{U}_h$ are the approximation of $T \in H^1_r(\omega)$ and $\overrightarrow{u} \in \mathbb{U}$ respectively. In further sections, we are going to describe the Lagrange finite element method used to approximate the solutions to problems $(WT2), (WM2), (WM2M)$ and $(WM2T)$.

We introduce the n_h- dimensional space $H^1_{r,h}(\omega) \subset H^1_r(\omega)$ and m_h- dimensional space $\mathbb{U}_h \subset \mathbb{U}$:

$$H^1_{r,h}(\omega) = \text{span}\{\psi_{1,h}, \psi_{2,h}, \ldots, \psi_{n_h,h}\} \ , \tag{4.1}$$

$$\mathbb{U}_h = \text{span}\{\overrightarrow{\phi}_{1,h}, \overrightarrow{\phi}_{2,h}, \ldots, \overrightarrow{\phi}_{m_h,h}\} \ . \tag{4.2}$$

Based on the Galerkin method of weighted residuals [106], we can express the approximated solutions T_h and $\overrightarrow{u}_h$ as,

$$T_h = \sum_{i=1}^{n_h} T_h^i \psi_{i,h} \ , \tag{4.3}$$

$$\overrightarrow{u}_h = \sum_{i=1}^{m_h} u_h^i \overrightarrow{\phi}_{i,h} \ , \tag{4.4}$$

where T_h^i and u_h^i are the nodal temperature and nodal displacement, respectively, and the basis functions $\psi_{i,h}$ and $\overrightarrow{\phi}_{i,h}$ are piecewise polynomial of degree $p \geq 1$ in (r, y) space.

The nodal values $\{T_h^i\}_{i=1}^{n_h}$ and $\{u_h^i\}_{i=1}^{m_h}$ are common only to elements which are sharing the same node. Hence, the computational stencil of the system matrices does not extend beyond immediate neighboring elements and accordingly the system matrices are sparse matrices.

4.3 Finite element formulation

4.3.1 Thermal model

In the finite element analysis, the bilinear form defined in (3.8), $a_T(T, \psi) : H_r^1(\omega) \times H_r^1(\omega) \to \mathbb{R}$ is restricted to the finite dimensional subspace as $a_{T,h}(T_h, \psi_h) : H_{r,h}^1(\omega) \times H_{r,h}^1(\omega) \to \mathbb{R}$ and it is defined in the similar way:

$$
\begin{aligned}
a_{T,h}(T_h, \psi_h) = \int_\omega rk \left(\frac{\partial T_h}{\partial y} \frac{\partial \psi_h}{\partial y} + \frac{\partial T_h}{\partial r} \frac{\partial \psi_h}{\partial r} \right) dr dy + \int_{\gamma_{sf}} \psi_h h_{c,f} T_h r d\gamma \\
+ \int_{\gamma_{out}} \psi_h h_{c,out} T_h r d\gamma + \int_{\gamma_-} \psi_h h_{c,-} T_h r d\gamma \ .
\end{aligned}
\tag{4.5}
$$

Analogously, the linear form introduced in (3.9), $l_T(\psi) : H_r^1(\omega) \to \mathbb{R}$ is restricted to the finite dimensional space as $l_{T,h}(\psi_h) : H_{r,h}^1(\omega) \to \mathbb{R}$, as:

$$
\begin{aligned}
l_{T,h}(\psi_h) = \int_\omega \psi_h Q r dr dy + \int_{\gamma_{sf}} \psi_h h_{c,f} T_f r d\gamma + \int_{\gamma_{out}} \psi_h h_{c,out} T_{out} r d\gamma + \\
\int_{\gamma_-} \psi_h h_{c,-} T_- \ r d\gamma - \int_{\gamma_+} \psi_h q^+ r d\gamma \ .
\end{aligned}
\tag{4.6}
$$

Therefore, the approximation of the problem $(WT2)$ in the finite dimensional space can be stated as,

Problem 7 *Problem $(WT2)_h$: Under the assumptions $(TH1) - (TH4)$, find $T_h \in H_{r,h}^1(\omega)$ such that:*

$$
a_{T,h}(T_h, \psi_h) = l_{T,h}(\psi_h) \ , \ \forall \psi_h \in H_{r,h}^1(\omega) \ .
\tag{4.7}
$$

The coercivity and continuity of $a_{T,h}(T_h, \psi_h)$ follows same explanation as coercivity and continuity of $a_T(T, \psi)$. There exist a coercivity constant $c_{T,h} > 0$ and a continuity constant $C_{T,h} > 0$ such that:

$$
c_{T,h} ||\psi_h||_{H_{r,h}^1(\omega)}^2 \leq a_{T,h}(\psi_h, \psi_h) \ , \ \forall \psi_h \in H_{r,h}^1(\omega) \ ,
\tag{4.8}
$$

$$
|a_{T,h}(T_h, \psi_h)| \leq C_{T,h} ||T_h||_{H_{r,h}^1(\omega)} ||\psi_h||_{H_{r,h}^1(\omega)} \ , \ \forall \psi_h, T_h \in H_{r,h}^1(\omega) \ .
\tag{4.9}
$$

We recall that, c_T and C_T are respectively coercivity and continuity constants for $a_T(\cdot, \cdot)$. Since $H_{r,h}^1 \subset H_r^1$, it can be deduced that:

$$c_{T,h} \geq c_T \ , \ \ C_{T,h} \leq C_T \ .$$

Similarly, it can be shown that the linear form $l_{T,h}(T_h, \psi_h)$ is linear and continuous following the same explanation as given for boundedness of $l_T(T, \psi)$. Hence the problem $(WT2)_h$ is well-posed.

4.3.2 Thermomechanical model

In the finite element analysis, the bilinear form $a_M(\overrightarrow{u}, \overrightarrow{\phi}) : \mathbb{U} \times \mathbb{U} \to \mathbb{R}$, defined in (3.15), is restricted to a finite dimensional subspace, $\mathbb{U}_h \times \mathbb{U}_h$, as $a_{M,h}(\overrightarrow{u}_h, \overrightarrow{\phi}_h) : \mathbb{U}_h \times \mathbb{U}_h \to \mathbb{R}$ defined by,

$$a_{M,h}(\overrightarrow{u}_h, \overrightarrow{\phi}_h) = \int_\omega \boldsymbol{A}\{\boldsymbol{\varepsilon}(\overrightarrow{u}_h)\} \cdot \{\boldsymbol{\varepsilon}(\overrightarrow{\phi}_h)\} r dr dy \ , \tag{4.10}$$

and the linear form $l_M[T](\overrightarrow{\phi}) : \mathbb{U} \to \mathbb{R}$ is restricted to the finite dimensional space as $l_{M,h}[T_h](\overrightarrow{\phi}_h) : \mathbb{U}_h \to \mathbb{R}$, being $\overrightarrow{\phi}_h = [\phi_{r,h} \ \phi_{y,h}]$,

$$l_{M,h}[T_h](\overrightarrow{\phi}_h) = \int_\omega (2\mu + 3\lambda)\alpha(T_h - T_0)\{\boldsymbol{I}\} \cdot \{\boldsymbol{\varepsilon}(\overrightarrow{\phi}_h)\} r dr dy +$$

$$\int_\omega (\phi_{r,h} f_{0,r} + \phi_{y,h} f_{0,y}) \, r dr dy + \int_{\gamma_{sf}} \overrightarrow{\phi}_h \cdot \overrightarrow{g}_{sf} r d\gamma + \tag{4.11}$$

$$\int_{\gamma_{out}} \overrightarrow{\phi}_h \cdot \overrightarrow{g}_{out} r d\gamma + \int_{\gamma_-} \overrightarrow{\phi}_h \cdot \overrightarrow{g}_- r d\gamma + \int_{\gamma_+} \overrightarrow{\phi}_h \cdot \overrightarrow{g}_+ r d\gamma \ .$$

To approach the solution of weak problem $(WM2)$ in the finite dimensional space $\mathbb{U}_h$, the discretized problem can be stated as:

Problem 8 *Problem $(WM2)_h$: Let $T_h \in H_{r,h}^1(\omega)$, be the solution of the discretized thermal model $(WT2)_h$. Under the assumptions $(MH1) - (MH4)$, find $\overrightarrow{u}_h \in \mathbb{U}_h$ such that:*

$$a_{M,h}(\overrightarrow{u}_h, \overrightarrow{\phi}_h) = l_{M,h}[T_h](\overrightarrow{\phi}_h) \ , \ \forall \overrightarrow{\phi}_h \in \mathbb{U}_h \ . \tag{4.12}$$

By superposition principle, from equation (3.21), it can be deduced that the solution $\overrightarrow{u}_h \in \mathbb{U}_h$ is the sum of $\overrightarrow{u}_{M,h} \in \mathbb{U}_h$ and $\overrightarrow{u}_{T,h} \in \mathbb{U}_h$ defined as the solutions of the following problems:

Problem 9 *Problem $(WM2M)_h$: Under the assumptions $(MH1) - (MH4)$, find $\overrightarrow{u}_{M,h} \in \mathbb{U}_h$ such that:*

$$a_{M,h}(\overrightarrow{u}_{M,h}, \overrightarrow{\phi}_h) = l_{M,h}[T_0](\overrightarrow{\phi}_h) \ , \ \forall \overrightarrow{\phi}_h \in \mathbb{U}_h \ . \tag{4.13}$$

Problem 10 *Problem $(WM2T)_h$: Let $T_h \in H^1_{r,h}(\omega)$, be the solution of the discretized thermal model $(WT2)_h$. Under the assumptions $(MH1) - (MH4)$, find find $\overrightarrow{u}_{T,h} \in \mathbb{U}_h$ such that:*

$$a_{M,h}(\overrightarrow{u}_{T,h}, \overrightarrow{\phi}_h) = l_{M,h}[T_h](\overrightarrow{\phi}_h) - l_{M,h}[T_0](\overrightarrow{\phi}_h) \ , \ \forall \overrightarrow{\phi}_h \in \mathbb{U}_h \ . \tag{4.14}$$

From both,

$$\overrightarrow{u}_h = \overrightarrow{u}_{M,h} + \overrightarrow{u}_{T,h} \ . \tag{4.15}$$

The coercivity and continuity of $a_{M,h}(\overrightarrow{u}_h, \overrightarrow{\phi}_h)$ follows same explanation as coercivity and continuity of $a_M(\overrightarrow{u}, \overrightarrow{\phi})$. There exist a coercivity constant $c_{M,h} > 0$ and a continuity constant $C_{M,h} > 0$ of $a_{M,h}(\cdot, \cdot)$ such that:

$$c_{M,h}\|\overrightarrow{\phi}_h\|^2_{\mathbb{U}_h} \leq a_{M,h}(\overrightarrow{\phi}_h, \overrightarrow{\phi}_h) \ , \ \forall \overrightarrow{\phi}_h \in \mathbb{U}_h \ , \tag{4.16}$$

$$|a_{M,h}(\overrightarrow{u}_h, \overrightarrow{\phi}_h)| \leq C_{M,h}\|\overrightarrow{u}_h\|_{\mathbb{U}_h}\|\overrightarrow{\phi}_h\|_{\mathbb{U}_h} \ , \ \forall \overrightarrow{u}_h, \overrightarrow{\phi}_h \in \mathbb{U}_h \ . \tag{4.17}$$

We recall that, c_M and C_M are respectively coercivity and continuity constants of $a_M(\cdot, \cdot)$. Since $\mathbb{U}_h \subset \mathbb{U}$, it can be deduced that:

$$c_{M,h} \geq c_M \ , \ C_{M,h} \leq C_M \ .$$

Similarly, it can be proved that the linear form $l_{M,h}[T_h](\overrightarrow{\phi}_h)$ is continuous in $\mathbb{U}_h$ following same explanation as given for the boundedness of $l_M[T](\overrightarrow{\phi})$. Hence the problem $(WM2)_h$ is well-posed.

We use the Cholesky decomposition [75] for thermal model $(WT2)_h$ as well as momentum equation thermomechanical model $(WM2)_h$.

4.4 Error analysis of thermal model

4.4.1 a_T-orthogonality of error

From equations (3.10), (4.7) and considering that $H^1_{r,h}(\omega)$ is a subspace of $H^1_r(\omega)$, the solutions $T \in H^1_r(\omega)$ and $T_h \in H^1_{r,h}(\omega)$ of problems $(WT2)$ and $(WT2)_h$, respectively, verify,

$$a_T(T, \psi) = l_T(\psi) \ , \ T \in H^1_r(\omega), \ \forall \ \psi \in H^1_r(\omega) \ ,$$

$$a_{T,h}(T_h, \psi_h) = l_{T,h}(\psi_h) \ , \ T_h \in H^1_{r,h}(\omega) \ , \ \forall \ \psi_h \in H^1_{r,h}(\omega) \ ,$$

therefore the following relation is deduced,

$$a_T(T - T_h, \psi_h) = 0 \ , \ T_h \in H^1_{r,h}(\omega) \ , \ T \in H^1_r(\omega) \ , \ \forall \psi_h \in H^1_{r,h}(\omega) \ . \tag{4.18}$$

This implies the a_T-orthogonality of the error function $T - T_h$.

4.4.2   Error in energy norm and application of Cea's lemma

Since the bilinear form $a_T(T, \psi)$ is continuous and coercive, it can be used as norm in $H^1_r(\omega)$ associated to the inner product defined by a_T. By Cauchy-Schwarz inequality and a_T−orthogonality of the error function:

$$a_T(T - T_h, T - T_h) = a_T(T - T_h, T - \psi_h)$$
$$\leq \sqrt{a_T(T - T_h, T - T_h)}\sqrt{a_T(T - \psi_h, T - \psi_h)} \ , \ \forall \psi_h \in H^1_{r,h}(\omega) \ . \tag{4.19}$$

The Cea's lemma in energy norm becomes:

$$a_T(T - T_h, T - T_h) \leq a_T(T - \psi_h, T - \psi_h) \ , \ \forall \psi_h \in H^1_{r,h}(\omega) \ . \tag{4.20}$$

This implies that T_h is the orthogonal projection of T with respect to the inner product induced by $a_T(\cdot, \cdot)$. In other words, $T_h \in H^1_{r,h}(\omega)$ is the best approximation of $T \in H^1_r(\omega)$ with respect to the energy norm.

Additionally, by coercivity and continuity of $a_T(\cdot, \cdot)$, and taking into account again (4.20), for all $\psi_h \in H^1_{r,h}(\omega)$ we obtain:

$$c_T||T - T_h||^2_{H^1_r(\omega)} \leq a_T(T - T_h, T - T_h)$$
$$\leq a_T(T - \psi_h, T - \psi_h) \leq C_T||T - \psi_h||^2_{H^1_r(\omega)} \ ,$$
$$\implies ||T - T_h||_{H^1_r(\omega)} \leq \sqrt{\frac{C_T}{c_T}}||T - \psi_h||_{H^1_r(\omega)} \ . \tag{4.21}$$

4.4.3   Error in $H^1_r(\omega)$ norm

We introduce now $\tilde{T}_h \in H^1_{r,h}(\omega)$ as the orthonormal projection of $T \in H^1_r(\omega)$ with respect to the inner product $< \cdot, \cdot >_{H^1_r(\omega)}$. It verifies:

$$||T - \tilde{T}_h||_{H^1_r(\omega)} \leq ||T - \psi_h||_{H^1_r(\omega)} \ , \ \forall \psi_h \in H^1_{r,h}(\omega) \ . \tag{4.22}$$

Additionally, we recall that $T_h \in H^1_{r,h}(\omega)$ is the orthogonal projection of T with respect to the inner product induced by $a_T(\cdot, \cdot)$:

$$||T - T_h||^2_{H^1_r(\omega)} = ||T - \tilde{T}_h||^2_{H^1_r(\omega)} + ||\tilde{T}_h - T_h||^2_{H^1_{r,h}(\omega)} \geq ||T - \tilde{T}_h||^2_{H^1_r(\omega)} \ . \tag{4.23}$$

By using the a_T orthogonality of the error function (see (4.18)):

$$a_T(T - \tilde{T}_h, T - \tilde{T}_h) = a_T(T - T_h, T - T_h) + a_{T,h}(T_h - \tilde{T}_h, T_h - \tilde{T}_h)$$
$$\geq a_T(T - T_h, T - T_h) \ . \tag{4.24}$$

By continuity and coercivity of $a_T(\cdot, \cdot)$ and $a_{T,h}(\cdot, \cdot)$ and above relations (4.22)-(4.24) (see [36]):

$$\frac{C_T}{c_{T,h}} ||T - \tilde{T}_h||^2_{H^1_r(\omega)} \geq \frac{1}{c_{T,h}} a_T(T - \tilde{T}_h, T - \tilde{T}_h)$$

$$= \frac{1}{c_{T,h}} \left(a_T(T - T_h, T - T_h) + a_{T,h}(\tilde{T}_h - T_h, \tilde{T}_h - T_h) \right)$$

$$\geq \frac{c_T}{c_{T,h}} ||T - T_h||^2_{H^1_r(\omega)} + ||\tilde{T}_h - T_h||^2_{H^1_{r,h}(\omega)}$$

$$= \frac{c_T}{c_{T,h}} ||T - T_h||^2_{H^1_r(\omega)} + ||T - T_h||^2_{H^1_r(\omega)} - ||T - \tilde{T}_h||^2_{H^1_r(\omega)}$$

$$\geq \frac{c_T}{c_{T,h}} ||T - \tilde{T}_h||^2_{H^1_r(\omega)} + ||T - T_h||^2_{H^1_r(\omega)} - ||T - \tilde{T}_h||^2_{H^1_r(\omega)}$$

$$= ||T - T_h||^2_{H^1_r(\omega)} + \left(\frac{c_T - c_{T,h}}{c_{T,h}} \right) ||T - \tilde{T}_h||^2_{H^1_r(\omega)} .$$

Hence, it can be estimated that,

$$
\begin{aligned}
||T - T_h||_{H^1_r(\omega)} &\leq \sqrt{\frac{C_T + c_{T,h} - c_T}{c_{T,h}}} ||T - \tilde{T}_h||_{H^1_r(\omega)} , \\
&\leq \sqrt{\frac{C_T + c_{T,h} - c_T}{c_{T,h}}} ||T - \psi_h||_{H^1_r(\omega)} , \quad \forall \psi_h \in H^1_{r,h}(\omega) .
\end{aligned}
\tag{4.25}
$$

Since, $c_{T,h} \geq c_T$, the error estimate provided by equation (4.25) is an improved estimate as compared to the error estimate provided by equation (4.21).

4.5 Error analysis of thermomechanical model

4.5.1 a_M-orthogonality of error

Similar to the proof of a_T-orthogonality of error for thermal model, it can be proven that:

$$a_M(\overrightarrow{u} - \overrightarrow{u}_h, \overrightarrow{\phi}_h) - \int_\omega (2\mu + 3\lambda)\alpha(T - T_h)\boldsymbol{I} : \varepsilon(\overrightarrow{\phi}_h) = 0 , \ \forall \ \overrightarrow{\phi}_h \in \mathbb{U}_h . \tag{4.26}$$

This implies that the error in the energy norm for mechanical equation is not a_M-orthogonal except in case $T = T_h$.

Taking into account the decomposition of the weak models $(WM2)$ and $(WM2)_h$ into $(WM2M), (WM2T), (WM2M)_h, (WM2T)_h$, it can be verified that,

$$a_M(\overrightarrow{u}_M - \overrightarrow{u}_{M,h}, \overrightarrow{\phi}_h) = 0 , \ \forall \overrightarrow{\phi}_h \in \mathbb{U}_h , \tag{4.27}$$

and

$$a_M(\overrightarrow{u}_T - \overrightarrow{u}_{T,h}, \overrightarrow{\phi}_h) - \int_\omega (2\mu + 3\lambda)\alpha(T - T_h)\boldsymbol{I} : \varepsilon(\overrightarrow{\phi}_h) = 0 , \ \forall \ \overrightarrow{\phi}_h \in \mathbb{U}_h . \tag{4.28}$$

4.5.2 Error in energy norm and application of Cea's lemma

From (4.26), it can be observed that for all $\overrightarrow{\phi}_h \in \mathbb{U}_h$:

$$
\begin{aligned}
a_M(\overrightarrow{u} - \overrightarrow{u}_h, \overrightarrow{u} - \overrightarrow{u}_h) &= a_M(\overrightarrow{u} - \overrightarrow{u}_h, \overrightarrow{u} - \overrightarrow{\phi}_h) + a_M(\overrightarrow{u} - \overrightarrow{u}_h, \overrightarrow{\phi}_h - \overrightarrow{u}_h) \\
&= a_M(\overrightarrow{u} - \overrightarrow{u}_h, \overrightarrow{u} - \overrightarrow{\phi}_h) + \int_\omega (2\mu + 3\lambda)\alpha(T - T_h)\boldsymbol{I} : \varepsilon(\overrightarrow{\phi}_h - \overrightarrow{u}_h) \ .
\end{aligned}
\tag{4.29}
$$

Thanks to the $\mathbb{U}-$coercivity of a_M and its continuity, a_M defines an equivalent norm in $\mathbb{U}$ to the $H_r^1(\omega)$ norm. For simplicity of notations, we use $a_M(\overrightarrow{\phi}, \overrightarrow{\phi}) = ||\overrightarrow{\phi}||_{a_M}^2$.

By Cauchy-Schwarz inequality, from equation (4.29) we obtain:

$$
\begin{aligned}
||\overrightarrow{u} - \overrightarrow{u}_h||_{a_M}^2 &\leq ||\overrightarrow{u} - \overrightarrow{u}_h||_{a_M}||\overrightarrow{u} - \overrightarrow{\phi}_h||_{a_M} \\
&+ (2\mu + 3\lambda)\alpha||T - T_h||_{L_r^2(\omega)}||Div(\overrightarrow{\phi}_h - \overrightarrow{u}_h)||_{L_r^2(\omega)} \ .
\end{aligned}
\tag{4.30}
$$

By coercivity and continuity of $a_M(\cdot, \cdot)$, $\exists c_M, C_M > 0$:

$$
\begin{aligned}
c_M||\overrightarrow{u} - \overrightarrow{u}_h||_{\mathbb{U}}^2 &\leq C_M||\overrightarrow{u} - \overrightarrow{u}_h||_{\mathbb{U}}||\overrightarrow{u} - \overrightarrow{\phi}_h||_{\mathbb{U}} \\
&+ (2\mu + 3\lambda)\alpha||T - T_h||_{L_r^2(\omega)}||Div(\overrightarrow{\phi}_h - \overrightarrow{u}_h)||_{L_r^2(\omega)} \ , \ \forall \ \overrightarrow{\phi}_h \in \mathbb{U}_h \ .
\end{aligned}
\tag{4.31}
$$

4.5.3 Error in $\mathbb{U}$ norm

Following the same procedure as followed for deriving equation (4.25), it can be verified that:

$$
||\overrightarrow{u}_M - \overrightarrow{u}_{M,h}||_{\mathbb{U}} \leq \sqrt{\frac{C_M + c_{M,h} - c_M}{c_{M,h}}}||\overrightarrow{u}_M - \overrightarrow{\phi}_h||_{\mathbb{U}} \ , \ \forall \overrightarrow{\phi}_h \in \mathbb{U}_h \ .
\tag{4.32}
$$

However, due to lack of a_M-orthogonality, we use error estimate from equation (4.31) for error $\overrightarrow{u}_T - \overrightarrow{u}_{T,h}$.

$$
\begin{aligned}
||\overrightarrow{u}_T - \overrightarrow{u}_{T,h}||_{\mathbb{U}} \leq \Bigg(&\frac{C_M}{c_M}||\overrightarrow{u}_T - \overrightarrow{u}_{T,h}||_{\mathbb{U}}||\overrightarrow{u}_T - \overrightarrow{\phi}_h||_{\mathbb{U}} \\
&+ \frac{(2\mu + 3\lambda)\alpha}{c_M}||T - T_h||_{L_r^2(\omega)}||Div(\overrightarrow{\phi}_h - \overrightarrow{u}_{T,h})||_{L_r^2(\omega)} \Bigg)^{\frac{1}{2}} \ , \ \forall \ \overrightarrow{\phi}_h \in \mathbb{U}_h \ .
\end{aligned}
\tag{4.33}
$$

Now we recall that $\overrightarrow{u}_h = \overrightarrow{u}_{T,h} + \overrightarrow{u}_{M,h}$ and provide the error estimate:

$$
\begin{aligned}
||\overrightarrow{u} - \overrightarrow{u}_h||_{\mathbb{U}} \leq &\sqrt{\frac{C_M + c_{M,h} - c_M}{c_{M,h}}}||\overrightarrow{u}_M - \overrightarrow{\phi}_h||_{\mathbb{U}} \\
&+ \left(\frac{C_M}{c_M}||\overrightarrow{u}_T - \overrightarrow{u}_{T,h}||_{\mathbb{U}}||\overrightarrow{u}_T - \overrightarrow{\phi}_h||_{\mathbb{U}} \right. \\
&+ \frac{(2\mu + 3\lambda)\alpha}{c_M}||T - T_h||_{L^2_r(\omega)}||Div(\overrightarrow{\phi}_h - \overrightarrow{u}_{T,h})||_{L^2_r(\omega)} \left. \right)^{\frac{1}{2}} , \ \forall \overrightarrow{\phi}_h \in \mathbb{U}_h .
\end{aligned}
$$

$$(4.34)$$

In this chapter, we introduced finite element formulation to approximate the solution field by solving system of equations. We now shift our focus to computational issues. In the next chapter, we describe the benchmark tests to verify the numerical implementation in open source software used in this work.

Chapter 5

Numerical examples

In this chapter we provide results for some benchmark tests to verify the numerical implementations of the axisymmetric models $(WT2)_h$ and $(WM2)_h$ introduced in Chapter 4. Given that a first objective is to apply a method of order reduction for the numerical resolution of the real problem, we focus first on the difficulty linked to the geometric shape of the vertical section. In section 5.1, we introduce the domain and its discretization under consideration. We then introduce the benchmark tests for thermal model and thermomechanical model (Section 5.2).

5.1 Computational domain and mesh

The coordinates of the 12 vertices constituting the domain illustrated in Figure 2.2 are reported in Table 5.1.

r	0	7.050	7.050	5.300	5.300	4.950	4.950	4.600	4.600	4.250	4.250	0
y	0	0	7.265	7.265	4.065	4.065	3.565	3.565	2.965	2.965	2.365	2.365

Table 5.1: coordinates (in m) of the vertices of domain ω (see Figure 2.2).

Since one of the main objectives of this work is to develop model order reduction approach able to work in a geometrical parametrization setting, before proceeding to the meshing, we consider a decomposition of the domain into n_{su} triangular subdomains as (see, e.g., [52, 82]):

$$\omega = \bigcup_{i=1}^{n_{su}} \omega_i \ , \ \omega_i \cap \omega_j = \emptyset \text{ for } i \neq j \ , \ 1 \leq i, j \leq n_{su} \ . \tag{5.1}$$

We set $n_{su} = 30$ (see Figure 5.1a). The considered mesh is compliant with the triangular subdomains and contains 121137 triangular elements and 61147 vertices (see Figure 5.1b).

(a) Domain decomposition   (b) Close up of the mesh   (c) Mesh quality
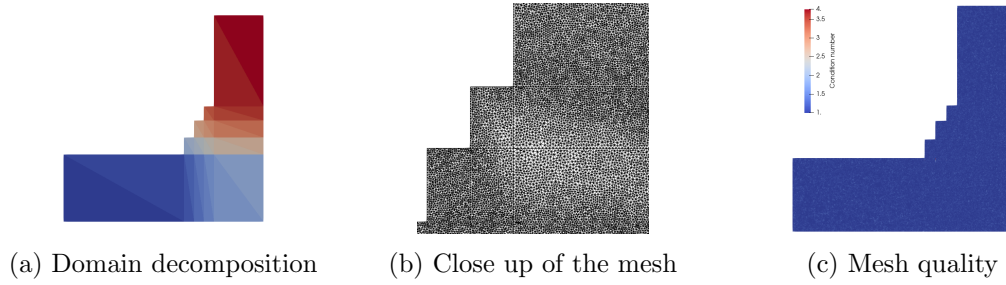
Figure 5.1: Discretization of the domain ω

The minimum and maximum mesh size, that is measured as the distance between vertices of an element of the mesh, are 0.011m and 0.045m respectively. The quality of each mesh element, q_e, could be estimated by using the following formula [101]:

$$q_e = \frac{4\sqrt{3}A}{l_1^2 + l_2^2 + l_3^2} \ ,$$

(5.2)

where A is the area of the element, and l_1, l_2 and l_3 are the lengths of its three edges. The minimum value of q_e was 0.25, that is sufficiently far from zero. The mesh condition number is also presented in Figure 5.1c. The decrease in condition number of an element increases its distance from the set of degenerate elements. The condition number of an element ranges from 1 to ∞, with 1 being a perfectly shaped element.

5.2   Benchmark tests

The pipeline that we follow for the design of reliable benchmark tests to be used for the FOM validation consists of three steps:

- We set analytical expressions for temperature and displacement.

- We calculate corresponding model data, including boundary conditions and source terms, in order to identify the FOM for which the analytical relationships are solutions.

- Finally, we numerically solve the problem and compare the computational solutions with the analytical ones.

We consider the physical properties reported in Table 5.2 for all numerical simulations shown in this section. We also introduce some definitions, which will be used in the subsequent sections:

Property	Value
Thermal conductivity k	$10\frac{W}{mK}$
Convection coefficient $h_{c,-}$	$2000\frac{W}{m^2K}$
Convection coefficient $h_{c,f}$	$200\frac{W}{m^2K}$
Convection coefficient $h_{c,out}$	$2000\frac{W}{m^2K}$
Young's modulus E	$5e9Pa$
Poisson's ratio ν	0.2
Thermal expansion coefficient α	$10^{-6}/K$
Reference temperature T_0	$298K$
Gravitational acceleration g	$9.81\frac{m}{s^2}$

Table 5.2: Physical properties values used for the FOM benchmark tests.

- Hydrostatic stress σ_m :

$$\sigma_m = \frac{1}{3}Tr(\boldsymbol{\sigma}) \ . \tag{5.3}$$

- Deviatoric part of the stress tensor $\boldsymbol{\sigma}_d$:

$$\boldsymbol{\sigma}_d = \boldsymbol{\sigma} - \frac{1}{3}Tr(\boldsymbol{\sigma})\boldsymbol{I} = \boldsymbol{\sigma} - \sigma_m\boldsymbol{I} \ . \tag{5.4}$$

- Von Mises effective stress σ_{vm}:

$$\sigma_{vm} = \sqrt{\frac{3}{2}\boldsymbol{\sigma}_d : \boldsymbol{\sigma}_d} \ . \tag{5.5}$$

5.2.1 Thermal model

We consider the following analytical expression for the temperature:

$$T_a(r, y) = C'r^2y, \quad \text{with } C' = 1K/m^3 \ . \tag{5.6}$$

Accordingly,

- the corresponding source term Q is obtained by using eq. (2.55),

$$Q(r, y) = -k\frac{\partial^2 T_a}{\partial r^2} - k\frac{\partial^2 T_a}{\partial y^2} - \frac{k}{r}\frac{\partial T_a}{\partial r} = -4C'ky \ , \tag{5.7}$$

- the heat flux q_+, as well as the temperatures T_f, T_{out} and T_-, are derived from eq. (2.56),

$$\text{on } \gamma_+ \ : \ q_+(r,y) = -k\frac{\partial T_a}{\partial y} = -C'kr^2 \ , \tag{5.8a}$$

$$\text{on } \gamma_{sf} \ : \ T_f = T_a + \frac{k}{h_{c,f}}\left(\frac{\partial T_a}{\partial r}n_r + \frac{\partial T_a}{\partial y}n_y\right)$$

$$= C'r^2 y + C'\frac{k}{h_{c,f}}(2ryn_r + r^2 n_y) \ , \tag{5.8b}$$

$$\text{on } \gamma_{out} \ : \ T_{out} = T_a + \frac{k}{h_{c,out}}\frac{\partial T_a}{\partial r} = C'r^2 y + C'\frac{2ryk}{h_{c,out}} \ , \tag{5.8c}$$

$$\text{on } \gamma_- \ : \ T_- = T_a - \frac{k}{h_{c,-}}\frac{\partial T_a}{\partial y} = C'r^2 y - C'\frac{r^2 k}{h_{c,-}} \ , \tag{5.8d}$$

and it is verified that

$$\text{on } \gamma_s \ : \ \frac{\partial T_a}{\partial r} = 0. \tag{5.9a}$$

We solve the $(WT)_h$ problem for the data $Q, q_+, T_f, T_{out}, T_-$ given by the equations (5.7)-(5.9a). We choose a discretized space of polynomial of degree 3. Analytical and numerical solutions are reported in Figure 5.2 (left and center). As we can see, a very good agreement is obtained. For a more quantitative comparison, we also display the absolute error in Figure 5.2 (right), and compute the relative error:

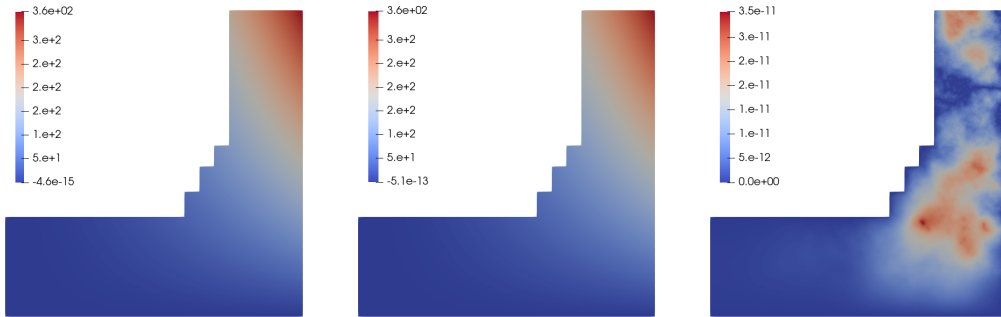$$\frac{||T_a - T_h||_{H^1_r(\omega)}}{||T_a||_{H^1_r(\omega)}} = 7e - 13.$$

Figure 5.2: Benchmark for the thermal model $(WT)_h$: analytical temperature T_a (left), numerical temperature T_h (center), and corresponding absolute error $|T_a - T_h|$ (right) in K.

5.2.2   Thermomechanical model

Firstly, we consider that the body is at reference temperature $T = T_0$, i.e. thermal stresses $(2\mu + 3\lambda)\alpha(T - T_0)$ are not present. Therefore, we refer to the problem $(WM2M)_h$. We consider a known displacement function:

$$\vec{u}_a = C(ry^2, r^2y), \quad \text{with } C = 1e - 4/m^2. \tag{5.10}$$

Accordingly,

- the components of the stress tensor $\boldsymbol{\sigma}$ are given by eqs. (2.58) as,

$$\sigma_{rr} = \frac{E}{(1 - 2\nu)(1 + \nu)}(Cy^2 + \nu Cr^2) \ , \tag{5.11a}$$

$$\sigma_{yy} = \frac{E}{(1 - 2\nu)(1 + \nu)}(2\nu Cy^2 + (1 - \nu)Cr^2) \ , \tag{5.11b}$$

$$\sigma_{\theta\theta} = \frac{E}{(1 - 2\nu)(1 + \nu)}(Cy^2 + \nu Cr^2) \ , \tag{5.11c}$$

$$\sigma_{ry} = \frac{2ECry}{(1 + \nu)} \ , \tag{5.11d}$$

- the source term $\vec{f}_0 = [f_{0,r} \ f_{0,y}]$ is obtained from eqs. (2.57) and (5.11) as,

$$f_{0,r} = -\left(\frac{\partial \sigma_{rr}}{\partial r} + \frac{\partial \sigma_{ry}}{\partial y} + \frac{\sigma_{rr} - \sigma_{\theta\theta}}{r}\right)$$
$$= -\left(\frac{2E\nu Cr}{(1 - 2\nu)(1 + \nu)} + \frac{2ECr}{(1 + \nu)}\right) \ , \tag{5.12a}$$

$$f_{0,y} = -\left(\frac{\partial \sigma_{ry}}{\partial r} + \frac{\partial \sigma_{yy}}{\partial y} + \frac{\sigma_{ry}}{r}\right)$$
$$= -\left(\frac{4ECy}{(1 + \nu)} + \frac{4E\nu Cy}{(1 - 2\nu)(1 + \nu)}\right) \ , \tag{5.12b}$$

- the boundary tractions are derived from eqs. (2.59) and (5.11) as,

$$\text{on } \gamma_+ \; : \; g_{+,r} = \frac{2ECry}{(1+\nu)} \; , \tag{5.13a}$$

$$g_{+,y} = \frac{E}{(1-2\nu)(1+\nu)} \left(2\nu Cy^2 + (1-\nu)Cr^2\right) \; , \tag{5.13b}$$

$$\text{on } \gamma_- \; : \; g_{-,r} = -\frac{2ECry}{(1+\nu)} \; , \tag{5.13c}$$

$$\text{on } \gamma_{sf} \; : \; g_{sf,r} = \frac{E}{(1-2\nu)(1+\nu)} \left(Cy^2 + \nu Cr^2\right) n_r + \frac{2ECry}{(1+\nu)} n_y \; , \tag{5.13d}$$

$$g_{sf,y} = \frac{2ECry}{(1+\nu)} n_r + \frac{E}{(1-2\nu)(1+\nu)} \left(2\nu Cy^2 + (1-\nu)Cr^2\right) n_y \; , \tag{5.13e}$$

$$\text{on } \gamma_{out} \; : \; g_{out,r} = \frac{E}{(1-2\nu)(1+\nu)} \left(Cy^2 + \nu Cr^2\right) \; , \tag{5.13f}$$

$$g_{out,y} = \frac{2ECry}{(1+\nu)} \; , \tag{5.13g}$$

and it is verified that

$$\text{on } \gamma_- \cup \gamma_s \; : \; \overrightarrow{u}_a \cdot \overrightarrow{n} = 0 \; . \tag{5.14a}$$

We solve the $(WM2M)_h$ problem for the data given by equations (5.12a) - (5.14a) by using a discretized space of polynomial of degree 3. The magnitude of the analytical and numerical displacement, as well as the associated absolute error, are represented in Figure 5.3. Moreover, we compute the relative error:

$$\frac{||\overrightarrow{u}_a - \overrightarrow{u}_h||_{\mathbb{U}}}{||\overrightarrow{u}_a||_{\mathbb{U}}} = 1.81e - 12.$$
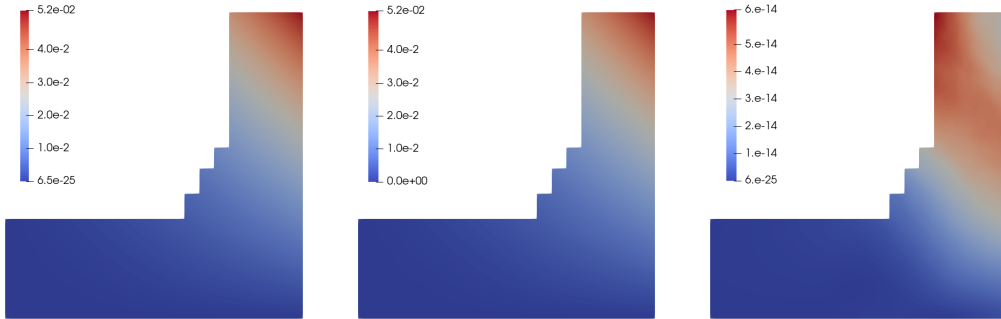

Figure 5.3: Benchmark for the mechanical model $(WM2M)_h$: analytical displacement magnitude $|\overrightarrow{u}_a|$ (left), numerical displacement magnitude $|\overrightarrow{u}_h|$ (center), and absolute error magnitude $|\overrightarrow{u}_a - \overrightarrow{u}_h|$ (right) in m.

Like the thermal model, even in this case we could observe that the two solutions show a very good agreement. For further comparison, we also compute the Von Mises stress:

$$\sigma_{vm} = \sqrt{\frac{3}{2}\boldsymbol{\sigma}_d : \boldsymbol{\sigma}_d} \ .\tag{5.15}$$

We display the magnitude of the analytical and numerical Von Mises stress, σ_{vma} and σ_{vmh} respectively, and the corresponding absolute error in Figure 5.4. We see that a very good agreement is obtained.
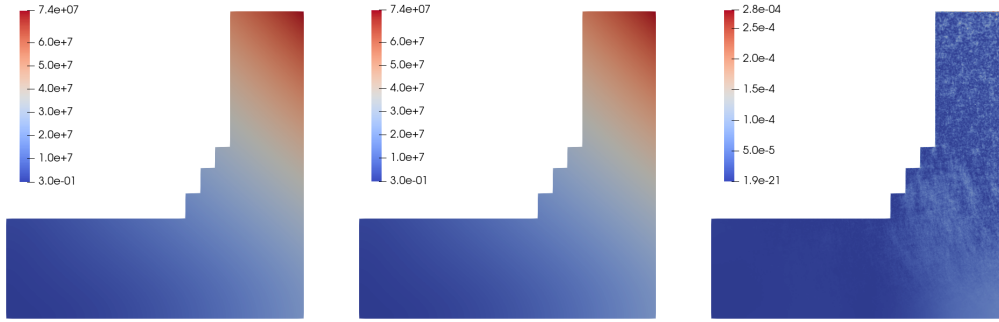
Figure 5.4: Benchmark for the mechanical model $(WM2M)_h$: analytical Von Mises stress magnitude σ_{vma} (left), numerical Von Mises stress magnitude σ_{vmh} (center), and absolute error $|\sigma_{vmh} - \sigma_{vma}|$ (right) in $\frac{N}{m^2}$.

Next, we address the coupling between the thermal and mechanical effects, so we refer to the problem $(WM2)_h$. We assume for the temperature the analytical field used for the problem $(WT)_h$, T_a (see eq. (5.6)), and for the displacement the analytical field used for the problem $(WM2M)_h$, $\overrightarrow{u}_a$ (see eq. (5.10)). Accordingly,

- the components of the stress tensor $\boldsymbol{\sigma}$ are given by eqs. (2.58),

$$\sigma_{rr} = \frac{E}{(1-2\nu)(1+\nu)}(Cy^2 + \nu Cr^2) - \frac{E}{(1-2\nu)}\alpha(C'r^2y - T_0) \ ,\tag{5.16a}$$

$$\sigma_{yy} = \frac{E}{(1-2\nu)(1+\nu)}(2\nu Cy^2 + (1-\nu)Cr^2) - \frac{E}{(1-2\nu)}\alpha(C'r^2y - T_0) \ ,\tag{5.16b}$$

$$\sigma_{\theta\theta} = \frac{E}{(1-2\nu)(1+\nu)}(Cy^2 + \nu Cr^2) - \frac{E}{(1-2\nu)}\alpha(C'r^2y - T_0) \ ,\tag{5.16c}$$

$$\sigma_{ry} = \frac{2ECry}{(1+\nu)} \ ,\tag{5.16d}$$

- the source term $\overrightarrow{f}_0 = [f_{0,r} \ f_{0,y}]$ is obtained from eqs. (2.57) and (5.11) by,

$$f_{0,r} = -\left(\frac{\partial \sigma_{rr}}{\partial r} + \frac{\partial \sigma_{ry}}{\partial y} + \frac{\sigma_{rr} - \sigma_{\theta\theta}}{r}\right)$$

$$= -\left(\frac{2E\nu Cr}{(1-2\nu)(1+\nu)} + \frac{2ECr}{(1+\nu)} - \frac{2C'ryE\alpha}{(1-2\nu)}\right) , \qquad (5.17a)$$

$$f_{0,y} = -\left(\frac{\partial \sigma_{ry}}{\partial r} + \frac{\partial \sigma_{yy}}{\partial y} + \frac{\sigma_{ry}}{r}\right)$$

$$= -\left(\frac{4ECy}{(1+\nu)} + \frac{4E\nu Cy}{(1-2\nu)(1+\nu)} - \frac{C'r^2 E\alpha}{(1-2\nu)}\right) , \qquad (5.17b)$$

- we obtain the thermal stresses. from eqs. (2.27) and (2.29):

$$(2\mu + 3\lambda)\alpha(T - T_0) = (2\mu + 3\lambda)\alpha(C'r^2y - T_0) = \frac{E}{(1-2\nu)}\alpha(C'r^2y - T_0) , \quad (5.18)$$

- the boundary tractions are derived from eqs. (2.59) and (5.11) as,

$$\text{on } \gamma_+ \ : g_{+,r} = \frac{2ECry}{(1+\nu)} , \qquad (5.19a)$$

$$g_{+,y} = \frac{E}{(1-2\nu)(1+\nu)}\left(2\nu Cy^2 + (1-\nu)Cr^2\right)$$

$$- \frac{E\alpha}{(1-2\nu)}(C'r^2y - T_0) , \qquad (5.19b)$$

$$\text{on } \gamma_- \ : g_{-,r} = -\frac{2ECry}{(1+\nu)} , \qquad (5.19c)$$

$$\text{on } \gamma_{sf} \ : g_{sf,r} = \frac{E}{(1-2\nu)(1+\nu)}(Cy^2 + \nu Cr^2)n_r$$

$$- \frac{E\alpha}{(1-2\nu)}(C'r^2y - T_0)n_r + \frac{2ECry}{(1+\nu)}n_y , \qquad (5.19d)$$

$$g_{sf,y} = \frac{E}{(1-2\nu)(1+\nu)}\left(2\nu Cy^2 + (1-\nu)Cr^2\right)n_y$$

$$- \frac{E\alpha}{(1-2\nu)}(C'r^2y - T_0)n_y + \frac{2ECry}{(1+\nu)}n_r , \qquad (5.19e)$$

$$\text{on } \gamma_{out} \ : g_{out,r} = \frac{E}{(1-2\nu)(1+\nu)}(Cy^2 + \nu Cr^2) - \frac{E\alpha}{(1-2\nu)}(C'r^2y - T_0) , \quad (5.19f)$$

$$g_{out,y} = \frac{2ECry}{(1+\nu)} . \qquad (5.19g)$$

We display the magnitude of the analytical displacement and Von Mises stress and their comparison with the corresponding numerical values in figures 5.5 and 5.6, respectively,

and compute the relative error:

$$\frac{||\overrightarrow{u}_a - \overrightarrow{u}_h||_{\mathbb{U}}}{||\overrightarrow{u}_a||_{\mathbb{U}}} = 2.2e - 12.$$

We could see that, as for mechanical model $(WM2M)_h$, the agreement between the two solutions is very good.
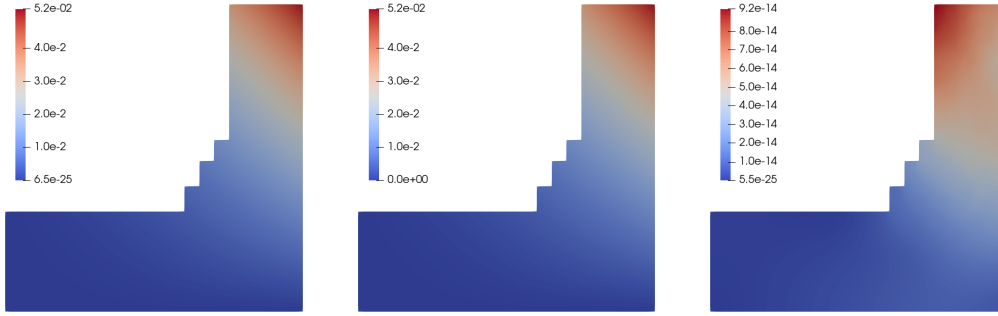
Figure 5.5: Benchmark for the mechanical problem $(WM2)_h$: analytical displacement magnitude $|\overrightarrow{u}_a|$ (left), numerical displacement magnitude $|\overrightarrow{u}_h|$ (center), and absolute error $|\overrightarrow{u}_a - \overrightarrow{u}_h|$(right) in m.
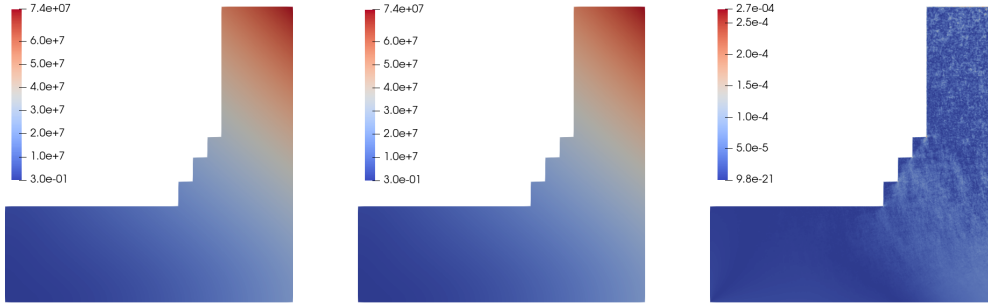
Figure 5.6: Benchmark for the mechanical problem $(WM2)_h$: analytical Von Mises stress σ_{vma} (left), numerical Von Mises stress σ_{vmh} (center) and absolute error $|\sigma_{vmh} - \sigma_{vma}|$ (right) in $\frac{N}{m^2}$.

Finally, we observe that the difference between the hydrostatic stress computed with the model $(WM2)_h$ and the one computed with the model $(WM2M)_h$, i.e. the hydrostatic stress related to the model $(WM2T)_h$, should be equal to the thermal stress:

$$\frac{1}{3}Tr\left(\boldsymbol{\sigma}(\overrightarrow{u_h})[T_h] - \boldsymbol{\sigma}(\overrightarrow{u_h})[T_0]\right) = (2\mu + 3\lambda)\alpha(T_h - T_0)\boldsymbol{I}. \tag{5.20}$$

The right and hand sides of eq. (5.20) are shown in Figure 5.7. We obtain a very good agreement.
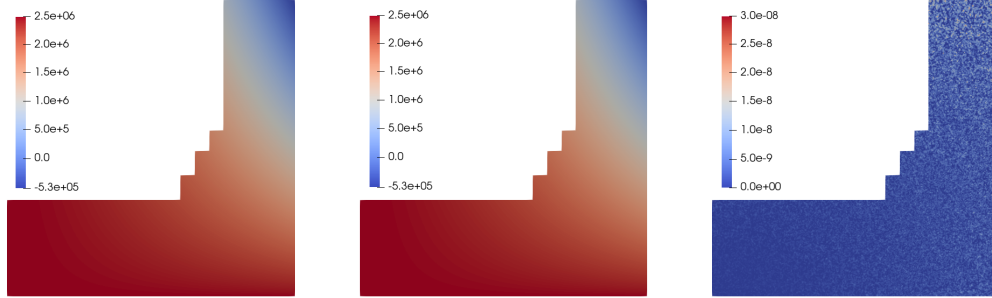
Figure 5.7:   Benchmark for the mechanical model $(WM2T)_h$:   difference between the hydrostatic stress computed with the $(WM2)_h$ model and the $(WM2M)_h$ model $\frac{1}{3}Tr\left(\sigma(\overrightarrow{u_h})[T_h] - \sigma(\overrightarrow{u_h})[T_0]\right)$ (left), thermal stress $(2\mu + 3\lambda)\alpha(T_h - T_0)$ (center) and corresponding absolute error $\left|\frac{1}{3}Tr\left(\sigma(\overrightarrow{u_h})[T_h] - \sigma(\overrightarrow{u_h})[T_0]\right) - (2\mu + 3\lambda)\alpha(T_h - T_0)\right|$ (right) in $\frac{N}{m^2}$.

After discussing theoretical and computational issues related to the full order model, we discuss the reduced basis approach for parametric PDEs, which is used to accelarate the computation of approximate solution field under the variation of parameters, in the next chapter.

Chapter 6

Problem parametrization and a reduced basis approach

In this chapter, we present our Model Order Reduction (MOR) framework. Firstly, we introduce the parameter space related to the problem under investigation (Sec. 6.1). Then, in Sec. 6.2, we describe the POD algorithm that is used for the construction of reduced basis space as well as the two methods adopted for the computation of the reduced degrees of freedom, Galerkin projection (G) and Artificial Neural Network (ANN). Finally, in Sec. 6.3, we show some numerical tests with the aim to validate our approach. The MOR computations have been carried out using RBniCS [46, 79], an in-house open source python library employing several reduced order techniques based on FEniCS [2, 35], and PyTorch [68, 71], a python machine learning library.

6.1   Parameter space

Let $\mathbb{P} \subset \mathbb{R}^d$ be the parameter space having dimensionality d with $\Xi \in \mathbb{P}$ a tuple of parameters. For the problem of blast furnace hearth, the relevant parameters are related both to the physical properties and the geometry of the domain ω. The physical parameters are the thermal conductivity of the material, k, the thermal expansion coefficient, α, the Young's modulus, E, and the Poisson's ratio, ν. On the other hand, the geometric parameters are the diameter of each section of the hearth D_0, D_1, D_2, D_3, D_4, and the thickness of each section of the hearth t_0, t_1, t_2, t_3, t_4 (see Figure 6.1). So for the problem under consideration, in the most general case (i.e., when all the parameters are considered), we have $\Xi = \{\Xi_p, \Xi_g\}$ where $\Xi_p = \{k, \alpha, E, \nu\} \in \mathbb{P}_p \subset \mathbb{R}^4$ is the physical parameters tuple and $\Xi_g = \{D_0, D_1, D_2, D_3, D_4, t_0, t_1, t_2, t_3, t_4\} \in \mathbb{P}_g \subset \mathbb{R}^{10}$ is the geometric parameters tuple, and $d = 14$.

Let us consider a geometrical parameters tuple $\bar{\Xi}_g$ and the corresponding domain $\hat{\omega} = \omega(\bar{\Xi}_g)$. We refer to $\hat{\omega}$ as the reference domain. As discussed in Sec. 5.1, the domain $\hat{\omega}$ is
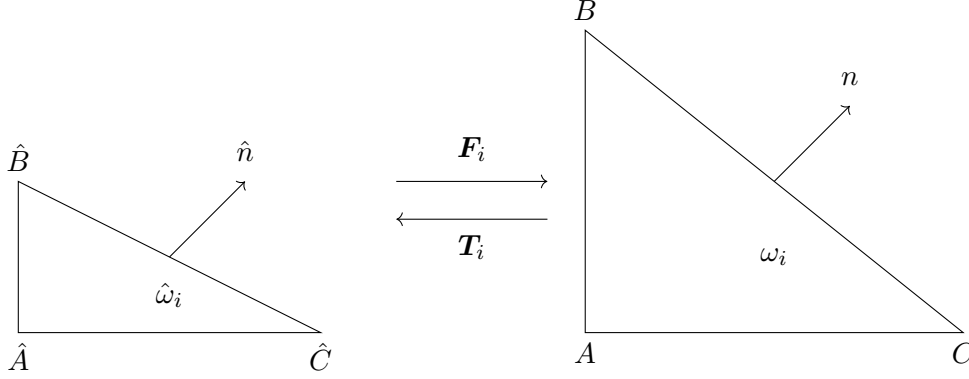
Figure 6.1: Hearth geometric parameters.

divided into n_{su} non-overlapping triangular subdomains i.e. $\hat{\omega} = \bigcup\limits_{i=1}^{n_{su}} \hat{\omega}_i$, $\hat{\omega}_i \cap \hat{\omega}_j = \emptyset$, $i \neq j$.
For each of the subdomains $\hat{\omega}_i$, one can consider an invertible mapping $\boldsymbol{F}_i$,

$$\boldsymbol{F}_i : \hat{\omega}_i \times \mathbb{P}_g \to \omega_i \ , \tag{6.1}$$

of the form,

$$\overrightarrow{x} = \boldsymbol{F}_i(\overrightarrow{\hat{x}}, \Xi_g) = \boldsymbol{G}_{F,i}(\Xi_g)\overrightarrow{\hat{x}} + \overrightarrow{c}_{F,i}(\Xi_g); \ , \ \forall \overrightarrow{\hat{x}} \in \hat{\omega}_i \ , \forall \overrightarrow{x} \in \omega_i(\Xi_g) \ , \tag{6.2}$$

where,

$$\boldsymbol{G}_{F,i} = \begin{bmatrix} G_{F,i,11} & G_{F,i,12} \\ G_{F,i,21} & G_{F,i,22} \end{bmatrix} \ , \ \overrightarrow{x} = \{r\ y\}^T \ , \ \overrightarrow{\hat{x}} = \{\hat{r}\ \hat{y}\}^T \ , \overrightarrow{c}_{F,i} = \{c_{F,i,1}\ c_{F,i,2}\}^T \ . \tag{6.3}$$

Equation (6.2) highlights that the Jacobian matrix $\boldsymbol{G}_{F,i}$ and the translation vector $\overrightarrow{c}_{F,i}$ are dependent only on the geometric parameters tuple Ξ_g and do not vary over a given subdomain. In the following, the domains ω will be the image by eq. (6.2) of the reference domain for the tuples of geometric parameters considered.

6.2   Main ingredients of MOR

The basic idea of MOR is the assumption that solutions live in a low dimensional manifold. Thus, any solution can be approximated based on a reduced number of global basis functions. We seek the reduced basis approximations $T_h^{rb} \in H_{r,h}^{1,rb}(\omega)$ and $\overrightarrow{u}_h^{rb} \in \mathbb{U}_h^{rb}$ of $T_h \in H_{r,h}^1(\omega)$ and $\overrightarrow{u}_h \in \mathbb{U}_h$, respectively. The reduced basis spaces $H_{r,h}^{1,rb}(\omega) \subset H_{r,h}^1(\omega)$ and $\mathbb{U}_h^{rb} \subset \mathbb{U}_h$ are given by,

$$H_{r,h}^{1,rb}(\omega) = \mathrm{span}\{\psi_h^1, \ldots, \psi_h^{N_T}\} \ , \ \mathbb{U}_h^{rb} = \mathrm{span}\{\overrightarrow{\phi}_h^1, \ldots, \overrightarrow{\phi}_h^{N_M}\} \ ,$$

Figure 6.2: Mapping between reference domain $\hat{\omega}_i$ and parametrized domain ω_i

where $N_M \ll m_h$ and $N_T \ll n_h$ are the number of basis functions forming the reduced basis spaces $H_{r,h}^{1,rb}(\omega)$ and $\mathbb{U}_h^{rb}$, respectively. Then we can represent $\overrightarrow{u}_h^{rb}$ and T_h^{rb} by,

$$T_h^{rb} = \sum_{i=1}^{N_T} \zeta_T^i \psi_h^i \ , \tag{6.4}$$

$$\overrightarrow{u}_h^{rb} = \sum_{i=1}^{N_M} \zeta_M^i \overrightarrow{\phi}_h^i \ , \tag{6.5}$$

where $\{\zeta_T^i\}_{i=1}^{N_T}$ and $\{\zeta_M^i\}_{i=1}^{N_M}$ are the temperature and displacement degrees of freedom, respectively. We also construct the reduced basis spaces for displacement fields $\overrightarrow{u}_T$ and $\overrightarrow{u}_M$, introduced in (4.13) and (4.14) as:

$$\mathbb{U}_{T,h}^{rb} = \text{span}\{\overrightarrow{\phi}_{T,h}^1, \dots, \overrightarrow{\phi}_{T,h}^{N_{M,T}}\} \ , \ \mathbb{U}_{M,h}^{rb} = \text{span}\{\overrightarrow{\phi}_{M,h}^1, \dots, \overrightarrow{\phi}_{M,h}^{N_{M,M}}\} \ .$$

So, the reduced basis approximations $\overrightarrow{u}_{M,h}^{rb} \in \mathbb{U}_{M,h}^{rb}$ of $\overrightarrow{u}_{M,h} \in \mathbb{U}_h$ and $\overrightarrow{u}_{T,h}^{rb} \in \mathbb{U}_{T,h}^{rb}$ of $\overrightarrow{u}_{T,h} \in \mathbb{U}_h$ can be represented as:

$$\overrightarrow{u}_{M,h}^{rb} = \sum_{i=1}^{N_{M,M}} \zeta_{M,M}^i \overrightarrow{\phi}_{M,h}^i \ , \ \overrightarrow{u}_{T,h}^{rb} = \sum_{i=1}^{N_{M,T}} \zeta_{M,T}^i \overrightarrow{\phi}_{T,h}^i \ . \tag{6.6}$$

Reduced basis method has found applications in real time computations, many query contexts and quick transfer of computational problems to industrial problems. The reduced basis method assumes that the solution provided by full order model is "truth solution". The reduced basis method can be decomposed into two stages : Offline phase and Online phase. The success of MOR depends on full decoupling between the offline phase and the online phase.

- **Offline phase**: The computationally expensive offline phase consists of FLOPS dependent on the dimension of full order model, $\mathcal{O}(n_h)$, such as solving finite element models. During the offline phase, reduced basis spaces $H_{r,h}^{1,rb}(\omega)$ and $\mathbb{U}_h^{rb}$ are constructed. In the case of POD-G, the operators are projected on the reduced basis space, which can later be assembled quickly. In the case of POD-ANN, the training of ANN, including computing high-fidelity snapshots and its projection on reduced basis space, incurs significant offline cost. The offline phase is performed only once and need not be performed for each new parameter.

- **Online phase**: The online phase consists of FLOPS dependent on the dimension of reduced basis model such as $\mathcal{O}(N_T)$. During the online phase, the coefficients of the reduced basis are computed. The online phase needs to be computationally efficient as it is performed for each new parameter.

Finally, by triangular inequality, errors between actual solution, finite element solution and reduced basis solution are related as:

$$||T - T_h^{rb}||_{H_r^1(\omega)} \leq ||T - T_h||_{H_r^1(\omega)} + ||T_h - T_h^{rb}||_{H_{r,h}^1(\omega)} \ , \tag{6.7}$$

$$||\overrightarrow{u} - \overrightarrow{u}_h^{rb}||_{\mathbb{U}} \leq ||\overrightarrow{u} - \overrightarrow{u}_h||_{\mathbb{U}} + ||\overrightarrow{u}_h - \overrightarrow{u}_h^{rb}||_{\mathbb{U}_h} \ . \tag{6.8}$$

It is to be noted that in equations (6.7) and (6.8), the first term on the right hand side is related to the accuracy of the finite element model and the second term on the right hand side is related to the accuracy of the reduced order model. For the reduced basis solution to be a good approximation of the actual solution, it is important that the finite element model is sufficiently accurate.

6.2.1 POD algorithm

In the literature, one can find several techniques to generate the reduced basis spaces, e.g. Proper Orthogonal Decomposition (POD), the Proper Generalized Decomposition (PGD) and the Reduced Basis (RB) with a greedy sampling strategy. See, e.g., [4, 17, 42, 46, 73]. In this work, the reduced basis spaces are constructed by POD that is able to capture the "dominant" modes by exploiting the information contained in the full order snapshots.

We are going to describe the procedure for the computation of the reduced basis space $H_{r,h}^{1,rb}(\omega)$. The reduced basis space $\mathbb{U}_h^{rb}$, $\mathbb{U}_{T,h}^{rb}$ and $\mathbb{U}_{M,h}^{rb}$ are constructed in an analogous way. First, n_s parameter tuples, $\{\Xi_k\}_{k=1}^{n_s}$, are considered that form the training set. We compute the snapshots $T_h(\Xi_k)$ related to each parameter tuple in the training set. Then a matrix $\boldsymbol{C}_T \in \mathbb{R}^{n_s \times n_s}$ is constructed,

$$(\boldsymbol{C}_T)_{kl} = < T_h(\Xi_k), T_h(\Xi_l) >_{H_{r,h}^1(\hat{\omega})} \ , \ 1 \leq k,l \leq n_s \ , \tag{6.9}$$

where transformation (6.2) is considered. Next, N_T largest eigenvalues $\{\theta_T^i\}_{i=1}^{N_T}$ of the matrix $\boldsymbol{C}_T$, sorted in descending order, $\theta_T^1 \geq \theta_T^2 \geq \ldots \geq \theta_T^{N_T}$, and corresponding eigenvectors $\{\boldsymbol{V}_T^i\}_{i=1}^{N_T}$, $\boldsymbol{V}_T^i \in \mathbb{R}^{n_s}$, are computed:

$$\boldsymbol{C}_T \boldsymbol{V}_T^i = \theta_T^i \boldsymbol{V}_T^i \ . \tag{6.10}$$

The reduced basis are then given by:

$$\psi_h^i = \frac{\sum\limits_{k=1}^{n_s} (\boldsymbol{V}_T^i)_k T_h(\Xi_k)}{\|\sum\limits_{k=1}^{n_s} (\boldsymbol{V}_T^i)_k T_h(\Xi_k)\|_{H^1_{r,h}(\hat{\omega})}} \ , \ 1 \leq i \leq N_T \ . \tag{6.11}$$

In order to determine the admissibility of a given eigenvector into the POD space, we refer to the following criterion:

$$\frac{\theta_T^i}{\theta_T^1} \geq 1e - 4 \ . \tag{6.12}$$

In the following subsections, we describe two different approaches for the computation of the degrees of freedom: Galerkin projection (G) and Artificial Neural Network (ANN).

6.2.2 Galerkin projection

Here we choose to consider $(WM2M)_h$ and $(WM2T)_h$ in the place of $(WM2)_h$ because each subsystem may have different scale effects: see, e.g., [50, 85, 105]. We consider an affine parametric dependence, i.e. the bilinear forms $a_T(\cdot, \cdot; \Xi)$ and $a_M(\cdot, \cdot; \Xi)$ are expressed as weighted sum of n_{a_T} and n_{a_M} parameter independent bilinear forms. Similarly, the linear forms $l_T(\cdot; \Xi)$ and $l_M[T](\cdot; \Xi)$ are expressed as weighted sum of n_{l_T} and n_{l_M} parameter independent linear forms. We have:

$$a_T(T, \psi; \Xi) = \sum_{i=1}^{n_{a_T}} \theta_{a_{T,i}}(\Xi) a_{T,i}(T, \psi; \bar{\Xi}) \ ,$$
$$l_T(\psi; \Xi) = \sum_{i=1}^{n_{l_T}} \theta_{l_{T,i}}(\Xi) l_{T,i}(\psi; \bar{\Xi}) \ , \tag{6.13}$$

and

$$a_M(\overrightarrow{u}, \overrightarrow{\phi}; \Xi) = \sum_{i=1}^{n_{a_M}} \theta_{a_{M,i}}(\Xi) a_{M,i}(\overrightarrow{u}, \overrightarrow{\phi}; \bar{\Xi}) \ ,$$
$$l_M[T](\overrightarrow{\phi}; \Xi) = \sum_{i=1}^{n_{l_M}} \theta_{l_{M,i}}(\Xi) l_{M,i}[T](\overrightarrow{\phi}; \bar{\Xi}) \ . \tag{6.14}$$

The affine expansion of operators is essentially a change of variables and has been widely addressed in the literature: see, e.g., [17, 42, 46]. The affinity assumption is particularly important as it leads to considerable efficiency. This is mainly due to the fact that the evaluation of bilinear forms, $a_{M,i}(\overrightarrow{u}, \overrightarrow{\phi})$ and $a_{T,i}(T, \psi)$, and linear forms, $l_{T,i}(\psi)$ and $l_{M,i}[T](\overrightarrow{\phi})$ are not required for each new tuple of parameters.

So for what concerns the model $(WT2)_h$, the bilinear form $a_{T,h} : H^1_{r,h}(\omega) \times H^1_{r,h}(\omega) \to \mathbb{R}$ is restricted to the reduced basis space as $a^{rb}_{T,h} : H^{1,rb}_{r,h}(\omega) \times H^{1,rb}_{r,h}(\omega) \to \mathbb{R}$. In the same way, the linear form $l_{T,h} : H^1_{r,h}(\omega) \to \mathbb{R}$ is restricted to the reduced basis space as $l^{rb}_{T,h} : H^{1,rb}_{r,h}(\omega) \to \mathbb{R}$. So the reduced basis approximation T^{rb}_h at a given parameter tuple Ξ^* is obtained by solving:

$$a^{rb}_{T,h}(T^{rb}_h, \psi^{rb}_h; \Xi^*) = l^{rb}_{T,h}(\psi^{rb}_h; \Xi^*) \ , \ \forall \psi^{rb}_h \in H^{1,rb}_{r,h}(\omega) \ . \tag{6.15}$$

On the other hand, for what concerns the model $(WM2M)_h$, the bilinear form $a_{M,h} : \mathbb{U}_h \times \mathbb{U}_h \to \mathbb{R}$ is restricted to the reduced basis space as $a^{rb}_{M,h} : \mathbb{U}^{rb}_{M,h} \times \mathbb{U}^{rb}_{M,h} \to \mathbb{R}$. The linear form $l_{M,h} : \mathbb{U}_h \to \mathbb{R}$ is restricted to the reduced basis space as $l^{rb}_{M,h} : \mathbb{U}^{rb}_{M,h} \to \mathbb{R}$. So the reduced basis approximation $\overrightarrow{u}^{rb}_{M,h}$ at a given parameter tuple Ξ^* is obtained by solving:

$$a^{rb}_{M,h}(\overrightarrow{u}^{rb}_{M,h}, \overrightarrow{\phi}^{rb}_{M,h}; \Xi^*) = l^{rb}_{M,h}[T_0](\overrightarrow{\phi}^{rb}_{M,h}; \Xi^*) \ , \ \forall \overrightarrow{\phi}^{rb}_{M,h} \in \mathbb{U}^{rb}_{M,h} \ . \tag{6.16}$$

Similarly, for the model $(WM2T)_h$ the bilinear form $a_{M,h} : \mathbb{U}_h \times \mathbb{U}_h \to \mathbb{R}$ is restricted to the reduced basis space as $a^{rb}_{M,h} : \mathbb{U}^{rb}_{T,h} \times \mathbb{U}^{rb}_{T,h} \to \mathbb{R}$. The linear form $l_{M,h} : \mathbb{U}_h \to \mathbb{R}$ is restricted to the reduced basis space as $l^{rb}_{M,h} : \mathbb{U}^{rb}_{T,h} \to \mathbb{R}$. So, the reduced basis approximation $\overrightarrow{u}^{rb}_{T,h}$ at a given parameter Ξ^* is obtained by solving:

$$a^{rb}_{M,h}(\overrightarrow{u}^{rb}_{T,h}, \overrightarrow{\phi}^{rb}_{T,h}; \Xi^*) = l^{rb}_{M,h}[T^{rb}_h](\overrightarrow{\phi}^{rb}_{T,h}; \Xi^*) - l^{rb}_{M,h}[T_0](\overrightarrow{\phi}^{rb}_{T,h}; \Xi^*) \ , \ \forall \overrightarrow{\phi}^{rb}_{T,h} \in \mathbb{U}^{rb}_{T,h} \ . \tag{6.17}$$

We introduce the coercivity constant $c^{rb}_{T,h} > 0$ and continuity constant $C^{rb}_{T,h} > 0, \forall T^{rb}_h, \psi^{rb}_h \in H^{1,rb}_{r,h}(\omega)$:

$$c^{rb}_{T,h}||\psi^{rb}_h||^2_{H^{1,rb}_{r,h}(\omega)} \le a^{rb}_{T,h}(\psi^{rb}_h, \psi^{rb}_h) \ , \tag{6.18}$$

$$|a^{rb}_{T,h}(T^{rb}_h, \psi^{rb}_h)| \le C^{rb}_{T,h}||T^{rb}_h||_{H^{1,rb}_{r,h}(\omega)}||\psi^{rb}_h||_{H^{1,rb}_{r,h}(\omega)} \ . \tag{6.19}$$

The reduced basis approximation T^{rb}_h is orthogonal projection of finite element approximation T_h with respect to $a_{T,h}(\cdot, \cdot)$,

$$a_{T,h}(T_h - T^{rb}_h, \psi^{rb}_h) = 0 \ , \ \forall \psi^{rb}_h \in H^{1,rb}_{r,h}(\omega) \ . \tag{6.20}$$

By following procedure for deriving error estimate (4.25), following error estimate can be derived:

$$||T_h - T_h^{rb}||_{H^1_{r,h}(\omega)} \leq \sqrt{\frac{C_{T,h} + c_{T,h}^{rb} - c_{T,h}}{c_{T,h}^{rb}}} ||T_h - \psi_h^{rb}||_{H^1_{r,h}(\omega)} \ , \ \forall \psi_h^{rb} \in H^{1,rb}_{r,h}(\omega) \ . \quad (6.21)$$

We introduce the coercivity constant $c_{MM,h}^{rb} > 0$ and continuity constant $C_{MM,h}^{rb} > 0, \forall \overrightarrow{u}_{M,h}^{rb}, \overrightarrow{\phi}_{M,h}^{rb} \in \mathbb{U}_{M,h}^{rb}$.

$$c_{MM,h}^{rb} ||\overrightarrow{\phi}_{M,h}^{rb}||^2_{\mathbb{U}_{M,h}^{rb}} \leq a_{M,h}^{rb}(\overrightarrow{\phi}_{M,h}^{rb}, \overrightarrow{\phi}_{M,h}^{rb}) \ , \quad (6.22)$$

$$|a_{M,h}^{rb}(\overrightarrow{u}_{M,h}^{rb}, \overrightarrow{\phi}_{M,h}^{rb})| \leq C_{MM,h}^{rb} ||\overrightarrow{u}_{M,h}^{rb}||_{\mathbb{U}_{M,h}^{rb}} ||\overrightarrow{\phi}_{M,h}^{rb}||_{\mathbb{U}_{M,h}^{rb}} \ . \quad (6.23)$$

The reduced basis approximation $\overrightarrow{u}_{M,h}^{rb}$ is orthogonal projection of finite element approximation $\overrightarrow{u}_{M,h}$ with respect to $a_{M,h}(\cdot,\cdot)$:

$$a_{M,h}(\overrightarrow{u}_{M,h} - \overrightarrow{u}_{M,h}^{rb}, \overrightarrow{\phi}_{M,h}^{rb}) = 0 \ , \ \forall \overrightarrow{\phi}_{M,h}^{rb} \in \mathbb{U}_{M,h}^{rb} \ . \quad (6.24)$$

By following procedure for deriving error estimate (4.32), following error estimate can be derived:

$$||\overrightarrow{u}_{M,h} - \overrightarrow{u}_{M,h}^{rb}||_{\mathbb{U}_{M,h}} \leq \sqrt{\frac{C_{MM,h} + c_{MM,h}^{rb} - c_{MM,h}}{c_{MM,h}^{rb}}} ||\overrightarrow{u}_{M,h} - \overrightarrow{\phi}_{M,h}^{rb}||_{\mathbb{U}_{M,h}} \ ,$$

$$\forall \overrightarrow{\phi}_{M,h}^{rb} \in \mathbb{U}_{M,h}^{rb} \ . \quad (6.25)$$

We introduce the coercivity constant $c_{MT,h}^{rb} > 0$ and continuity constant $C_{MT,h}^{rb} > 0, \forall \overrightarrow{u}_{T,h}^{rb}, \overrightarrow{\phi}_{T,h}^{rb} \in \mathbb{U}_{T,h}^{rb}$:

$$c_{MT,h}^{rb} ||\overrightarrow{\phi}_{T,h}^{rb}||^2_{\mathbb{U}_{T,h}^{rb}} \leq a_{T,h}^{rb}(\overrightarrow{\phi}_{T,h}^{rb}, \overrightarrow{\phi}_{T,h}^{rb}) \ , \quad (6.26)$$

$$|a_{T,h}^{rb}(\overrightarrow{u}_{T,h}^{rb}, \overrightarrow{\phi}_{T,h}^{rb})| \leq C_{MT,h}^{rb} ||\overrightarrow{u}_{T,h}^{rb}||_{\mathbb{U}_{T,h}} ||\overrightarrow{\phi}_{T,h}^{rb}||_{\mathbb{U}_{T,h}^{rb}} \ . \quad (6.27)$$

However, due to lack of $a_{M,h}-$orthogonality, similar to equation (4.33) following error estimate can be derived:

$$||\overrightarrow{u}_{T,h} - \overrightarrow{u}_{T,h}^{rb}||_{\mathbb{U}_h} \leq \left(\frac{C_{M,h}}{c_{M,h}} ||\overrightarrow{u}_{T,h} - \overrightarrow{u}_{T,h}^{rb}||_{\mathbb{U}_h} ||\overrightarrow{u}_{T,h} - \overrightarrow{\phi}_{T,h}^{rb}||_{\mathbb{U}_h} \right.$$

$$\left. + \frac{(2\mu + 3\lambda)\alpha}{c_{M,h}} ||T_h - T_h^{rb}||_{L^2_r(\omega)} ||Div(\overrightarrow{\phi}_{T,h}^{rb} - \overrightarrow{u}_{T,h}^{rb})||_{L^2_r(\omega)} \right)^{\frac{1}{2}} \ , \quad (6.28)$$

$$\forall \overrightarrow{\phi}_{T,h}^{rb} \in \mathbb{U}_{T,h}^{rb} \ .$$

The bilinear forms and the linear forms in equations (6.15), (6.16) and (6.17) are evaluated using affine decomposition. The equation (6.15) has dimensionality $N_T \ll n_h$. Hence, at a given parameter, much smaller system of equations needs to be solved. Same explanation also holds for equations (6.16),(6.17). The online phase of POD-Galerkin approach involves assembling, using affine expansion, and solving smaller system of equations (6.15), (6.16) and (6.17).

### 6.2.3   Artificial Neural Network

The Galerkin projection has several advantages as discussed earlier. However, there are two aspects which need consideration:

- The efficiency of POD-Galerkin approach depends on efficient evaluation of the bilinear form by suitable method such as affine decomposition. However, such efficient assembly may not always be possible. Especially, since the non-linearity will be introduced at later stage, where Empirical interpolation method will be required, the efficiency of the assembly will be seriously compromised.

- Also, the system matrices are not always available. This is especially true, if commercial softwares are used instead of open source softwares.

In order to address both these issues, we introduce now Proper Orthogonal Decomposition(POD) - Artificial Neural Network(ANN) approach. As the name suggests, we use the Proper Orthogonal Decomposition for generating the reduced basis space, but replace Galerkin projection with the Artificial Neural Network (ANN). The POD-ANN approach has shown promising capabilities also for non linear equations [45]. Artificial Neural Network (ANN) is a computational model that takes inspiration from the human brain consisting of an interconnected network of simple processing units that can learn from experience by modifying their connections (see, e.g., [29, 43, 51, 80]).

Recently, the application of deep learning methods to partial differential equations has shown promising capabilities: see, e.g., [27, 58, 59, 76, 77, 90]. Concerning the application of the ANN approach in a MOR context, the reader is referred, e.g., to [27, 45, 69, 83, 100, 102]. We highlight that, unlike the Galerkin projection, ANN is a data-driven approach, i.e. based only on the data and does not require the knowledge of the original equations describing the system. It is also non-intrusive, in the sense that no modification of the simulation software, used for high-fidelity FEM solution field, is required.

In this work, we use a feed-forward ANN consisting of input layer, hidden layers, and output layer, with n_l the total number of layers and d_l the number of unit cells (the so-called neurons) of the $l-$th layer. The neurons of each layer are connected to the neurons of the next layer by synapses. See Figure 6.3 for an illustrative representation of a feed-forward ANN.
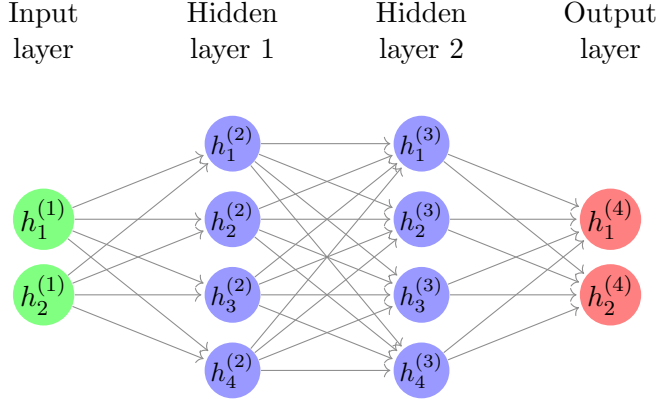
Figure 6.3: Sketch of a feed-forward ANN with $n_l = 4$.

Each neuron of the $l-$th layer takes a set of inputs s_i^l from the $(l-1)$-th layer provided by [34]:

$$s_i^l = \sum_{j=1}^{d_{(l-1)}} w_{ij}^l h_j^{(l-1)} \ , \ i = 1, \dots, d_l \ , \tag{6.29}$$

where $w_{ij}^{(l)}$ are weights linking the $(l-1)$-th and l-th layers. Then the output of the $l-$th layer is given by,

$$h_i^{(l)} = f_a \left(s_i^l + b_i^l \right) \ , \ i = 1, \dots, d_l \ , \tag{6.30}$$

where $b_i^{(l)}$ are the biasing parameters of the layer l. The weights $w_{ij}^{(l)}$ as well as the biasing parameters $b_i^{(l)}$ are iteratively adjusted by the backpropagation process using an optimization algorithm [56]. The function f_a is a non-linear differentiable function, called activation function [104]. In this work, we consider for hidden layers the Sigmoid activation function that can be expressed as:

$$f_a(x) = \frac{1}{1 + e^{-x}} \ , \tag{6.31}$$

whilst for the initial and final layer we use the identity function.

Unlike what done for the Galerkin projection approach, concerning the mechanical problem, we consider the model $(WM2)_h$. This choice is due to the fact that ANN suffers from high offline cost because of the training phase, so it is beneficial to train one only model instead of training two models.

Now we are going to describe the training phase of ANN. We use two hidden layers whose depth $d_l = H$ is determined by trial and error [45]. For the input layer we have $d_l = d$ whilst for the output layer $d_l = N_T$ for $(WT2)_h$ and $d_l = N_M$ for $(WM2)_h$.

We consider N_t^T parameter tuples $\{\Xi_k\}_{k=1}^{N_t^T}$ and compute the temperature field $T_h(\Xi_k)$ by solving problem $(WT2)_h$ at each parameter tuple Ξ_k. Next, the temperature field $T_h(\Xi_k)$ is projected on the reduced basis space so to obtain the projected solution $T_h^\pi(\Xi_k)$ and corresponding degrees of freedom $\boldsymbol{\zeta}_{T,\pi}(\Xi_k)$:

$$T_h^\pi(\Xi_k) = \operatorname*{arg\,min}_{\psi_h^{rb} \in H_{r,h}^{1,rb}(\omega)} ||T_h(\Xi_k) - \psi_h^{rb}||_{H_{r,h}^1(\omega)} = \sum_{i=1}^{N_T} \zeta_{T,\pi}^i(\Xi_k)\psi_h^i \ , \ \boldsymbol{\zeta}_{T,\pi}(\Xi_k) = \{\zeta_{T,\pi}^i(\Xi_k)\}_{i=1}^{N_T} \ .$$

$$(6.32)$$

Similarly, we consider N_t^M parameter tuples $\{\Xi_k\}_{k=1}^{N_t^M}$ and compute the displacement fields $\overrightarrow{u}_h(\Xi_k)$ by solving problem $(WM2)_h$ at each parameter tuple Ξ_k. Next, the displacement field $\overrightarrow{u}_h(\Xi_k) \in \mathbb{U}_h$ is projected on the reduced basis space so to obtain the projected solution $\overrightarrow{u}_h^\pi(\Xi_k)$ and corresponding degrees of freedom $\boldsymbol{\zeta}_{M,\pi}(\Xi_k)$:

$$\overrightarrow{u}_h^\pi(\Xi_k) = \operatorname*{arg\,min}_{\overrightarrow{\phi}_h^{rb} \in \mathbb{U}_h^{rb}} ||\overrightarrow{u}_h(\Xi_k) - \overrightarrow{\phi}_h^{rb}||_{\mathbb{U}_h} = \sum_{i=1}^{N_M} \zeta_{M,\pi}^i(\Xi_k)\overrightarrow{\phi}_h^i \ , \ \boldsymbol{\zeta}_{M,\pi}(\Xi_k) = \{\zeta_{M,\pi}^i(\Xi_k)\}_{i=1}^{N_M} \ .$$

$$(6.33)$$

We consider two collections of (known) training input-desidered output pairs, $\{\Xi_k, \zeta_{T,\pi}(\Xi_k)\}_{k=1}^{N_t^T}$ and $\{\Xi_k, \zeta_{M,\pi}(\Xi_k)\}_{k=1}^{N_t^M}$. The goal is to approximate the functions f_T and f_M that map these training input-desidered output pairs. After training the two ANNs, we consider them as black boxes that can then be used to compute the POD coefficients related to a new parameter instance Ξ^*.

We split the full order data into two parts: one to be used for training and one to be used for validation. While the training data are used to adjust weights and biasing parameters of the ANN, the validation data are used to measure its accuracy. A common issue is that ANN may perform better on training data but may not perform well on data other than training data. To avoid this overfitting phenomenon, we use the early stopping criteria [43]: the training is stopped when the the mean squared error

$$\epsilon_T = \frac{\sum\limits_{i=1}^{N_T} \left(\zeta_{T,\pi}^i(\Xi_k) - \zeta_T^i(\Xi_k)\right)^2}{N_T} \ , \ \epsilon_M = \frac{\sum\limits_{i=1}^{N_M} \left(\zeta_{M,\pi}^i(\Xi_k) - \zeta_M^i(\Xi_k)\right)^2}{N_M} \ , \tag{6.34}$$

as measured on validation data starts to increase.

The online phase of POD-ANN approach involves, predicting the coefficients of the reduced basis using feed-forward procedure. The training of neural network is performed during the offline phase.

6.3 Validation of MOR

We use a mesh of $\hat{\omega}$ containing 8887 triangular elements and 4608 vertices. The minimum mesh size is 0.047 m and the maximum one is 0.16 m. Its minimum quality is $q_e = 0.25$ (eq. 5.2). Notice that we use a coarser mesh with respect to the one used for the FOM benchmark tests in Sec. 5.1. Such a choice is justified by the fact that the FOM solution is required to be solved at many parameters values, so using a fine mesh can be very costly and make prohibitive the collection of the high-fidelity database.

The ranges of physical and geometrical parameters for training and testing are reported in Table 6.1. Concerning ANN, the training data are related to the 70% of the total data provided by the full order model whilst the remaining 30% is used for the validation.

Parameter	Minimum value	Maximum value
t_0	2.3	2.4
t_1	0.5	0.7
t_2	0.5	0.7
t_3	0.4	0.6
t_4	3.05	3.35
D_0	13.5	14.5
D_1	8.3	8.7
D_2	8.8	9.2
D_3	9.8	10.2
D_4	10.4	10.8
k	9.8	10.2
μ	1.9e9	2.5e9
λ	1.2e9	1.8e9
α	0.8e-6	1.2e-6

Table 6.1: Parameters ranges used for MOR training and testing.

The accuracy of our MOR approach is quantified by the relative error:

$$\epsilon_{rel,X_h} = \frac{||X_h - X_h^{rb}||}{||X_h||} \quad . \tag{6.35}$$

Here, X_h and X_h^{rb} are the finite element solution and the corresponding reduced basis solution, respectively. $||\cdot||$ is the relevant norm ($||\cdot||_{H_{r,h}^1(\omega)}$ and $||\cdot||_{\mathbb{U}_h}$). As benchmark for the relative error, we consider the projection error:

$$\epsilon_{proj,X_h} = \frac{||X_h - X_h^{\pi}||}{||X_h||} \quad . \tag{6.36}$$

6.3.1   Thermal model

We consider four experiments that differ in terms of kind (physical and/or geometrical) and the number of parameters considered:

- *experiment (i)*: 1 physical parameter: $\Xi = \{k\}$.

- *experiment (ii)*: 1 physical parameter and 3 geometric parameters:
  $\Xi = \{k, t_0, D_2, D_4\}$.

- *experiment (iii)*: 1 physical parameter and 6 geometric parameters:
  $\Xi = \{k, t_0, t_2, t_4, D_0, D_2, D_4\}$.

- *experiment (iv)*: 1 physical parameter and all (10) geometric parameters:
  $\Xi = \{k, t_0, t_1, t_2, t_3, t_4, D_0, D_1, D_2, D_3, D_4\}$.

Regarding the computation of POD space, for *experiment (i)*, 50 FOM snapshots were considered while for the other ones 1000. The eigenvalues decay is shown in Fig. 6.4. We see that the decay related to the experiment (iv) is the slowest. This is due to the fact that in the experiment (iv) we consider a larger number of parameters, so the system exhibits a greater complexity, and the modal content is more wide.
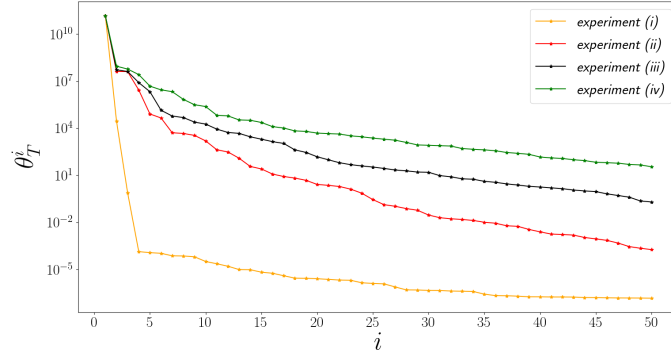

Figure 6.4: Thermal model: eigenvalues decay for all the experiments considered.

Fig. 6.5 shows the relative error (6.35) both for POD-ANN, related to different values of the number of samples provided by the full order model, $n_{tr} = N_t^T$, and depth of hidden layers, H, and POD-G. We also report the projection error (6.36). We observe that the performance of the POD-ANN method crucially depends on the values of n_{tr} and H. As expected, if we expand the training set and increase the depth of hidden layers, we obtain more accurate predictions when the number of parameters considered starts to get significative (experiments (iii) and (iv)). Unlike [45], we observe that the POD-G method

(a) experiment (i)   (b) experiment (ii)

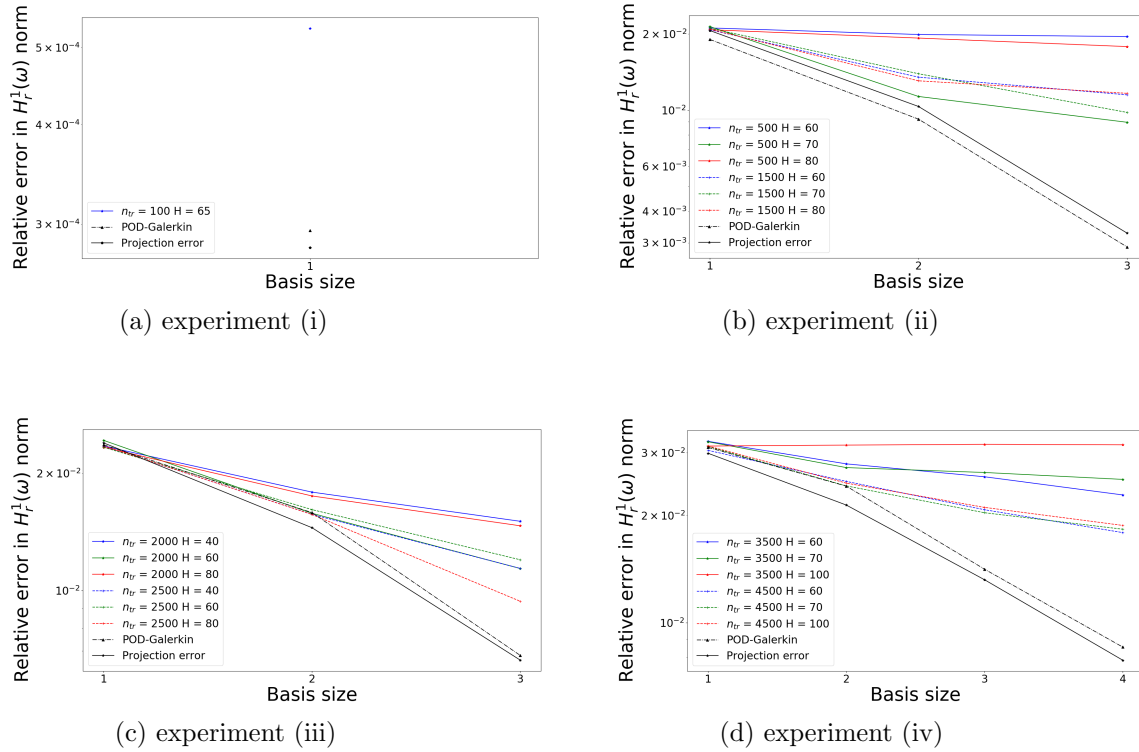(c) experiment (iii)   (d) experiment (iv)

Figure 6.5: Thermal model: error analysis for POD-G and POD-ANN for all the experiments carried out.

results to be in general more accurate than the POD-ANN method. This could be justified by considering that in the nonlinear framework the affine expansion could not be enforced and an Empirical Interpolation Method (EIM) [13] is used within the POD-G approach. Its implementation introduces interpolation error during the assembling of the reduced equations system by significantly affecting the accuracy of the POD-G method.

Illustrative representations of the computed FOM and MOR are displayed in Fig. 6.6 related to the experiment (iv) for the parameters tuple:

$$\Xi = \{2.365, 0.6, 0.6, 0.5, 3.2, 14.10, 8.50, 9.2, 9.9, 10.6, 10\} \ .$$

We use 4 POD basis. The POD-ANN solution was computed with $n_{tr} = 4500$ and $H = 70$. As we can see from Fig. 6.6, both MOR approaches are able to provide a good reconstruction of the temperature field.

We conclude by proving some information about the efficiency of our MOR approach. We report in Table 6.2 the online time related to the POD-G and POD-ANN methods for all the experiments carried out. As can be seen, the online time of POD-G method increases

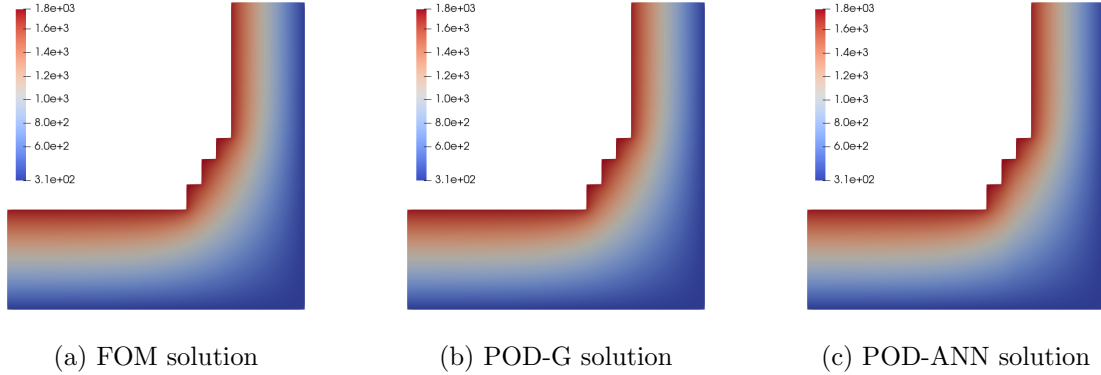(a) FOM solution   (b) POD-G solution   (c) POD-ANN solution

Figure 6.6: Thermal model: comparison between the temperature field (in K) computed by the FOM and by the POD-G and POD-ANN methods related to the experiment (iv) for $\Xi = \{2.365, 0.6, 0.6, 0.5, 3.2, 14.10, 8.50, 9.2, 9.9, 10.6, 10\}$. We consider 4 POD modes. For POD-ANN, we set $n_{tr} = 4500$ and $H = 70$.

experiment	Basis size	POD-G	POD-ANN
(i)	1	7e-4	4.9e-4
(ii)	3	1.3e-2	4.8e-4
(iii)	3	1.5e-2	4.9e-4
(iv)	4	1.3e-2	5.1e-4

Table 6.2: Thermal model: online time (in s) for all the experiments under investigation. Concerning POD-ANN, we use $n_{tr} = 100, H = 65$ for the experiment (i), $n_{tr} = 500, H = 70$ for the experiment ii), $n_{tr} = 2500, H = 80$ for the experiment (iii) and $n_{tr} = 4500, H = 70$ for the experiment (iv).

significantly in the presence of geometric parameters by moving from $7e - 4$ s (experiment (i)) to $1.3/1.5e - 2$ s (experiment (ii)-(iv)). On the other hand, the time taken by POD-ANN online stage remains relatively constant for all the experiments under investigation, around $5e - 4$. So the computational efficiency of POD-ANN is much higher, of almost two order of magnitude, than POD-G when geometrical parametrization is considered.

6.3.2   Thermomechanical model

We remark that for POD-ANN we refer to the $(WM2)_h$ model, whilst we consider $(WM2M)_h$ and $(WM2T)_h$ models for POD-G. As done for the thermal model, we consider four different experiments having different kinds and numbers of parameters:

- *experiment (i)*: 4 physical parameters: $\Xi = \{k, \mu, \lambda, \alpha\}$.

- *experiment (ii)*: 4 physical parameters and all 3 geometric parameters:
  $\Xi = \{k, \mu, \lambda, \alpha, t_0, D_2, D_4\}$.

- *experiment (iii)*: 4 physical parameters and 6 geometric parameters:
  $\Xi = \{k, \mu, \lambda, \alpha, t_0, t_2, t_4, D_0, D_2, D_4\}$.

- *experiment (iv)*: 4 physical parameters and all (10) geometric parameters:
  $\Xi = \{k, \mu, \lambda, \alpha, t_0, t_1, t_2, t_3, t_4, D_0, D_1, D_2, D_3, D_4\}$.

For all the experiments, the POD space was computed by considering 1000 snapshots. The eigenvalue plot is shown in Figure 6.7. Like the thermal model, we observe that the experiment (iv), characterized by the larger number of parameters, shows the lowest decay. On the other hand, as expected, among the different mechanical models we consider, the model $(WM2)_h$ exhibits the slowest eigenvalues decay including it both thermal and mechanical effects.
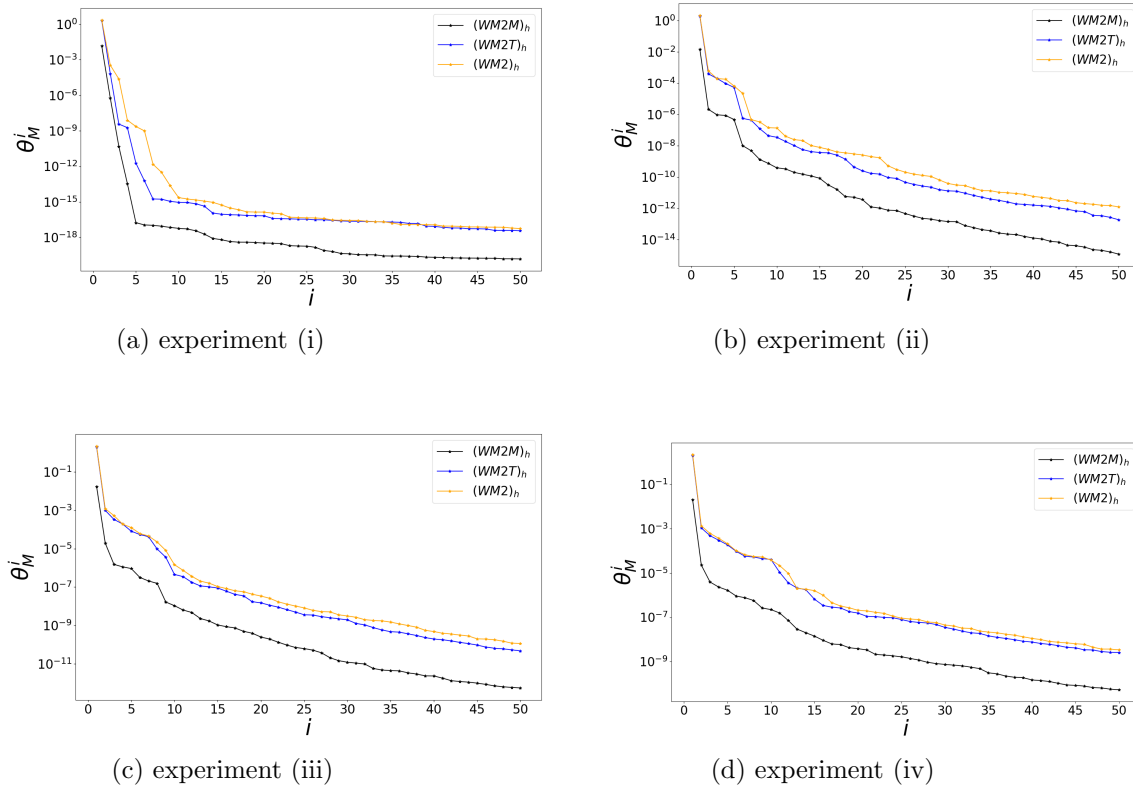

(a) experiment (i)

(b) experiment (ii)

(c) experiment (iii)
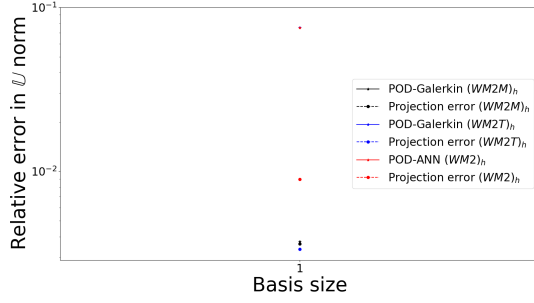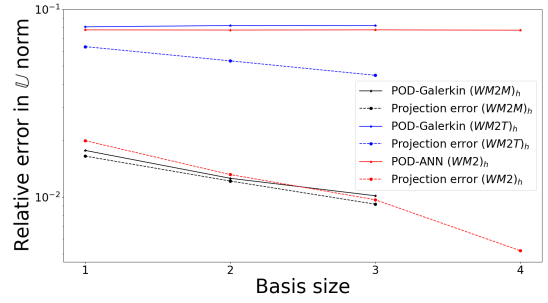
(d) experiment (iv)

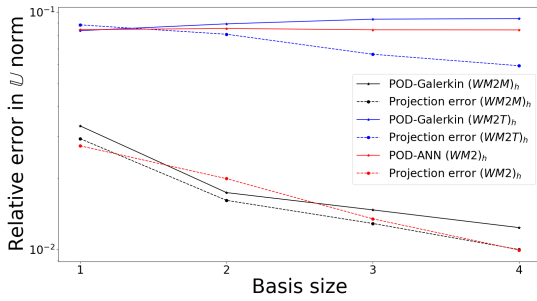Figure 6.7: Mechanical model: eigenvalues decay for all the experiments considered.

Figure 6.8 shows the relative error (6.35) both for POD-ANN and POD-G with rspect to
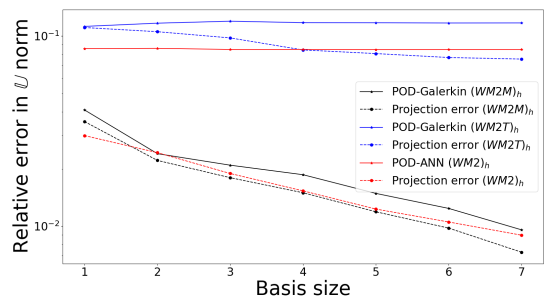
(a) experiment (i). For POD-ANN $n_{tr} = 500$ and $H = 60$.

(b) experiment (ii). For POD-ANN $n_{tr} = 500$ and $H = 80$.

(c) experiment (iii). For POD-ANN $n_{tr} = 1000$ and $H = 170$.

(d) experiment (iv). For POD-ANN $n_{tr} = 2500$ and $H = 130$.

Figure 6.8: Mechanical model: error analysis for POD-G and POD-ANN for all the experiments considered.

different number of training set, $n_{tr} = N_t^M$, and depth of hidden layers, H. The projection error (6.36) is also depicted. As observed for the thermal model, POD-G is able to provide more accurate results with respect to POD-ANN.

Figure 6.9 shows the qualitative comparison between the computed FOM and MOR related to the experiment (iv) for the parameters tuple:

$$\Xi = \{2.365, 0.6, 0.6, 0.5, 3.2, 14.10, 8.50, 9.2, 9.9, 10.6, 10, 2.08e9, 1.39e9, 1e-6\} \ .$$

We use 7 POD basis. The POD-ANN solution was computed with $n_{tr} = 2500$ and $H = 130$. We could observe that both MOR approaches are able to provide a good reconstruction of the displacement field.

Finally, we briefly discuss the efficiency of our MOR approach. We report in Table 6.3 the online time related to the POD-G and POD-ANN methods for all the experiments carried out.

(a) FOM solution related to the problem $(WM2M)_h$

(b) FOM solution related to the problem $(WM2T)_h$

(c) FOM solution related to the problem $(WM2)_h$

(d) POD-G solution related to the problem $(WM2M)_h$

(e) POD-G solution related to the problem $(WM2T)_h$
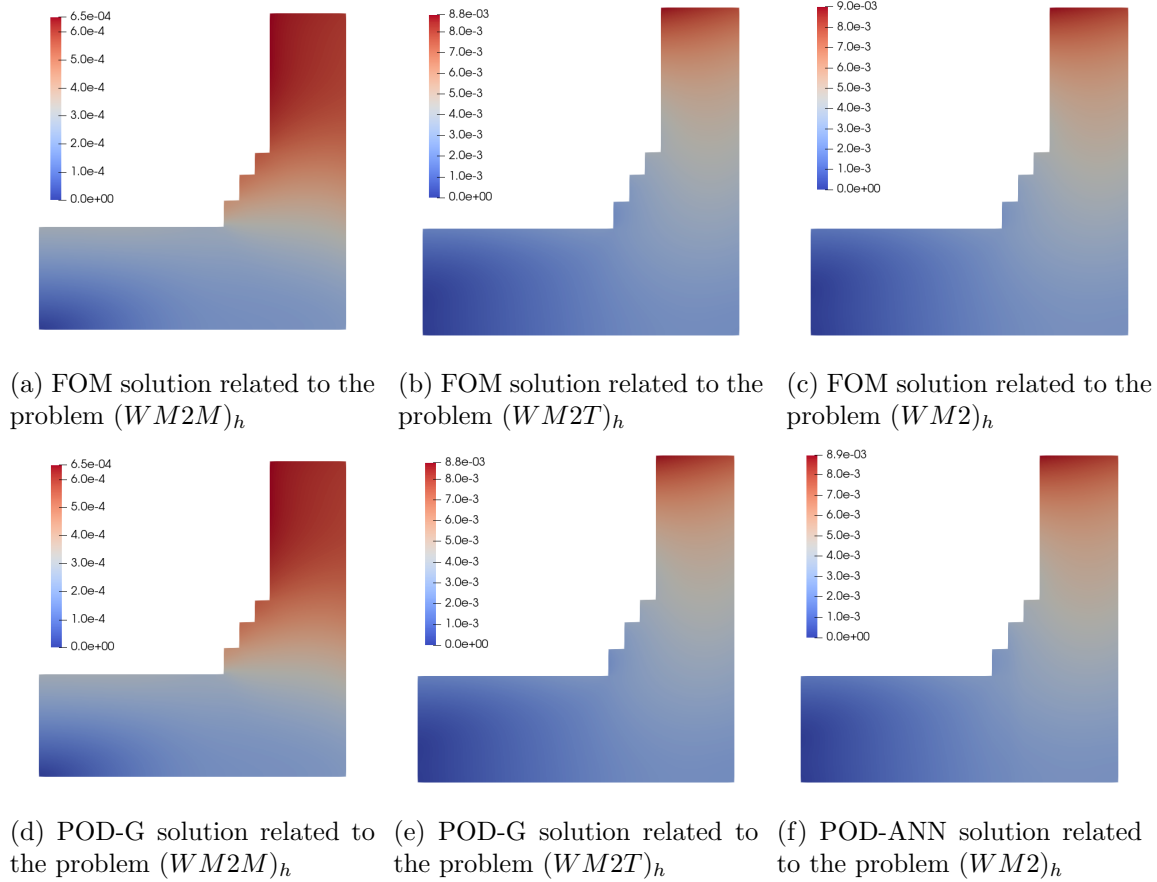
(f) POD-ANN solution related to the problem $(WM2)_h$

Figure 6.9: Mechanical model: comparison between the displacement (in m) computed by FOM and by the POD-G and POD-ANN methods related to the experiment (iv) for $\Xi = \{2.365, 0.6, 0.6, 0.5, 3.2, 14.10, 8.50, 9.2, 9.9, 10.6, 10, 2.08e9, 1.39e9, 1e-6\}$. We consider 7 POD modes. For POD-ANN, we set $n_{tr} = 2500$ and $H = 130$.

Like the thermal model, the online time of POD-G method increases significantly in the presence of geometric parameters by moving from $8e-4$ s (experiment (i)) to $2.6/6.9e-2$ s (experiments (ii)-(iv)) for the model $(WM2M)_h$ and from $4.5e-2$ s (experiment (i)) to $1.9/2.6e-1$ s (experiments (ii)-(iv)) for the model $(WM2T)_h$. We could observe that the online time taken by the model $(WM2T)_h$ is significantly greater than that taken by the model $(WM2M)_h$. This is expected because for the model $(WM2T)_h$ a reduced basis approximation of temperature needs to be computed due to the thermomechanical coupling. On the other hand, the POD-ANN, that does not need reduced basis approximation of temperature thanks to its non intrusive nature, is able to provide a higher computational efficiency. Moreover, like the thermal model, the POD-ANN online time remains relatively

experiment	Basis size	POD-G $(WM2M)_h$	POD-G $(WM2T)_h$	POD-ANN $(WM2)_h$
(i)	1	8e-4	4.5e-2	6.7e-4
(ii)	3	2.6e-2	1.9e-1	5.3e-4
(iii)	4	5.4e-2	2.1e-1	5.2e-4
(iv)	7	6.9e-2	2.6e-1	4.9e-4

Table 6.3: Mechanical model: online time (in s) for all the experiments under investigation. Concerning POD-ANN, we use $n_{tr} = 500, H = 60$ for the experiment (i), $n_{tr} = 500, H = 80$ for the experiment (ii), $n_{tr} = 1000, H = 170$ for the experiment (iii) and $n_{tr} = 2500, H = 130$ for the experiment (iv).

constant for all the experiments under investigations, around $5e-4$, by showing a low sensitivity at varying of the kind and number of parameters considered.

In this first part of the thesis, we developed axisymmetric thermomechanical model, which was solved using finite element method. In next part, we introduce further complexities to make thermomechanical model more realistic. In addition, we apply the POD-ANN approach, introduced in this chapter, to the complex thermomechanical model.

Part II

Thermomechanical model with temperature dependent material properties, presence of different materials and orthotropy

Chapter 7

Thermomechanical model and weak formulation

We now relax some of the assumptions introduced in Part I. The assumptions were aimed at simplifying the real model. By relaxing these assumptions, we shift our focus to a thermomechanical model, characterised by complexities such as non-linearity due to temperature dependence of material properties, presence of different materials and homogenization of subdomains replacing periodic assembly of different materials with an equivalent orthotropic material. We discuss the domain and the governing equations alongwith temperature dependence of material properties and homogenization to identify equivalent orthotropic material for ceramic cup from periodic assembly of bricks and mortar (Section 7.1). Subsequently, in section 7.2, we introduce the governing equations in cylindrical coordinates. Finally, we discuss the axisymmetry hypothesis (Section 7.3) and corresponding weak formulation (Section 7.4).

7.1   Domain and governing equations

Blast furnace hearth is made up of different materials: standard carbon, micropore carbon, super-micropore carbon, ceramic cup, corondum brick and steel shell. The material selection is based on the suitability of material properties to the blast furnace operating conditions, in order to control the temperature profile within the system. We consider three dimensional domain Ω as in Figure 7.1. The domain is divided into 6 non-overlapping subdomains based on the material of each subdomain:

$$\bar{\Omega} = \bar{\Omega}_{sc} \cup \bar{\Omega}_{mc} \cup \bar{\Omega}_{smc} \cup \bar{\Omega}_{cc} \cup \bar{\Omega}_{cb} \cup \bar{\Omega}_{ss} \ .$$

Each of the subdomains corresponds to different material except the ceramic cup:

$$\text{Standard carbon: } \Omega_{sc} = \omega_{sc} \times [0, 2\pi) \ ,$$
$$\text{Micropore carbon: } \Omega_{mc} = \omega_{mc} \times [0, 2\pi) \ ,$$
$$\text{Super-micropore carbon: } \Omega_{smc} = \omega_{smc} \times [0, 2\pi) \ ,$$
$$\text{Ceramic cup: } \Omega_{cc} = \omega_{cc} \times [0, 2\pi) \ ,$$
$$\text{Corondum brick: } \Omega_{cb} = \omega_{cb} \times [0, 2\pi) \ ,$$
$$\text{Steel shell: } \Omega_{ss} = \omega_{ss} \times [0, 2\pi) \ .$$

Ceramic cup is periodic assembly of brick and mortar,

$$\bar{\Omega}_{cc} = \bar{\Omega}_{br} \cup \bar{\Omega}_{mo} \ ,$$

where, Ω_{br} and Ω_{mo} represent the open subdomains corresponding to brick and mortar respectively. Each of the above subdomains are further divided into triangular subdomains (Figure 8.1) such that the domain Ω is divided into n_{su} subdomains,

$$\bar{\Omega} = \bigcup_{i}^{n_{su}} \bar{\Omega}_i \ , \Omega_i \cap \Omega_j = \emptyset \ , \text{ for } i \neq j \ , \ 1 \leq i, j \leq n_{su} \ ,$$

in accordance with the geometric parametrization introduced later.

The governing equation for the thermal model is given by,

$$-Div(\boldsymbol{K}(T(x), x)\nabla T(x)) = Q(x) \ , \ x \in \Omega \ , \tag{7.1}$$

assuming the natural continuity for temperature and heat flux at the inner boundaries.

Thermal conductivity is given by:

$$\boldsymbol{K}(s, x) = \boldsymbol{K}^{(i)}(s) \text{ if } x \in \Omega_i \text{ and } s \in \mathbb{R} \ . \tag{7.2}$$

The governing equation for mechanical model is given by,

$$-Div(\boldsymbol{\sigma}) = \overrightarrow{f_0} \text{ in } \Omega \ , \tag{7.3}$$

assuming natural continuity of displacement and the action-reaction principle at each inner interface.

Since the temperature T and heat flux $\overrightarrow{q} \cdot \overrightarrow{n}$ are continuous, the gradient of temperature ∇T is discontinuous along the interfaces. Similarly, the continuity of $\overrightarrow{u}$ and stress vector $\boldsymbol{\sigma}\overrightarrow{n}$ results in discontinuity of strain tensor along the interfaces. For any two neighboring subdomains ω_i, ω_j , $i \neq j$, with outward pointing normal vectors $\overrightarrow{n}_i = -\overrightarrow{n}_j$ and their interface $\gamma_{ij} = \partial\omega_i \cap \partial\omega_j$ (Figure 7.2), following interface conditions are imposed:
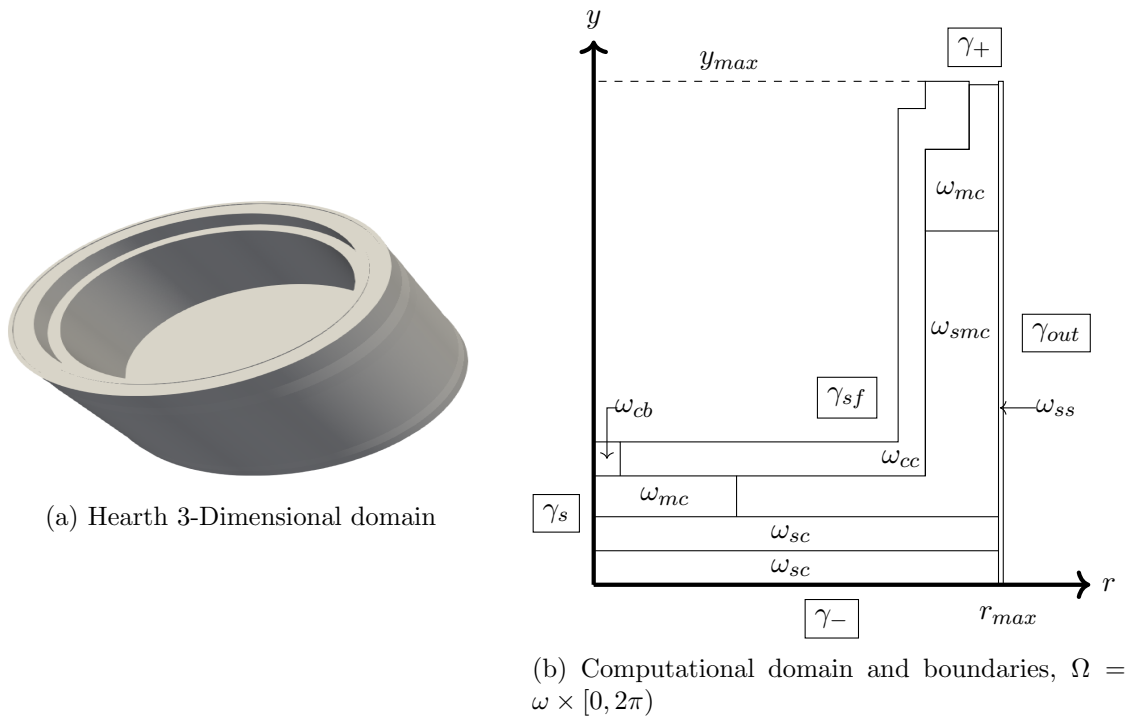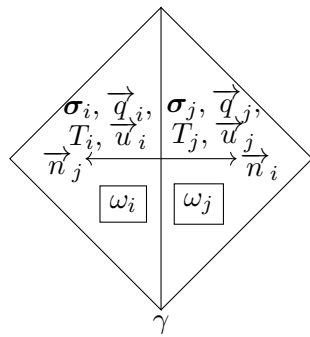
(a) Hearth 3-Dimensional domain

(b) Computational domain and boundaries, $\Omega = \omega \times [0, 2\pi)$

Figure 7.1: Blast furnace hearth

Figure 7.2: Subdomain interface

- Continuity of heat flux:

$$\overrightarrow{q}_i \cdot \overrightarrow{n}_i|_{\gamma_{ij}} = -\overrightarrow{q}_j \cdot \overrightarrow{n}_j|_{\gamma_{ij}} . \tag{7.4}$$

- Action-reaction principle:

$$\boldsymbol{\sigma}_i \overrightarrow{n}_i|_{\gamma_{ij}} = -\boldsymbol{\sigma}_j \overrightarrow{n}_j|_{\gamma_{ij}} . \tag{7.5}$$

- Continuity of temperature field and displacement field:

$$T_i|_{\gamma_{ij}} = T_j|_{\gamma_{ij}} , \quad \overrightarrow{u}_i|_{\gamma_{ij}} = \overrightarrow{u}_j|_{\gamma_{ij}} . \tag{7.6}$$

As the materials under consideration are either orthotropic or isotropic, the thermomechanical stress tensor $\boldsymbol{\sigma}$ is related to the strain tensor in vector form as:

$$\{\boldsymbol{\varepsilon}(\overrightarrow{u})(x)\} = \boldsymbol{S}(T(x), x)\{\boldsymbol{\sigma}(x)\} + \alpha(x)(T(x) - T_0)\{\boldsymbol{I}\} , \tag{7.7}$$

where all materials are considered isotropic (as in Chapter 2), except the ceramic cup that is orthotropic:

$$\boldsymbol{S} = \begin{bmatrix} \frac{1}{E_1} & \frac{-\nu_{21}}{E_2} & \frac{-\nu_{31}}{E_3} & 0 & 0 & 0 \\ \frac{-\nu_{12}}{E_1} & \frac{1}{E_2} & \frac{-\nu_{32}}{E_3} & 0 & 0 & 0 \\ \frac{-\nu_{13}}{E_1} & \frac{-\nu_{23}}{E_2} & \frac{1}{E_3} & 0 & 0 & 0 \\ 0 & 0 & 0 & \frac{1}{\mu_{23}} & 0 & 0 \\ 0 & 0 & 0 & 0 & \frac{1}{\mu_{13}} & 0 \\ 0 & 0 & 0 & 0 & 0 & \frac{1}{\mu_{12}} \end{bmatrix} , \text{ in } \Omega_{cc} , \tag{7.8}$$

with the property,

$$\frac{\nu_{ij}}{E_i} = \frac{\nu_{ji}}{E_j} , \text{ for } i, j = 1, 2, 3 . \tag{7.9}$$

The inverse of stiffness matrix $\boldsymbol{S}$ is the compliance matrix $\boldsymbol{C}$ i.e. $\boldsymbol{S} = \boldsymbol{C}^{-1}$. The strain tensor is defined as:

$$\varepsilon(\overrightarrow{u}) = \frac{1}{2}\left(\nabla\overrightarrow{u} + \nabla\overrightarrow{u}^T\right) . \tag{7.10}$$

In case i^{th} subdomain Ω_i corresponds to ceramic cup with Young's modulus $E_n^{(i)}$ and Poisson's ratio $\nu_{nm}^{(i)}$:

$$E_n(s, x) = E_n^{(i)}(s) , \quad \nu_{nm}(s, x) = \nu_{nm}^{(i)}(s) , \quad n, m = 1, 2, 3 , \quad x \in \Omega_i , \quad s \in \mathbb{R} .$$

In case i^{th} subdomain Ω_i corresponds to isotropic material with Young's modulus $E^{(i)}$ and Poisson's ratio $\nu^{(i)}$:

$$E_n(s, x) = E^{(i)}(s) , \quad \nu_{nm}(s, x) = \nu^{(i)}(s) , \quad n, m = 1, 2, 3 , \quad x \in \Omega_i , \quad s \in \mathbb{R} .$$

Thermal expansion coefficient α is scalar and independent of the temperature for all materials under consideration. Thermal expansion coefficient corresponding to i^{th} subdomain is given by $\alpha^{(i)}$:

$$\alpha(x) = \alpha^{(i)}(x) , \quad x \in \Omega_i .$$

7.1.1 Boundary conditions

In the following, we state the boundary conditions on the domain Ω considering heterogeneity and temperature dependence of material properties. We recall the definition of normal force σ_n and tangential force $\overrightarrow{\sigma_t}$ from equation (2.30). On Ω, and therefore on ω, the following boundaries need to be identified,

$$\Gamma_{out} = \partial\Omega \cap (r \equiv r_{max}) = \gamma_{out} \times [0, 2\pi) \ ,$$
$$\Gamma_+ = \partial\Omega \cap (y \equiv y_{max}) = \gamma_+ \times [0, 2\pi) \ ,$$
$$\Gamma_- = \partial\Omega \cap (y \equiv 0) = \gamma_- \times [0, 2\pi) \ ,$$
$$\Gamma_{sf} = \partial\Omega \backslash (\Gamma_{out} \cup \Gamma_+ \cup \Gamma_-) = \gamma_{sf} \times [0, 2\pi) \ ,$$
$$\gamma_s = \partial\omega \cap (r \equiv 0) \ ,$$

where, $r_{max} \in \mathbb{R}^+$ and $y_{max} \in \mathbb{R}^+$.

- On the upper boundary, Γ_+, the applied tangential force, $\overrightarrow{g}_+$, and the density of heat flux, q_+, are known. Therefore, on Γ_+, the following boundary conditions are considered:

$$(-\boldsymbol{K}(T(x), x)\nabla T(x)) \cdot \overrightarrow{n} = q_+(x) \ , \quad \overrightarrow{\sigma}_t = \overrightarrow{g}_+ \ , \quad \overrightarrow{u} \cdot \overrightarrow{n} = 0 \ . \tag{7.11}$$

  Here, q_+ is the heat flux flowing from the upper boundary.

- On the bottom boundary, Γ_-, convection heat transfer with heat exchanger at temperature T_- and heat transfer coefficient $h_{c,-}$ occurs. We also apply zero displacement at bottom boundary. Therefore, on Γ_-, it is verified:

$$(-\boldsymbol{K}(T(x), x)\nabla T(x)) \cdot \overrightarrow{n} = h_{c,-}(x)(T(x) - T_-(x)) \ , \quad \overrightarrow{u} = \overrightarrow{0} \ . \tag{7.12}$$

- On the inner boundary, Γ_{sf}, convection heat transfer with the fluid phase occurs and hydrostatic pressure due to fluid is acting on the surface. Hence, on this boundary the following boundary conditions are considered:

$$(-\boldsymbol{K}(T(x), x)\nabla T(x)) \cdot \overrightarrow{n} = h_{c,f}(x)(T(x) - T_f(x)) \ ,$$
$$\boldsymbol{\sigma}\overrightarrow{n} = -p\overrightarrow{n} = -\rho_m g h \overrightarrow{n} = \overrightarrow{g}_{sf} \ . \tag{7.13}$$

  Here, T_f is the fluid temperature, assumed to be known and constant at the steady state, and $h_{c,f}$ the convective heat transfer coefficient on Γ_{sf}. The density of fluid ρ_m, gravitational acceleration g, and the maximum height of the fluid column on the blast furnace inner wall Γ_{sf}, that is h, are known and used to compute hydrostatic pressure through (7.13).

- On the outer boundary, Γ_{out}, a convective heat flux and known applied force $\overrightarrow{g}_{out}$ are assumed:

$$(-\boldsymbol{K}(T(x),x)\nabla T(x)) \cdot \overrightarrow{n} = h_{c,out}(x)(T(x) - T_{out}(x)) \ , \ \boldsymbol{\sigma}\overrightarrow{n} = \overrightarrow{g}_{out} \ . \qquad (7.14)$$

Here, $h_{c,out}$ being the convective heat transfer coefficient on Γ_{out}, and T_{out} the ambient temperature.

7.1.2   Material properties

In the case of thermomechanical problems with temperature dependent material properties, it is not possible to experimentally measure material properties at each temperature. Instead, material properties are measured at few intermediate temperatures and polynomial interpolation is used to approximate the material properties at all temperatures. Quadratic spline interpolation is used in the present work to obtain thermal conductivity and Young's modulus at intermediate temperatures such that the material properties as the function of temperature are smooth enough (see figure 7.3). Splines allow piecewise interpolation with global smoothness [74]. Tables 7.1 - 7.4, show the available material data. We note that thermal conductivity for steel shell, mortar and corondum brick; Young's modulus for steel shell and mortar; Poisson's ratio and thermal expansion coefficient were considered constant with respect to temperature.

Thermal conductivity k		
Material	Temperature $T(K)$	$k\left(\frac{W}{mK}\right)$
Standard carbon	293	15
	473	15.2
	873	16.2
	1273	15.1
Micropore carbon	293	35.8
	473	37.3
	873	42.7
	1273	15.2
Super-micropore carbon	293	19.2
	473	18.6
	873	20.7
	1273	21.3
Steel shell		48
Mortar		3.5
Corondum brick		5.5

Table 7.1: Thermal conductivities at various temperatures for isotropic materials

Young's modulus E		
Material	Temperature $T(K)$	$E(GPa)$
Standard carbon	293	9.88
	573	9.79
	1073	9.72
	1273	9.98
Micropore carbon	293	13.3
	573	13.6
	1073	14.7
	1273	15.4
Super-micropore carbon	293	13.7
	573	13.1
	1073	14.4
	1273	15.3
Corondum brick	293	31.9
	573	53.5
	1073	74.4
	1273	82.3
Steel shell		200
Mortar		0.01

Table 7.2: Young's modulus at various temperatures for isotropic materials

Poisson's ratio ν	
Material	ν
Standard Carbon	0.30
Micropore Carbon	0.20
Super-micropore Carbon	0.20
Steel shell	0.25
Mortar	0.20
Corondum brick	0.08

Table 7.3: Poisson's ratio for isotropic materials

Thermal expansion coefficient α	
Material	$\alpha(K^{-1})$
Standard Carbon	2.5e-06
Micropore Carbon	4.56e-06
Super-micropore Carbon	6.04e-06
Steel shell	11.55e-06
Mortar	4.50E-06
Corondum brick	4.66E-06

Table 7.4: Thermal expansion coefficient for isotropic materials

(a) Thermal conductivity vs Temperature   (b) Young's modulus vs Temperature
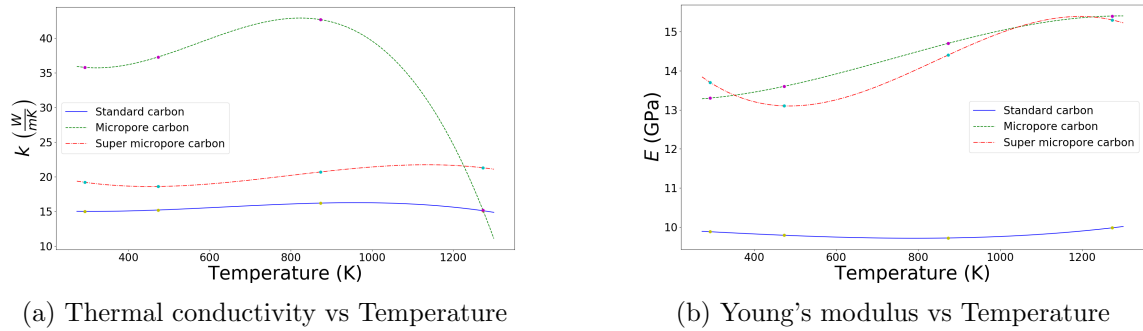
Figure 7.3: Interpolation of thermal conductivity and Young's modulus with respect to temperature

7.1.3   Homogenization

Homogenization is a process used for identifying an equivalent orthotropic material from the periodic assembly of homogeneous isotropic materials. In the context of blast furnace hearth, the ceramic cup is made up of mortar and bricks (Figure 7.4). We replace this periodic assembly of mortar and bricks with equivalent orthotropic material (Figure 7.5). The idea is to estimate stiffness tensor $\boldsymbol{S}$ and thermal conductivity $\boldsymbol{K}$ for the ceramic cup subdomain Ω_{cc} representing equivalent material. As can be seen in Table 7.4, there is very small difference between thermal expansion coefficient of these two materials and hence, we do not consider the homogenization for thermal expansion coefficient.

We refer to work [7] for homogenization of Lamé parameters corresponding to the ceramic cup of our interest. For the subdomain Ω_{cc}, authors estimate 36 components of the stiffness matrix $\boldsymbol{S}$ from equation (7.7). They start with an assumption that the stiffness matrix is not symmetric, hence they compute all 36 components and assess whether the computed stiffness matrix is symmetric, subject to round-off errors. For estimating the 36 components of the stiffness matrix, authors numerically perform 3 compression stress

test and 3 shear stress test on a Representative Unit Cell (RUC), which represents whole assembly when repeated along 3 directions, computing 6 stress-strain components in each test. Details of the procedure followed can be found in article [7]. The values included for the equivalent material in this section have been obtained thanks to the collaboration of the co-authors of [7] for this purpose. As can be seen from the table 7.2, Young's modulus of brick varies with temperature while Young's modulus of mortar remains constant. Also, Poisson's ratio of corondum brick and Poisson's ratio of mortar remain constant w.r.t. temperature (Table 7.3). Accordingly, the tests are performed at discrete temperature values and equivalent material properties are computed at these discrete temperature values. For intermediate temperature values, the material properties are interpolated using quadratic spline interpolation (Figure 7.6).

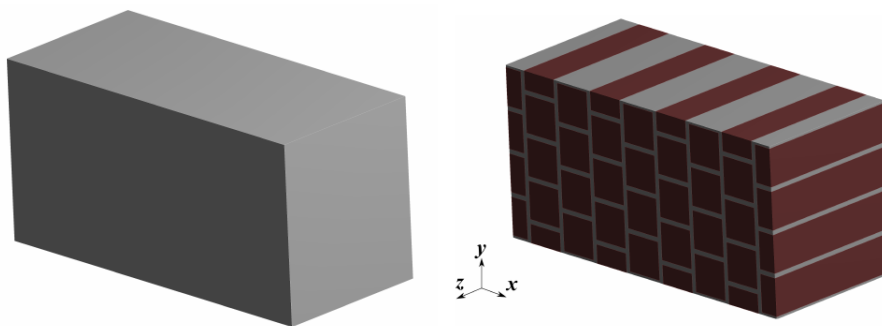Figure 7.4: Ceramic cup [Courtesy: ArcelorMittal]

Figure 7.5: Equivalent orthotropic material (left) from periodic assembly of brick and mortar (right) [7]

For thermal conductivity, we need to estimate 9 components of thermal conductivity. Considering the same unit cell, 3 numerical tests for heat conduction equation were perfomed to compute heat flux and gradient of temperature in each test. It is preferable to adjust the parameters of these tests such that the material response to applied heat flux is measured in three perpendicular directions. Since the thermal conductivity of corondum brick and thermal conductivity of mortar do not vary with temperature, the numerical tests were only performed once with properties reported in Table 7.1.

For the thermal expansion coefficient, it is possible to estimate the equivalent thermal expansion coefficient for equivalent material. However, considering that the values of thermal expansion coefficient for mortar and thermal expansion coefficient for corondum brick are almost equal, we do not perform the homogenization and approximate the thermal expansion coefficient of equivalent material as arithmetic mean of brick and mortar thermal expansion coefficients.

The equivalent properties corresponding to equivalent orthotropic material representing ceramic cup are reported in table 7.5. The quadratic spline interpolation for E_3 and ν_{31} is shown in figure 7.6.

Temperature (K)	Young's modulus $E(GPa)$	Poisson's ratio
293	$E_1 = 0.092$	$\nu_{21} = 0.08$
	$E_2 = 0.097$	$\nu_{31} = 0.13$
	$E_3 = 1.72$	$\nu_{32} = 0.13$
573	$E_1 = 0.092$	$\nu_{21} = 0.08$
	$E_2 = 0.097$	$\nu_{31} = 0.14$
	$E_3 = 1.77$	$\nu_{32} = 0.13$
1073	$E_1 = 0.092$	$\nu_{21} = 0.08$
	$E_2 = 0.097$	$\nu_{31} = 0.14$
	$E_3 = 1.79$	$\nu_{32} = 0.13$
1273	$E_1 = 0.092$	$\nu_{21} = 0.08$
	$E_2 = 0.097$	$\nu_{31} = 0.14$
	$E_3 = 1.80$	$\nu_{32} = 0.13$

(a) Young's modulus and Poisson's ratio

Thermal conductivity $\boldsymbol{K} \left(\frac{W}{Km}\right)$

$$\begin{bmatrix} 5.00 & 0.00 & 0.00 \\ 0.00 & 5.00 & 0.00 \\ 0.00 & 0.00 & 5.09 \end{bmatrix} \frac{W}{Km}$$

(b) Thermal conductivity

Thermal expansion coefficient $\alpha(K^{-1})$
4.58e-6 K^{-1}

(c) Thermal expansion coefficient

Table 7.5: Ceramic cup (Ω_{cc}) material properties

(a) E_3 vs Temperature
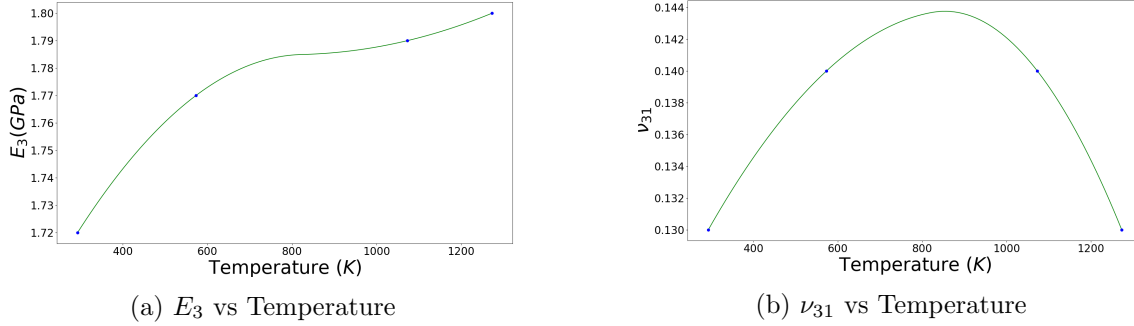

(b) ν_{31} vs Temperature

Figure 7.6: Interpolation of E_3 and ν_{31} with respect to temperature for the equivalent ceramic cup material.

7.2 Thermomechanical model in cylindrical coordinates

Following similar approach as used for the simplified model, we express now the governing equations (7.1), (7.3) and boundary conditions (7.11)-(7.14) in cylindrical coordinate system (r, y, θ) having corresponding unit vectors $(\overrightarrow{e}_r, \overrightarrow{e}_y, \overrightarrow{e}_\theta)$. The material point $x = (r, y, \theta)$, with $(r, y) \in \omega$ (Figure 7.1b), and $\theta \in [0, 2\pi)$. We use the same notation as used in Section 2.2.2.

- The normal vector will now be represented as:

$$\overrightarrow{n} = n_r \overrightarrow{e}_r + n_y \overrightarrow{e}_y + n_\theta \overrightarrow{e}_\theta \ .$$

- The body force term $\overrightarrow{f}_0$ is expressed as:

$$\overrightarrow{f}_0 = f_{0,r} \overrightarrow{e}_r + f_{0,y} \overrightarrow{e}_y + f_{0,\theta} \overrightarrow{e}_\theta \ .$$

- The displacement vector $\overrightarrow{u}$ is expressed as:

$$\overrightarrow{u} = u_r(r, y, \theta) \overrightarrow{e}_r + u_y(r, y, \theta) \overrightarrow{e}_y + u_\theta(r, y, \theta) \overrightarrow{e}_\theta \ .$$

- The thermal conductivity tensor of equivalent material for ceramic cup is given as:

$$\boldsymbol{K} = \begin{bmatrix} k_{rr} & 0 & 0 \\ 0 & k_{yy} & 0 \\ 0 & 0 & k_{\theta\theta} \end{bmatrix} = \begin{bmatrix} 5 & 0 & 0 \\ 0 & 5 & 0 \\ 0 & 0 & 5.09 \end{bmatrix} \ , \ \text{in } \Omega_{cc} \ .$$

Thermal conductivity for all other materials are given in the table 7.1.

- The temperature scalar, T, is expressed as:

$$T = T(r, y, \theta) \ .$$

- The divergence of displacement field $\overrightarrow{u}$ in cylindrical coordinate system is given by:

$$Div(u) = \frac{1}{r}\frac{\partial\left(u_r r\right)}{\partial r} + \frac{\partial u_y}{\partial y} + \frac{1}{r}\frac{\partial u_\theta}{\partial \theta} \ .$$

- The gradient of temperature field, T, in cylindrical coordinate system, is given by:

$$\nabla T = \frac{\partial T}{\partial r}\overrightarrow{e_r} + \frac{\partial T}{\partial y}\overrightarrow{e_y} + \frac{1}{r}\frac{\partial T}{\partial \theta}\overrightarrow{e_\theta} \ .$$

- The heat flux vector $\overrightarrow{q}$ is expressed as:

$$\overrightarrow{q} = q_r\,\overrightarrow{e}_r + q_y\,\overrightarrow{e}_y + q_\theta\,\overrightarrow{e}_\theta \ .$$

- The strain tensor in cylindrical coordinate system (r, y, θ) is expressed as:

$$\varepsilon(\overrightarrow{u}) = \begin{bmatrix} \frac{\partial u_r}{\partial r} & \frac{1}{2}\left(\frac{\partial u_r}{\partial y} + \frac{\partial u_y}{\partial r}\right) & \frac{1}{2}\left(\frac{\partial u_\theta}{\partial r} + \frac{1}{r}\frac{\partial u_r}{\partial \theta} - \frac{u_\theta}{r}\right) \\ \frac{1}{2}\left(\frac{\partial u_r}{\partial y} + \frac{\partial u_y}{\partial r}\right) & \frac{\partial u_y}{\partial y} & \frac{1}{2r}\left(\frac{\partial u_y}{\partial \theta} + r\frac{\partial u_\theta}{\partial y}\right) \\ \frac{1}{2}\left(\frac{\partial u_\theta}{\partial r} + \frac{1}{r}\frac{\partial u_r}{\partial \theta} - \frac{u_\theta}{r}\right) & \frac{1}{2r}\left(\frac{\partial u_y}{\partial \theta} + r\frac{\partial u_\theta}{\partial y}\right) & \frac{1}{r}\frac{\partial u_\theta}{\partial \theta} + \frac{u_r}{r} \end{bmatrix} \ .$$

- The stress tensor and strain tensor are defined in vector form as:

$$\{\boldsymbol{\sigma}\} = \{\sigma_{rr} \quad \sigma_{yy} \quad \sigma_{\theta\theta} \quad \sigma_{y\theta} \quad \sigma_{r\theta} \quad \sigma_{ry}\}^T \ ,$$
$$\{\boldsymbol{\varepsilon}\} = \{\varepsilon_{rr} \quad \varepsilon_{yy} \quad \varepsilon_{\theta\theta} \quad 2\varepsilon_{y\theta} \quad 2\varepsilon_{r\theta} \quad 2\varepsilon_{ry}\}^T \ .$$

- The stress-strain relationship is given by:

$$\{\boldsymbol{\varepsilon}\} = \boldsymbol{S}\{\boldsymbol{\sigma}\} + (T - T_0)\{\boldsymbol{\alpha}\} \ . \tag{7.15}$$

The governing equations can now be written as below:

- Stationary thermal model: The energy conservation equation (7.1) can be rewritten as:

$$\frac{1}{r}\frac{\partial\left(rq_r\right)}{\partial r} + \frac{1}{r}\frac{\partial q_\theta}{\partial \theta} + \frac{\partial q_y}{\partial y} = Q \ , \text{ in } \Omega \ . \tag{7.16}$$

Corresponding thermal boundary conditions in (7.11)-(7.14) are:

$$\begin{aligned} \text{on } \Gamma_+ \ &: -(\boldsymbol{K}\nabla T)\cdot\overrightarrow{n} = q_+ \ , \\ \text{on } \Gamma_- \ &: -(\boldsymbol{K}\nabla T)\cdot\overrightarrow{n} = h_{c,-}(T - T_-) \ , \\ \text{on } \Gamma_{sf} \ &: -(\boldsymbol{K}\nabla T)\cdot\overrightarrow{n} = h_{c,f}(T - T_f) \ , \\ \text{on } \Gamma_{out} \ &: -(\boldsymbol{K}\nabla T)\cdot\overrightarrow{n} = h_{c,out}(T - T_{out}) \ . \end{aligned} \tag{7.17}$$

- Stationary mechanical model: Equation (7.3) in cylindrical coordinates corresponds to the three following equations:

$$\frac{\partial \sigma_{rr}}{\partial r} + \frac{\partial \sigma_{ry}}{\partial y} + \frac{1}{r}\frac{\partial \sigma_{r\theta}}{\partial \theta} + \frac{\sigma_{rr} - \sigma_{\theta\theta}}{r} + f_{0,r} = 0 \ , \ \text{in } \Omega \ ,$$

$$\frac{\partial \sigma_{r\theta}}{\partial r} + \frac{\partial \sigma_{\theta y}}{\partial y} + \frac{1}{r}\frac{\partial \sigma_{\theta\theta}}{\partial \theta} + 2\frac{\sigma_{r\theta}}{r} + f_{0,\theta} = 0 \ , \ \text{in } \Omega \ , \tag{7.18}$$

$$\frac{\partial \sigma_{ry}}{\partial r} + \frac{1}{r}\frac{\partial \sigma_{\theta y}}{\partial \theta} + \frac{\partial \sigma_{yy}}{\partial y} + \frac{\sigma_{ry}}{r} + f_{0,y} = 0 \ , \ \text{in } \Omega \ .$$

Corresponding mechanical boundary conditions introduced in (7.11)-(7.14) are:

$$
\begin{aligned}
\text{on } \Gamma_+ \ : \ & \overrightarrow{\sigma}_t = \overrightarrow{g}_+ \ , \ \overrightarrow{u} \cdot \overrightarrow{n} = 0 \ , \\
\text{on } \Gamma_- \ : \ & \overrightarrow{u} = \overrightarrow{0} \ , \\
\text{on } \Gamma_{sf} \ : \ & \boldsymbol{\sigma}\overrightarrow{n} = \overrightarrow{g}_{sf} = -\rho_m g(y_{max} - y)\overrightarrow{n} \ , \\
\text{on } \Gamma_{out} \ : \ & \boldsymbol{\sigma}\overrightarrow{n} = \overrightarrow{g}_{out} \ .
\end{aligned} \tag{7.19}
$$

7.3 Axisymmetry hypothesis

Similar to axisymmetric hypothesis applied to simplified model (section 2.3), we can assume following:

- In the context of blast furnace application, the body force density term $\overrightarrow{f}_0$ can be expressed as,

$$\overrightarrow{f}_0 = f_{0,r}\overrightarrow{e}_r + f_{0,y}\overrightarrow{e}_y \ ,$$

  and it depends only on (r, y) coordinates.

- The applied surface forces have zero component in $\overrightarrow{e}_\theta$ direction and they do not depend on θ.

- The heat source term, Q, the heat flux density, q_+, are assumed to be only dependent on (r, y) coordinates.

- The heat transfer coefficients, $h_{c,-}, h_{c,f}, h_{c,out}$, and temperatures T_-, T_f, T_{out} are assumed to be only dependent on (r, y) coordinates.

- The reference temperature T_0 is independent of θ.

As shown by [24], axisymmetric model can give results closer to reality also under the presence of temperature dependence of material property and in the presence of equivalent orthotropic material. Hence, we consider axisymmetric hypothesis in our analysis.

We consider the two dimensional domain ω as in Figure 7.1b. The domain is divided into 6 subdomains based on the material of the subdomain:

$$\bar{\omega} = \bar{\omega}_{sc} \cup \bar{\omega}_{mc} \cup \bar{\omega}_{smc} \cup \bar{\omega}_{cc} \cup \bar{\omega}_{cb} \cup \bar{\omega}_{ss} \ .$$

Here, $\omega_{sc}, \omega_{mc}, \omega_{smc}, \omega_{cc}, \omega_{cb}, \omega_{ss}$ respectively represent the non-overlapping open subdomains corresponding to standard carbon, micropore carbon, super-micropore carbon, ceramic cup, corondum brick and steel shell. Ceramic cup is periodic assembly of brick and mortar:

$$\bar{\omega}_{cc} = \bar{\omega}_{br} \cup \bar{\omega}_{mo} \ .$$

Here, ω_{br} and ω_{mo} represent the non-overlapping open subdomains corresponding to brick and mortar respectively. Each of the above subdomains are further divided into triangular subdomains such that the domain ω is divided into n_{su} non-overlapping subdomains,

$$\bar{\omega} = \bigcup_{i=1}^{n_{su}} \bar{\omega}_i \ , \omega_i \cap \omega_j = \emptyset \ , \ \text{for } i \neq j \ , \ 1 \leq i, j \leq n_{su} \ ,$$

in accordance with the geometric parametrization introduced later.

- The normal vector will now be represented as:

$$\overrightarrow{n} = n_r \overrightarrow{e}_r + n_y \overrightarrow{e}_y \ .$$

- The displacement vector $\overrightarrow{u}$ is expressed as:

$$\overrightarrow{u} = u_r(r, y) \overrightarrow{e}_r + u_y(r, y) \overrightarrow{e}_y \ .$$

- The temperature scalar, T, is expressed as:

$$T = T(r, y) \ .$$

- The heat flux vector $\overrightarrow{q}$ is expressed as:

$$\overrightarrow{q} = q_r \overrightarrow{e}_r + q_y \overrightarrow{e}_y \ .$$

- The thermal conductivity tensor for equivalent material of ceramic cup $\boldsymbol{K}$ is now represented as:

$$\boldsymbol{K} = \begin{bmatrix} k_{rr} & 0 \\ 0 & k_{yy} \end{bmatrix} = \begin{bmatrix} 5 & 0 \\ 0 & 5 \end{bmatrix} = 5\boldsymbol{I} \ , \ \text{in } \Omega_{cc} \ .$$

Accordingly, thermal conductivity for any material can now be written as:

$$\boldsymbol{K}^{(i)} = k^{(i)}\boldsymbol{I} \ , \ 1 \leq i \leq n_{su} \ .$$

- The strain tensor is given by:

$$\varepsilon(\overrightarrow{u}) = \begin{bmatrix} \frac{\partial u_r}{\partial r} & \frac{1}{2}\left(\frac{\partial u_r}{\partial y} + \frac{\partial u_y}{\partial r}\right) & 0 \\ \frac{1}{2}\left(\frac{\partial u_r}{\partial y} + \frac{\partial u_y}{\partial r}\right) & \frac{\partial u_y}{\partial y} & 0 \\ 0 & 0 & \frac{u_r}{r} \end{bmatrix} .$$

- The stress tensor and strain tensor are defined in vector form as:

$$\{\boldsymbol{\sigma}\} = \{\sigma_{rr} \quad \sigma_{yy} \quad \sigma_{\theta\theta} \quad \sigma_{ry}\}^T ,$$
$$\{\boldsymbol{\varepsilon}\} = \{\varepsilon_{rr} \quad \varepsilon_{yy} \quad \varepsilon_{\theta\theta} \quad 2\varepsilon_{ry}\}^T .$$

- The stress-strain relationship is given by:

$$\{\boldsymbol{\varepsilon}\} = \boldsymbol{S}\{\boldsymbol{\sigma}\} + (T - T_0)\alpha\{\boldsymbol{I}\} . \tag{7.20}$$

- The stiffness matrix for ceramic material is given by,

$$\boldsymbol{S} = \begin{bmatrix} \frac{1}{E_1} & \frac{-\nu_{21}}{E_2} & \frac{-\nu_{31}}{E_3} & 0 \\ \frac{-\nu_{12}}{E_1} & \frac{1}{E_2} & \frac{-\nu_{32}}{E_3} & 0 \\ \frac{-\nu_{13}}{E_1} & \frac{-\nu_{23}}{E_2} & \frac{1}{E_3} & 0 \\ 0 & 0 & 0 & \frac{1}{\mu_{12}} \end{bmatrix} , \text{ in } \omega_{cc} , \tag{7.21}$$

  with material properties reported in the Section 7.1.3. Since, all other materials are isotropic, the stiffness matrix for these materials are given same as the equation (2.58) with the material properties as reported in the Section 7.1.2.

- Symmetry boundary conditions are applied on γ_s.

The governing equations can now be written as below.

- Stationary thermal model (T2):

$$\frac{1}{r}\frac{\partial(rq_r)}{\partial r} + \frac{\partial q_y}{\partial y} = Q , \text{ in } \omega . \tag{7.22}$$

Corresponding thermal boundary conditions along with interface conditions at the interface of different subdomains are:

$$\begin{aligned} \text{on } \gamma_+ &: -(k\nabla T) \cdot \overrightarrow{n} = q_+ , \\ \text{on } \gamma_- &: -(k\nabla T) \cdot \overrightarrow{n} = h_{c,-}(T - T_-) , \\ \text{on } \gamma_{sf} &: -(k\nabla T) \cdot \overrightarrow{n} = h_{c,f}(T - T_f) , \\ \text{on } \gamma_{out} &: -(k\nabla T) \cdot \overrightarrow{n} = h_{c,out}(T - T_{out}) , \\ \text{on } \gamma_s &: -(k\nabla T) \cdot \overrightarrow{n} = 0 , \\ \text{on } \gamma_{ij} &: T_i|_{\gamma_{ij}} = T_j|_{\gamma_{ij}} , \quad \overrightarrow{q}_i \cdot \overrightarrow{n}_i|_{\gamma_{ij}} = -\overrightarrow{q}_j \cdot \overrightarrow{n}_j|_{\gamma_{ij}} . \end{aligned} \tag{7.23}$$

- Stationary mechanical model (M2):

$$
\begin{aligned}
\frac{\partial \sigma_{rr}}{\partial r} + \frac{\partial \sigma_{ry}}{\partial y} + \frac{\sigma_{rr} - \sigma_{\theta\theta}}{r} + f_{0,r} = 0 \ , \ \text{in } \omega \ , \\
\frac{\partial \sigma_{ry}}{\partial r} + \frac{\partial \sigma_{yy}}{\partial y} + \frac{\sigma_{ry}}{r} + f_{0,y} = 0 \ , \ \text{in } \omega \ .
\end{aligned}
\tag{7.24}
$$

Corresponding mechanical boundary conditions along with interface conditions at the interface of different subdomains are:

$$
\begin{aligned}
\text{on } \gamma_+ \ : \ & \overrightarrow{\sigma}_t = \overrightarrow{g}_+ \ , \ \overrightarrow{u} \cdot \overrightarrow{n} = 0 \ , \\
\text{on } \gamma_- \ : \ & \overrightarrow{u} = \overrightarrow{0} \ , \\
\text{on } \gamma_{sf} \ : \ & \sigma_{rr} n_r + \sigma_{ry} n_y = -\rho_m g(y_{max} - y) n_r \ , \\
& : \ \sigma_{yr} n_r + \sigma_{yy} n_y = -\rho_m g(y_{max} - y) n_y \ , \\
\text{on } \gamma_{out} \ : \ & \sigma_{rr} n_r + \sigma_{ry} n_y = g_{out,r} \ , \\
& : \ \sigma_{yr} n_r + \sigma_{yy} n_y = g_{out,y} \ , \\
\text{on } \gamma_s \ : \ & \overrightarrow{\sigma}_t = \overrightarrow{0} \ , \ \overrightarrow{u} \cdot \overrightarrow{n} = 0 \ , \\
\text{on } \gamma_{ij} \ : \ & \overrightarrow{u}_i|_{\gamma_{ij}} = \overrightarrow{u}_j|_{\gamma_{ij}} \ , \ \boldsymbol{\sigma}_i \overrightarrow{n}_i|_{\gamma_{ij}} = -\boldsymbol{\sigma}_j \overrightarrow{n}_j|_{\gamma_{ij}} \ .
\end{aligned}
\tag{7.25}
$$

7.4   Weak formulation

We now derive the axisymmetric weak formulation for the axisymmetric thermomechanical model. We use weighted Sobolev spaces in our analysis (Section 3.1). As compared to the simplified model, below are significant changes:

- The presence of non-linearity in thermal model and use of Newton's method require additional smoothness of thermal conductivity with respect to temperature.

- Heterogeneity due to different materials in contact with each other and corresponding interface conditions are the reason for discontinuity in gradient of temperature and strain tensor across the interface of neighboring subdomains.

7.4.1   Thermal model

Before discussing the weak formulation for the thermal model (T2), introduced in the Section 7.3, the following space $\mathbb{T}$ for the admissible temperature field is considered,

$$
\mathbb{T} = \{\psi \in L_r^2(\omega) \ , \ \tilde{\psi}_i \in H_r^1(\omega_i) \ , \ \tilde{\psi}_i|_{\gamma_{ij}} = \tilde{\psi}_j|_{\gamma_{ij}}\} \ ,
$$

where, γ_{ij} denotes the common edge between two neighboring subdomains, such that,

$$
\gamma_{ij} = \partial \omega_i \cap \partial \omega_j \neq \emptyset \ , \ \forall 1 \leq i, j \leq n_{su} \ ,
$$

and $\tilde{\psi}_i$ denotes the restriction of ψ to ω_i. It is equipped with the norm:

$$||\psi||_{\mathbb{T}}^2 = \left(\sum_{i=1}^{n_{su}} ||\tilde{\psi}_i||_{H_r^1(\omega_i)}^2 \right) .$$

We assume the following hypotheses on the thermal data:

(TH1) The heat source term, Q, verifies:

$$Q \in L_r^2(\omega) .$$

(TH2) The convection temperatures belong to the spaces:

$$T_{sf} \in L_r^2(\gamma_{sf}) , \ T_- \in L_r^2(\gamma_-) , \ T_{out} \in L_r^2(\gamma_{out}) .$$

(TH3) The boundary heat flux verifies:

$$q_+ \in L_r^2(\gamma_+) .$$

(TH4) There exists a constant $k_0 > 0$, such that all thermal conductivities, $k^{(i)}$, are positive:

$$k^{(i)}(s) \geq k_0 > 0 , \ s \in \mathbb{R} , \ 1 \leq i \leq n_{su} .$$

(TH5) There exist constants $h_{c,f,0} > 0, h_{c,out,0} > 0, h_{c,-,0} > 0$ such that:

$$h_{c,f}(r, y) \in L^\infty(\gamma_{sf}) , \ h_{c,f}(r, y) > h_{c,f,0} , \ \text{on } \gamma_{sf} ,$$
$$h_{c,out}(r, y) \in L^\infty(\gamma_{out}) , \ h_{c,out}(r, y) > h_{c,out,0} \text{ on } \gamma_{out} ,$$
$$h_{c,-}(r, y) \in L^\infty(\gamma_-) , \ h_{c,-}(r, y) > h_{c,-,0} , \ \text{on } \gamma_- .$$

In order to propose a weak formulation for the thermal model (7.22) and (7.23), in the following we assume sufficient regularity to perform the following calculations. Multiplying equation (7.22) by $r\psi, \psi \in \mathbb{T}$ gives,

$$\psi \frac{\partial r q_r}{\partial r} + r\psi \frac{\partial q_y}{\partial y} = \psi Q r ,$$

$$\frac{\partial(\psi r q_r)}{\partial r} - r q_r \frac{\partial \psi}{\partial r} + \frac{\partial(r\psi q_y)}{\partial y} - q_y \frac{\partial(r\psi)}{\partial y} = \psi Q r ,$$

and integrating gives,

$$\sum_{i=1}^{n_{su}} \int_{\omega_i} div(r\psi \overrightarrow{q})drdy - \sum_{i=1}^{n_{su}} \int_{\omega_i} \overrightarrow{q} : \nabla \psi r drdy = \sum_{i=1}^{n_{su}} \int_{\omega_i} \psi Q r drdy .$$

By applying Gauss-Divergence theorem, we get:

$$\sum_{i=1}^{n_{su}} \int_{\partial\omega_i\backslash\partial\omega} \psi\overrightarrow{q}\cdot\overrightarrow{n}rdrdy - \sum_{i=1}^{n_{su}} \int_{\omega_i} \overrightarrow{q}:\nabla\psi rdrdy + \int_{\partial\omega} \psi\overrightarrow{q}\cdot\overrightarrow{n}rdrdy = \int_\omega \psi Qrdrdy \ .$$

Notice that the first integral on the left hand side is zero due to interface conditions (Section 7.1). Considering, $\overrightarrow{q} = -k\nabla T$,

$$\sum_{i=1}^{n_{su}} \int_{\omega_i} k^{(i)}\nabla T:\nabla\psi rdrdy - \int_{\partial\omega} \psi(k\nabla T)\cdot\overrightarrow{n}rdrdy = \int_\omega \psi Qrdrdy \ ,$$

and using boundary conditions (equation (7.23)), we get,

$$\sum_{i=1}^{n_{su}} \int_{\omega_i} k^{(i)}(T)\nabla T:\nabla\psi rdrdy + \int_{\gamma_{sf}} h_{c,f}\psi Trdrdy + \int_{\gamma_-} h_{c,-}\psi Trdrdy$$

$$+ \int_{\gamma_{out}} h_{c,out}\psi Trdrdy = \int_\omega \psi rQdrdy + \int_{\gamma_{sf}} h_{c,f}\psi T_f rdrdy \qquad (7.26)$$

$$+ \int_{\gamma_-} h_{c,-}\psi T_- rdrdy + \int_{\gamma_{out}} h_{c,out}\psi T_{out}rdrdy - \int_{\gamma_+} \psi q^+ rdrdy \ .$$

It can be noted that under assumptions (TH1)-(TH5), all integrals of the proposed weak formulation are well defined. The left hand side of the equation (7.26) contains non-linear as well as bilinear terms. We introduce the operators:

$$a_T(T,\psi) = \sum_{i=1}^{n_{su}} \int_{\omega_i} k^{(i)}(T)\nabla T:\nabla\psi rdrdy \ ,$$

$$c_T(T,\psi) = \int_{\gamma_{sf}} h_{c,f}\psi Trdrdy + \int_{\gamma_-} h_{c,-}\psi Trdrdy + \int_{\gamma_{out}} h_{c,out}\psi Trdrdy \ ,$$

$$l_T(\psi) = \int_\omega \psi rQdrdy + \int_{\gamma_{sf}} h_{c,f}\psi T_f rdrdy + \int_{\gamma_-} h_{c,-}\psi T_- rdrdy$$

$$+ \int_{\gamma_{out}} h_{c,out}\psi T_{out}rdrdy - \int_{\gamma_+} \psi q^+ rdrdy \ .$$

Operator a_T contains the non linear term, whereas operator c_T is bilinear and symmetric, and operator l_T is linear. We seek a solution $T \in \mathbb{T}$, which satisfies equation (7.26) for all $\psi \in \mathbb{T}$. Therefore, we propose the following weak formulation for thermal problem $(T2)$:

Problem 11 *Weak thermal formulation $(WT3)$: Under the assumptions (TH1)-(TH5), find $T \in \mathbb{T}$, such that equality (7.26) is verified for all $\psi \in \mathbb{T}$:*

$$a_T(T,\psi) + c_T(T,\psi) = l_T(\psi) \ , \ \forall\psi \in \mathbb{T} \ .$$

Newton's method for thermal model

The nonlinear equation (7.26) is solved using Newton's method [23, 75]. At iteration $\kappa + 1, \kappa > 1$, the solution of

$$\sum_{i=1}^{n_{su}} \int_{\omega_i} k^{(i)}(T^{\kappa+1}) \nabla T^{\kappa+1} : \nabla \psi r dr dy + c_T(T^{\kappa+1}, \psi) = l_T(\psi) \ , \ \forall \psi \in \mathbb{T} \ ,$$

is approached by taking a linearisation around T^κ and neglecting higher order terms of second order, so at each iteration the weak formulation to be solved is given by:

$$\sum_{i=1}^{n_{su}} \int_{\omega_i} \left(k^{(i)}(T^\kappa) \nabla T^{\kappa+1} : \nabla \psi \right) r dr dy + \sum_{i=1}^{n_{su}} \int_{\omega_i} \left(T^{\kappa+1} k^{(i)'}(T^\kappa) \nabla T^\kappa : \nabla \psi \right) r dr dy$$

$$+ c_T(T^{\kappa+1}, \psi) = l_T(\psi) + \sum_{i=1}^{n_{su}} \int_{\omega_i} T^\kappa k^{(i)'}(T^\kappa) \nabla T^\kappa : \nabla \psi r dr dy \ . \tag{7.27}$$

We define operators $J_a[T^\kappa](T^{\kappa+1}, \psi)$ and $J_l[T^\kappa](\psi)$:

$$J_a[T^\kappa](T^{\kappa+1}, \psi) = \sum_{i=1}^{n_{su}} \int_{\omega_i} \left(k^{(i)}(T^\kappa) \nabla T^{\kappa+1} : \nabla \psi \right) r dr dy$$

$$+ \sum_{i=1}^{n_{su}} \int_{\omega_i} \left(T^{\kappa+1} k^{(i)'}(T^\kappa) \nabla T^\kappa : \nabla \psi \right) r dr dy \ , \ T^\kappa, T^{\kappa+1}, \psi \in \mathbb{T} \ ,$$

$$J_l[T^\kappa](\psi) = \sum_{i=1}^{n_{su}} \int_{\omega_i} T^\kappa k^{(i)'}(T^\kappa) \nabla T^\kappa : \nabla \psi r dr dy \ , \ T^\kappa, \psi \in \mathbb{T} \ .$$

Next, we propose below weak formulation corresponding to Newton's method used for the weak thermal formulation $(WT3)$:

Problem 12 *Weak thermal formulation* $(WT4)$ *: Under the assumptions (TH1)-(TH5), and known* T^κ, $\kappa \geq 0$, *find* $T^{\kappa+1} \in \mathbb{T}$, *such that equality (7.27) is verified for all* $\psi \in \mathbb{T}$:

$$J_a[T^\kappa](T^{\kappa+1}, \psi) + c_T(T^{\kappa+1}, \psi) = l_T(\psi) + J_l[T^\kappa](\psi) \ , \ \forall \psi \in \mathbb{T} \ .$$

The choice of initial guess T^0 is crucial for convergence of the Newton's method. The residual r^κ at solution field T^κ is defined as:

$$r^\kappa(\psi) = a_T(T^\kappa, psi) + c_T(T^\kappa, \psi) - l_T(\psi) \ .$$

The Newton's method corresponding to weak formulation $(WT3)$ is stopped when either maximum number of iterations N are reached or sufficient relative residual tolerance *tol*, with respect to residual r^0 at initial guess T^0, as measured in suitable norm $||\cdot||$ is achieved:

$$\frac{||r^\kappa||}{||r^0||} \leq tol \ , \kappa < N \ . \tag{7.28}$$

7.4.2   Thermomechanical model

Before discussing the weak formulation for the mechanical model ($M2$), the following space $\mathbb{V}$ for the displacements is considered,

$$\mathbb{V} = \{ \overrightarrow{\phi} \in \left[H_r^1(\omega) \right]^2 \ , \ \varepsilon(\tilde{\phi}_i) \in \left[L_r^2(\omega_i) \right]^{3\times 3} \ , \ \tilde{\phi}_i|_{\gamma_{ij}} = \tilde{\phi}_j|_{\gamma_{ij}} \} \ ,$$

where, $\varepsilon(\tilde{\phi}_i)$ is the axisymmetric strain tensor, γ_{ij} is the common edge between two neighboring subdomains such that,

$$\gamma_{ij} = \partial\omega_i \cap \partial\omega_j \neq \emptyset \ , \ 1 \leq i,j \leq n_{su} \ ,$$

and $\tilde{\phi}_i$ is the restriction of $\overrightarrow{\phi}$ on ω_i. Its closed and convex subspace,

$$\mathbb{U} = \{ \overrightarrow{\phi} = (\phi_r \ \phi_y) \in \mathbb{V} \ , \ \overrightarrow{\phi} = \overrightarrow{0} \text{ on } \gamma_- \ , \ \overrightarrow{\phi} \cdot \overrightarrow{n} = 0 \text{ on } \gamma_+ \ , \ \phi_r = 0 \text{ on } \gamma_s \} \ ,$$

will be the set of admissible displacements. It is equipped with the norm:

$$|| \overrightarrow{\phi} ||_{\mathbb{U}}^2 = \sum_{i=1}^{n_{su}} \left(\int_{\omega_i} \tilde{\phi}_i \cdot \tilde{\phi}_i r dr dy + \int_{\omega_i} \varepsilon(\tilde{\phi}_i) : \varepsilon(\tilde{\phi}_j) r dr dy \right) \ .$$

The function space for stress tensor is defined as:

$$\mathbb{S} = \{ \boldsymbol{\sigma} = [\sigma_{ij}] \in [L_r^2(\omega)]^{3\times 3}, \sigma_{ij} = \sigma_{ji}, \sigma_{\alpha 3} = 0 \} \ .$$

We assume the following hypotheses on the mechanical data:

(MH1) The source term $\overrightarrow{f}$ verifies:

$$\overrightarrow{f} \in [L_r^2(\omega)]^2 \ .$$

(MH2) The boundary forces verify the following regularity assumptions:

$$\overrightarrow{g}_+ \in [L_r^2(\gamma_+)]^2 \ , \ \overrightarrow{g}_{sf} \in [L_r^2(\gamma_{sf})]^2 \ , \ \overrightarrow{g}_{out} \in [L_r^2(\gamma_{out})]^2, \ \overrightarrow{g}_- \in [L_r^2(\gamma_-)]^2 \ .$$

(MH3) There exist constants $E_0 > 0, \nu_0 > 0, \nu_1 < 0.5, \alpha_0 > 0$ such that the material properties for ceramic cup verify,

$$\nu_{nm}^{(i)} \in L^\infty(\omega_i) \ , \ 0 < \nu_0 \leq \nu_{nm}^{(i)} \leq \nu_1 < 0.5 \ , \ E_n^{(i)} \in L^\infty(\omega_i) \ , \ 0 < E_0 \leq E_n^{(i)} \ ,$$
$$\alpha^{(i)} \in L^\infty(\omega_i) \ , \ 0 < \alpha_0 \leq \alpha^{(i)} \ , \ n, m = 1,2,3 \ , \ 1 \leq i \leq n_{su} \ , \ \text{in } \omega_{cc} \ ,$$

and the material properties for other isotropic materials verify,

$$\nu^{(i)} \in L^\infty(\omega_i) \ , \ 0 < \nu_0 \leq \nu^{(i)} \leq \nu_1 < 0.5 \ , \ E^{(i)} \in L^\infty(\omega_i) \ , \ 0 < E_0 \leq E^{(i)} \ ,$$
$$\alpha^{(i)} \in L^\infty(\omega_i) \ , \ 0 < \alpha_0 \leq \alpha^{(i)} \ , \ 1 \leq i \leq n_{su} \ , \ \text{in } \omega \backslash \omega_{cc} \ .$$

In order to propose a weak formulation of the mechanical model (7.24) - (7.25), we assume that all functions have sufficiently regularity as necessary for the following calculations. In equation (7.24), multiplying first equation by $r\phi_r$ and second equation by $r\phi_y$, $\overrightarrow{\phi} = (\phi_r \ \phi_y) \in \mathbb{U}$, we get:

$$r\phi_r \frac{\partial \sigma_{rr}}{\partial r} + r\phi_r \frac{\partial \sigma_{ry}}{\partial y} + \phi_r(\sigma_{rr} - \sigma_{\theta\theta}) + r\phi_r f_{0,r} = 0 \ ,$$

$$r\phi_y \frac{\partial \sigma_{ry}}{\partial r} + r\phi_y \frac{\partial \sigma_{yy}}{\partial y} + \phi_y \sigma_{ry} + r\phi_y f_{0,y} = 0 \ .$$

Adding them, it is easy obtain:

$$\frac{\partial}{\partial r}(\sigma_{rr} r\phi_r) - \sigma_{rr}\frac{\partial}{\partial r}(r\phi_r) + \frac{\partial}{\partial y}(\sigma_{ry} r\phi_r) - \sigma_{ry}\frac{\partial}{\partial y}(r\phi_r) + \phi_r\sigma_{rr} - \phi_r\sigma_{\theta\theta} + r\phi_r f_{0,r} +$$

$$\frac{\partial}{\partial r}(\sigma_{ry} r\phi_y) - \sigma_{ry}\frac{\partial}{\partial r}(r\phi_y) + \frac{\partial}{\partial y}(\sigma_{yy} r\phi_y) - \sigma_{yy}\frac{\partial}{\partial y}(r\phi_y) + \phi_y\sigma_{ry} + r\phi_y f_{0,y} = 0 \ .$$

By integrating and applying Gauss-Divergence theorem:

$$\sum_{i=1}^{n_{su}} \int_{\omega_i} \{\boldsymbol{\sigma}(\overrightarrow{u})\} : \{\boldsymbol{\varepsilon}(\overrightarrow{\phi})\} r dr dy = \int_{\omega} \overrightarrow{\phi} \cdot \overrightarrow{f} r dr dy +$$

$$\int_{\partial\omega} [(\sigma_{rr} r\phi_r)n_r + (\sigma_{ry} r\phi_r)n_y + (\sigma_{ry} r\phi_y)n_r + (\sigma_{yy} r\phi_y)n_y] \, dr dy$$

$$+ \sum_{i=1}^{n_{su}} \int_{\partial\omega_i \backslash \partial\omega} [(\sigma_{rr} r\phi_r)n_r + (\sigma_{ry} r\phi_r)n_y + (\sigma_{ry} r\phi_y)n_r + (\sigma_{yy} r\phi_y)n_y] \, dr dy \ .$$

It is to be noted that, the last integral is zero due to interface conditions (Section 7.1). Using stress strain relationship (7.20) and boundary conditions (7.25), the weak form corresponding to equation (7.24) is given as,

$$\sum_{i=1}^{n_{su}} \int_{\omega_i} \boldsymbol{C}^{(i)}\{\boldsymbol{\varepsilon}(\overrightarrow{u})\} : \{\boldsymbol{\varepsilon}(\overrightarrow{\phi})\} r dr dy = \sum_{i=1}^{n_{su}} \int_{\omega_i} \boldsymbol{C}^{(i)}(T - T_0)\alpha\{\boldsymbol{I}\} \cdot \{\boldsymbol{\varepsilon}(\overrightarrow{\phi})\} r dr dy$$

$$+ \int_{\gamma_{out}} \overrightarrow{\phi} \cdot \overrightarrow{g}_{out} r dr dy + \int_{\gamma_+} \overrightarrow{g}_+ \cdot \overrightarrow{\phi} r dr dy - \int_{\gamma_{sf}} \rho_m g(y_{max} - y)\overrightarrow{n} \cdot \overrightarrow{\phi} r dr dy \quad (7.29)$$

$$+ \int_{\omega} \overrightarrow{\phi} \cdot \overrightarrow{f} r dr dy \ ,$$

where T is assumed to be the solution of the weak thermal model ($WT2$).

Firstly, notice that under assumptions (MH1)-(MH3), and since $T \in \mathbb{T}$, all integrals in (7.29) are well defined. Therefore, we propose the following weak formulation for the mechanical model ($M2$):

Problem 13 *Weak mechanical formulation* $(WM3)$: *Let* $T \in \mathbb{T}$ *be the solution of the weak thermal model* $(WT3)$. *Under assumptions (MH1)-(MH3), find* $\overrightarrow{u} \in \mathbb{U}$, *such that equality (7.29) is verified for all* $\overrightarrow{\phi} \in \mathbb{U}$.

The left hand side of equation (7.29) is bilinear in $\mathbb{V} \times \mathbb{V}$,

$$a_M(\overrightarrow{u}, \overrightarrow{\phi}) = \sum_{i=1}^{n_{su}} \int_{\omega_i} \boldsymbol{C}^{(i)}\{\boldsymbol{\varepsilon}(\overrightarrow{u})\} : \{\boldsymbol{\varepsilon}(\overrightarrow{\phi})\}rdrdy \ , \tag{7.30}$$

while the right hand side of the equation is linear in $\mathbb{V}$,

$$l_M[T](\overrightarrow{\phi}) = \sum_{i=1}^{n_{su}} \int_{\omega_i} \boldsymbol{C}^{(i)}(T - T_0)\alpha\{\boldsymbol{I}\} \cdot \{\boldsymbol{\varepsilon}(\overrightarrow{\phi})\}rdrdy + \int_{\omega} \overrightarrow{\phi} \cdot \overrightarrow{f} rdrdy +$$
$$\int_{\gamma_{out}} \overrightarrow{\phi} \cdot \overrightarrow{g}_{out}rdrdy + \int_{\gamma+} \overrightarrow{g}_+ \cdot \overrightarrow{\phi} rdrdy - \int_{\gamma_{sf}} \rho_m g(y_{max} - y)\overrightarrow{n} \cdot \overrightarrow{\phi} rdrdy \ . \tag{7.31}$$

With the help of these two operators, the weak formulation of the mechanical problem can be written in the simplified and equivalent form as:

Problem 14 *Weak mechanical problem* $(WM4)$: *Let* $T \in \mathbb{T}$ *be the solution of the weak thermal model* $(WT3)$. *Under the assumptions (MH1)-(MH3), find* $\overrightarrow{u} \in \mathbb{U}$ *such that:*

$$a_M(\overrightarrow{u}, \overrightarrow{\phi}) = l_M[T](\overrightarrow{\phi}) \ , \ \forall \ \overrightarrow{\phi} \in \mathbb{U} \ . \tag{7.32}$$

Since the mechanical problem includes as parameter the temperature, which is the solution of the thermal model, a one way coupling between both models is considered.

We began part II by introducing complexities: presence of different materials, temperature dependence of material properties and homogenization. We further introduced axisymmetric thermomechanical model involving these complexities and corresponding weak formulation. In the next chapter, we introduce finite element formulation based on this weak formulation and perform the model order reduction using POD-ANN approach introduced in part I: chapter 6.

Chapter 8

Finite element formulation and reduced basis approach

We now derive the finite element formulation from weak forms (WT4) and (WM4) introduced in Chapter 7. We first introduce the domain discretization in line with the geometric shape parametrization introduced later. First, we introduce the domain discretization (Section 8.1) and relevant function spaces (Section 8.2). In section 8.3, we introduce the finite element formulations for thermal model (WT4) and for mechanical model (WM4). In section 8.4, a numerical example with computations of temperature field and displacement field is presented. Next, we apply the Model Order Reduction (MOR) to the finite element formulation (Section 8.5). We introduce the parameter space and relevant geometric parameters. Next, construction of reduced basis space using Proper Orthogonal Decomposition (POD) and computation of degrees of freedom using Artificial Neural Network (ANN) are described. Finally, MOR approach is validated by performing numerical experiments using open source libraries FEniCS [2, 35], RBniCS [46, 79], PyTorch [68, 71], and relevant conclusions are drawn in section 8.6.

8.1 Domain discretization

We consider a decomposition of the domain ω into n_{su} triangular subdomains as:

$$\bar{\omega} = \bigcup_{i=1}^{n_{su}} \bar{\omega}_i \ , \ \omega_i \cap \omega_j = \emptyset \text{ for } i \neq j \ , \ 1 \leq i, j \leq n_{su} \ .$$

Each subdomain ω_i is further divided into $\mathcal{N}_{el,i}$ smaller triangular elements τ_k. The total number of triangular elements in ω is $\mathcal{N}_{el}$. Grid $\mathcal{T}$ is the set of all triangular elements of ω,

that is assumed a mesh, that is the meshes of subdomains are compatible at the interfaces:

$$\bar{\omega} = \bigcup_{k=1}^{\mathcal{N}_{el}} \bar{\tau}_k \ , \ \mathcal{N}_{el} = \sum_{i=1}^{n_{su}} \mathcal{N}_{el,i} \ , \ \mathcal{T} = \{\tau_k\}_{k=1}^{\mathcal{N}_{el}} \ .$$

The edges of a triangular element τ_k are denoted as $\partial \tau_k$. The unit normal vector pointing outwards to $\partial \tau_k$ is denoted as $\vec{n}_k$.

8.2   Function space in finite dimension

We introduce now the finite dimensional subspaces $\mathbb{T}_h, \mathbb{U}_h$ of continuous spaces $\mathbb{T}, \mathbb{U}$ respectively:

$$\mathbb{T}_h \subset \mathbb{T} \ , \ \mathbb{U}_h \subset \mathbb{U} \ .$$

The n_h-dimensional space $\mathbb{T}_h$ is specified by,

$$\mathbb{T}_h = \text{span}\{\psi_{h,1}, \psi_{h,2}, \ldots, \psi_{h,n_h}\} \ ,$$

and the m_h-dimensional space $\mathbb{U}_h$ is specified by,

$$\mathbb{U}_h = \text{span}\{\vec{\phi}_{h,1}, \vec{\phi}_{h,2}, \ldots, \vec{\phi}_{h,m_h}\} \ ,$$

with all functions independent. Therefore, $\{\psi_{h,i}\}_{i=1}^{n_h}$ and $\{\vec{\phi}_{h,i}\}_{i=1}^{m_h}$ are the basis of the spaces $\mathbb{T}_h$ and $\mathbb{U}_h$, respectively. In the course of finite dimensional analysis, we seek the solutions $T_h \in \mathbb{T}_h$ and $\vec{u}_h \in \mathbb{U}_h$ of the discretized models corresponding to $(WT4)$ and $(WM4)$ respectively, restricting the test functions to the corresponding discrete spaces. It is to be noted that $T_h \in \mathbb{T}_h$ and $\vec{u}_h \in \mathbb{U}_h$ are the approximation of $T \in \mathbb{T}$ and $\vec{u} \in \mathbb{U}$ respectively.

We introduce here the Galerkin method of weighted residuals i.e. the shape function and the test function are in the same space. The solutions T_h and $\vec{u}_h$ are given by:

$$T_h = \sum_{i=1}^{i=n_h} T_h^i \psi_{h,i} \ , \ \vec{u}_h = \sum_{i=1}^{i=m_h} u_h^i \vec{\phi}_{h,i} \ .$$

Here, the coefficients T_h^i and u_h^i are known as nodal temperature and nodal displacement. As we will see later, these coefficients are obtained by solving system of equations. The basis functions for displacement and temperature are piecewise polynomial of degree $p \geq 1$.

8.3 Finite element formulation

8.3.1 Thermal model

In the finite element analysis, the forms defined in (7.27), $J_a[T^\kappa] : \mathbb{T} \times \mathbb{T} \to \mathbb{R}$ and $c_T : \mathbb{T} \times \mathbb{T} \to \mathbb{R}$ are restricted to the finite dimensional subspace as $J_{a,h}[T_h^\kappa] : \mathbb{T}_h \times \mathbb{T}_h \to \mathbb{R}$ and $c_{T,h} : \mathbb{T}_h \times \mathbb{T}_h \to \mathbb{R}$ and they are defined in the similar way:

$$
\begin{aligned}
J_{a,h}[T_h^\kappa](T_h^{\kappa+1}, \psi_h) &= \sum_{i=1}^{n_{su}} \int_{\omega_i} \left(k^{(i)}(T_h^\kappa) \nabla T_h^{\kappa+1} : \nabla \psi_h \right) r dr dy \\
&+ \sum_{i=1}^{n_{su}} \int_{\omega_i} \left(T_h^{\kappa+1} k^{(i)'}(T_h^\kappa) \nabla T_h^\kappa : \nabla \psi_h \right) r dr dy , \\
c_{T,h}(T_h^{\kappa+1}, \psi_h) &= \int_{\gamma_{sf}} h_{c,f} \psi_h T_h^{\kappa+1} r dr dy + \int_{\gamma_-} h_{c,-} \psi_h T_h^{\kappa+1} r dr dy \\
&+ \int_{\gamma_{out}} h_{c,out} \psi_h T_h^{\kappa+1} r dr dy , \ T_h^\kappa, T_h^{\kappa+1}, \psi_h \in \mathbb{T}_h .
\end{aligned}
\tag{8.1}
$$

Analogously, the linear forms introduced in (7.27), $J_l[T^\kappa] : \mathbb{T} \to \mathbb{R}$ and $l_T : \mathbb{T} \to \mathbb{R}$ are restricted to the finite dimensional space as $J_{l,h}[T_h^\kappa] : \mathbb{T}_h \to \mathbb{R}$ and $l_{T,h} : \mathbb{T}_h \to \mathbb{R}$:

$$
\begin{aligned}
J_{l,h}[T_h^\kappa](\psi_h) &= \sum_{i=1}^{n_{su}} \int_{\omega_i} T_h^\kappa k^{(i)'}(T_h^\kappa) \nabla T_h^\kappa : \nabla \psi_h r dr dy , \\
l_{T,h}(\psi_h) = \int_\omega \psi_h r Q dr dy &+ \int_{\gamma_{sf}} h_{c,f} \psi_h T_f r dr dy + \int_{\gamma_-} h_{c,-} \psi_h T_- r dr dy \\
&+ \int_{\gamma_{out}} h_{c,out} \psi_h T_{out} r dr dy - \int_{\gamma_+} \psi_h q^+ r dr dy , \ \psi_h \in \mathbb{T}_h .
\end{aligned}
\tag{8.2}
$$

Therefore, the approximation of the problem $(WT4)$ in the finite dimensional space can be stated as:

Problem 15 *Problem* $(WT4)_h$: *Under the assumptions* $(TH1) - (TH5)$ *and known* T_h^κ, *find* $T_h^{\kappa+1} \in \mathbb{T}_h$ *such that:*

$$
J_{a,h}[T_h^\kappa](T_h^{\kappa+1}, \psi_h) + c_{T,h}(T_h^{\kappa+1}, \psi_h) = J_{l,h}[T_h^\kappa](\psi_h) + l_{T,h}(\psi_h) , \ \forall \psi_h \in \mathbb{T}_h .
\tag{8.3}
$$

8.3.2 Thermomechanical model

In the finite element analysis, the bilinear form $a_M : \mathbb{U} \times \mathbb{U} \to \mathbb{R}$, defined in (7.30), is restricted to a finite dimensional subspace, $\mathbb{U}_h \times \mathbb{U}_h$, as $a_{M,h} : \mathbb{U}_h \times \mathbb{U}_h \to \mathbb{R}$ defined by,

$$
a_{M,h}(\overrightarrow{u}_h, \overrightarrow{\phi}_h) = \sum_{i=1}^{n_{su}} \int_{\omega_i} C^{(i)} \{\varepsilon(\overrightarrow{u}_h)\} : \{\varepsilon(\overrightarrow{\phi}_h)\} r dr dy ,
\tag{8.4}
$$

and the linear form $l_M[T]$, as defined in (7.31), is restricted to the finite dimensional space as $l_{M,h}[T_h]$:

$$
l_{M,h}[T_h](\overrightarrow{\phi}_h) = \sum_{i=1}^{n_{su}} \int_{\omega_i} \boldsymbol{C}^{(i)}(T_h - T_0)\alpha\{\boldsymbol{I}\} \cdot \{\boldsymbol{\varepsilon}(\overrightarrow{\phi}_h)\}rdrdy + \int_{\omega} \overrightarrow{\phi}_h \cdot \overrightarrow{f}\, rdrdy +
$$

$$
\int_{\gamma_{out}} \overrightarrow{\phi}_h \cdot \overrightarrow{g}_{out}rdrdy + \int_{\gamma_+} \overrightarrow{g}_+ \cdot \overrightarrow{\phi}_h rdrdy - \int_{\gamma_{sf}} \rho_m g(y_{max} - y)\overrightarrow{n} \cdot \overrightarrow{\phi}_h rdrdy \ . \tag{8.5}
$$

To approach the solution of weak problem $(WM4)$ in the finite dimensional space $\mathbb{U}_h$, the discretized problem can be stated as:

Problem 16 *Problem $(WM4)_h$: Let $T_h \in \mathbb{T}_h$, be the solution of the discretized thermal model $(WT4)_h$. Under the assumptions $(MH1) - (MH4)$, find $\overrightarrow{u}_h \in \mathbb{U}_h$ such that:*

$$
a_{M,h}(\overrightarrow{u}_h, \overrightarrow{\phi}_h) = l_{M,h}[T_h](\overrightarrow{\phi}_h) \ , \ \forall \overrightarrow{\phi}_h \in \mathbb{U}_h \ . \tag{8.6}
$$

8.4   Numerical example

The domain ω was divided into $n_{su} = 90$ non-overlapping triangular subdomains as shown in the Figure 8.1. The coordinates of the domain ω are given in Table 8.1. Number of triangular subdomains in each section of the domain are given in Table 8.2. The mesh contained 4428 vertices and $\mathcal{N}_{el} = 7981$ triangular elements. The average mesh quality (equation (5.2)) is 0.92.

As explained in section 7.4.1, Newton's method was used to compute the temperature field. The initial guess was constant temperature of $350K$, i.e. $T^0 = 350$, and iterations were stopped, when relative residual reaches closer to machine precision. The displacement field was computed using (LU) decomposition. We consider the reference temperature of $300K$ i.e. $T_0 = 300K$. From Table 8.1, we notice $y_{max} = 7.4m$. For the boundary conditions, we consider below data:

$$
\text{on } \gamma_{sf} : h_{c,f} = 2000\frac{W}{m^2K} \ , T_{sf} = 1773K \ , \ \rho_m = 7860\frac{Kg}{m^3}, \ g = 9.81\frac{m}{s^2} \ ,
$$

$$
h = y_{max} - y \ ,
$$

$$
\text{on } \gamma_{out} : h_{c,out} = 200\frac{W}{m^2K} \ , \ T_{out} = 300K \ , \ \overrightarrow{g}_{out} = \overrightarrow{0} \ ,
$$

$$
\text{on } \gamma_- : h_{c,-} = 2000\frac{W}{m^2K} \ , \ T_- = 300K \ ,
$$

$$
\text{on } \gamma_+ : q_+ = 0 \ , \ \overrightarrow{g}_+ = \overrightarrow{0} \ .
$$

The temperature profile and the displacement profile are shown in Figure 8.2. The location of critical isotherms are of importance for safe operation and longer lifetime of blast furnace hearth. The displacement profile is useful for locations corresponding to maximum deflection and maximum stresses.

ω_{sc}	r	0	5.9501	5.9501	1	/	/	/	/	/	/
	y	0	0	1	1	/	/	/	/	/	/
ω_{mc}	r	0	2.1	2.1	0	4.875	5.9501	5.9501	5.5188	5.5188	4.875
	y	1	1	1.6	1.6	5.2	5.2	7.35	7.35	7	7
ω_{cb}	r	0	0.39	0.39	0	/	/	/	/	/	/
	y	1	1	1.6	1.6	/	/	/	/	/	/
ω_{cc}	r	0.39	4.875	4.875	5.5188	5.5188	4.875	4.875	4.475	4.475	0.39
	y	1.6	1.6	6.4	6.4	7.4	7.4	7	7	2.1	2.1
ω_{smc}	r	2.1	5.9501	5.9501	4.875	4.875	2.1	/	/	/	/
	y	1	1	5.2	5.2	1.6	1.6	/	/	/	/
ω_{ss}	r	5.9501	6.0201	6.0201	5.9501	/	/	/	/	/	/
	y	0	0	7.4	7.4	/	/	/	/	/	/

Table 8.1: Coordinates (in (m)) of the vertices of subdomains

Section/Domain	ω_{sc}	ω_{mc}	ω_{smc}	ω_{cc}	ω_{cb}	ω_{ss}	ω
Number of subdomains	24	12	16	18	2	18	90

Table 8.2: Sectionwise triangular subdomains

Close up of the mesh   Subdomains decomposition
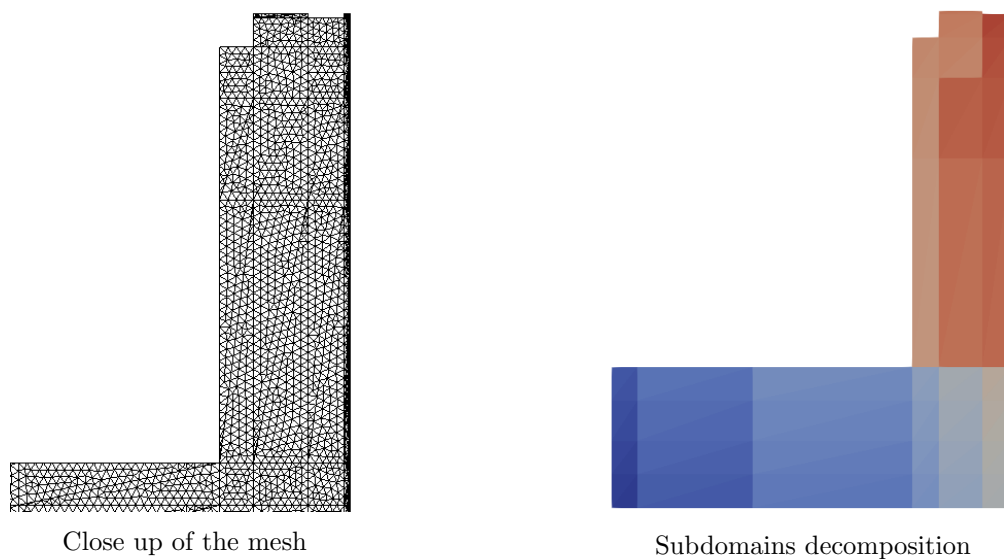
Figure 8.1: Discretisation of domain $\omega = \bigcup\limits_{i=1}^{n_{su}} \omega_i$

Temperature profile (in K)   Displacement magnitude (in m)
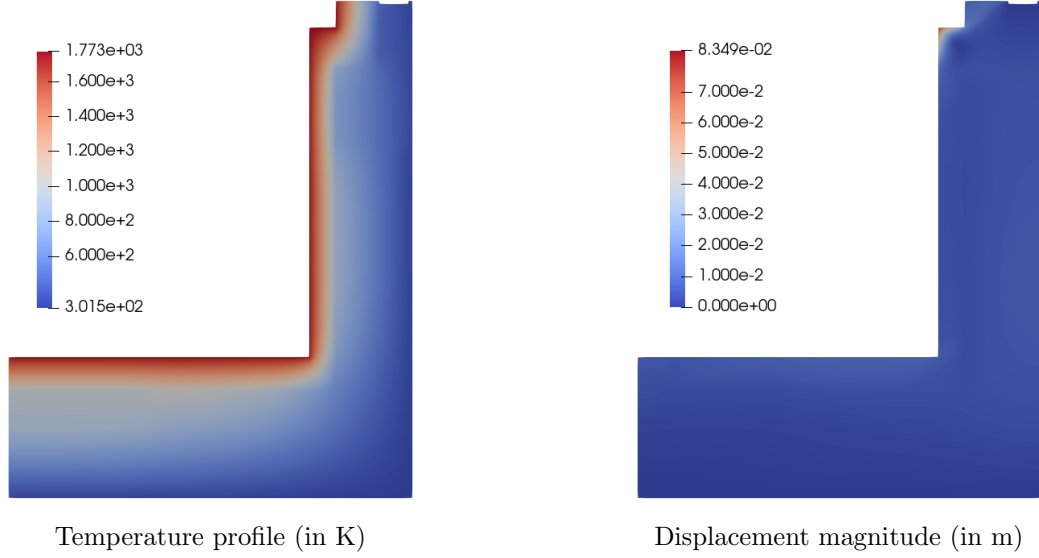
Figure 8.2: Furnace wall : Temperature (left) and Displacement (right)

8.5   Parameter space and model order reduction approach

We consider the parameter space $\mathbb{P} \subset \mathbb{R}^5$ as the parameter space and $\Xi \in \mathbb{P}$ as a parameter tuple. In chapter 6, material and geometric parameters were considered. In our present analysis, we consider only 5 geometric parameters. Specifically, we consider parameters (see Figure 8.3):

$$\Xi = \{t_0, t_1, t_2, D_0, D_1\} \ .$$

The reference domain $\hat{\omega}$ corresponds to:

$$\Xi = \{0.5, 0.5, 0.5, 0.6438, 0.4313\} \ .$$

It can be noticed that $\hat{\omega}$ corresponds to domain introduced in the section 8.4. We consider affine shape parametrization as introduced in the equations (6.1)-(6.3). The domains $\omega(\Xi)$ will be the image of $\hat{\omega}$ under the variation of parameter tuple $\Xi \in \mathbb{P}$.

8.5.1   Model order reduction using POD-ANN approach

We construct the reduced basis space $\mathbb{T}_h^{rb} \subset \mathbb{T}_h$ and compute the reduced basis solution $T_h^{rb} \in \mathbb{T}_h^{rb}$ to approximate the solution field $T_h \in \mathbb{T}_h$ corresponding to the problem $(WT4)_h$. Similarly, we construct the reduced basis space $\mathbb{U}_h^{rb} \subset \mathbb{U}_h$ and compute the reduced basis solution $\overrightarrow{u}_h^{rb} \in \mathbb{U}_h^{rb}$ to approximate the solution field $\overrightarrow{u}_h \in \mathbb{U}_h$ corresponding to the
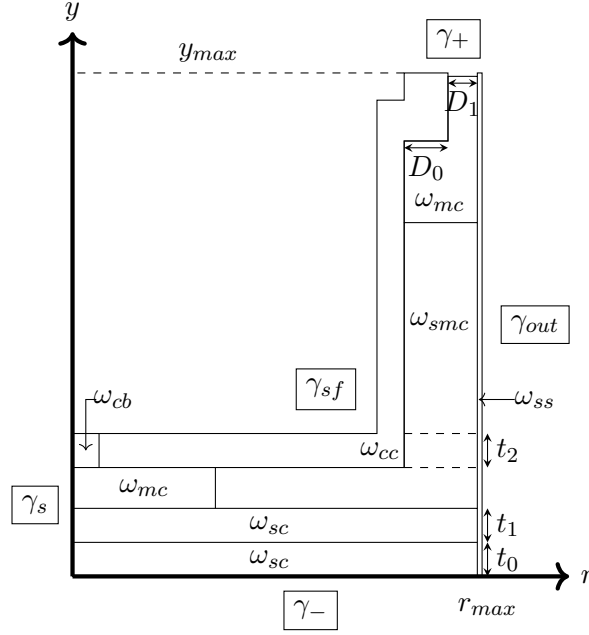
Figure 8.3: Hearth geometric parameters

problem $(WM4)_h$:

$$\mathbb{T}_h^{rb} = \text{span}\{\psi_h^1, \ldots, \psi_h^{N_T}\} \ , \tag{8.7}$$

$$\mathbb{U}_h^{rb} = \text{span}\{\overrightarrow{\phi}_h^1, \ldots, \overrightarrow{\phi}_h^{N_M}\} \ . \tag{8.8}$$

Here, $N_T \ll n_h$ and $N_M \ll m_h$ are the number of basis functions forming the reduced basis spaces $\mathbb{T}_h^{rb}$ and $\mathbb{U}_h^{rb}$ respectively. The reduced basis solutions can be represented as:

$$T_h^{rb} = \sum_{i=1}^{N_T} \zeta_T^i \psi_h^i \ , \ \ \overrightarrow{u}_h^{rb} = \sum_{i=1}^{N_M} \zeta_M^i \overrightarrow{\phi}_h^i \ .$$

In the present analysis, reduced basis spaces $\mathbb{T}_h^{rb}, \mathbb{U}_h^{rb}$ are constructed using Proper orthogonal Decomposition (POD) and degrees of freedom of the reduced basis solutions $\{\zeta_T^i\}_{i=1}^{N_T}, \{\zeta_M^i\}_{i=1}^{N_M}$ are computed using Artificial Neural Network (ANN). Precisely, we use POD-ANN approach as introduced in the chapter 6.

For constructing the reduced basis space $\mathbb{T}_h^{rb}$ using POD (Section 6.2.1), n_s^T parameter tuples are sampled from the parameter space $\mathbb{P}$ to construct the snapshot matrix $\boldsymbol{C}_T$:

$$(\boldsymbol{C}_T)_{kl} = \ < T_h(\Xi_k), T_h(\Xi_l) >_{\mathbb{T}_h} \ , \ 1 \le k, l \le n_s^T \ , \ \boldsymbol{C}_T \in \mathbb{R}^{n_s^T \times n_s^T} \ .$$

By performing eigenvalue decomposition of $\boldsymbol{C}_T$, N_T largest eigenvalues $\{\theta_T^i\}_{i=1}^{N_T}$, sorted in descending order $\theta_T^1 \geq \theta_T^2 \geq \ldots \geq \theta_T^{N_T}$, and corresponding eigenvectors $\{\boldsymbol{V}_T^i\}_{i=1}^{N_T}, \boldsymbol{V}_T^i \in \mathbb{R}^{n_s^T}$ are computed. The reduced basis space $\mathbb{T}_h^{rb}$ are constructed from the eigenvectors $\{\boldsymbol{V}_T^i\}_{i=1}^{N_T}$.

Similarly, reduced basis space $\mathbb{U}_h^{rb}$ is contructed using POD. n_s^M parameter tuples are sampled from the parameter space $\mathbb{P}$ to contruct the snapshot matrix $\boldsymbol{C}_M$:

$$(\boldsymbol{C}_M)_{kl} = < \overrightarrow{u}_h(\Xi_k), \overrightarrow{u}_h(\Xi_l) >_{\mathbb{U}_h} , \ 1 \leq k, l \leq n_s^M , \ \boldsymbol{C}_M \in \mathbb{R}^{n_s^M \times n_s^M} .$$

By performing eigenvalue decomposition of $\boldsymbol{C}_M$, N_M largest eigenvalues $\{\theta_M^i\}_{i=1}^{N_M}$, sorted in descending order $\theta_M^1 \geq \theta_M^2 \geq \ldots \geq \theta_M^{N_M}$, and corresponding eigenvectors $\{\boldsymbol{V}_M^i\}_{i=1}^{N_M}, \boldsymbol{V}_M^i \in \mathbb{R}^{n_s^M}$ are computed. The reduced basis space $\mathbb{U}_h^{rb}$ are constructed from the eigenvectors $\{\boldsymbol{V}_M^i\}_{i=1}^{N_M}$.

In order to determine the admissibility of a given eigenvector in the reduced basis space, we refer to below criterion:

$$\frac{\theta_T^i}{\theta_T^1} \geq 1e - 6 , \ \frac{\theta_M^i}{\theta_M^1} \geq 1e - 6 .$$

After constructing the reduced basis spaces $\mathbb{T}_h^{rb}$ and $\mathbb{U}_h^{rb}$, two separate ANNs are trained to predict the degrees of freedom $\{\zeta_T^i(\Xi)\}_{i=1}^{N_T}$ and $\{\zeta_M^i(\Xi)\}_{i=1}^{N_M}$ of the reduced basis solutions $T_h^{rb}(\Xi)$ and $\overrightarrow{u}_h^{rb}(\Xi)$, respectively, at a given parameter tuple $\Xi \in \mathbb{P}$. In order to create training sets for ANNs, N_t^T and N_t^M parameter tuples are sampled from the parameter space $\mathbb{P}$. Full order model $(WT4)_h$ is solved to compute the solution field $\{T_h(\Xi_k)\}_{k=1}^{n_t^T}$ at each of the N_t^T parameter tuples. Similarly, full order model $(WM4)_h$ is solved to compute the solution field $\{\overrightarrow{u}_h(\Xi_k)\}_{k=1}^{n_t^M}$ at each of the N_t^M parameter tuples. The computed solution fields are projected on the respective reduced basis spaces to create training data for ANNs:

$$
\begin{aligned}
T_h^\pi(\Xi_k) &= \underset{\psi_h^{rb} \in \mathbb{T}_h^{rb}}{\arg\min} ||T_h(\Xi_k) - \psi_h^{rb}||_{\mathbb{T}_h^{rb}} = \sum_{i=1}^{N_T} \zeta_{T,\pi}^i(\Xi_k)\psi_h^i , \\
\boldsymbol{\zeta}_{T,\pi}(\Xi_k) &= \{\zeta_{T,\pi}^i(\Xi_k)\}_{i=1}^{N_T} , \ 1 \leq k \leq N_t^T , \\
\overrightarrow{u}_h^\pi(\Xi_k) &= \underset{\overrightarrow{\phi}_h^{rb} \in \mathbb{U}_h^{rb}}{\arg\min} ||\overrightarrow{u}_h(\Xi_k) - \overrightarrow{\phi}_h^{rb}||_{\mathbb{U}_h} = \sum_{i=1}^{N_M} \zeta_{M,\pi}^i(\Xi_k) \overrightarrow{\phi}_h^i , \\
\boldsymbol{\zeta}_{M,\pi}(\Xi_k) &= \{\zeta_{M,\pi}^i(\Xi_k)\}_{i=1}^{N_M} , \ 1 \leq k \leq N_t^M .
\end{aligned}
\tag{8.9}
$$

ANN for thermal model is trained to learn the map f_T by training against input-output pair $\{\Xi_k, \boldsymbol{\zeta}_{T,\pi}(\Xi_k)\}_{k=1}^{N_t^T}$ and ANN for mechanical model to learn the map f_M by training against input-output pair $\{\Xi_k, \boldsymbol{\zeta}_{M,\pi}(\Xi_k)\}_{k=1}^{N_t^M}$. As explained in the section 6.2.3, we consider the two ANNs as black boxes that can then be used to compute the POD coefficients related

to a new parameter instance Ξ^* after training. We split the full order data into two parts: one to be used for training of ANN and one to be used for validation of ANN. We use early stopping criteria to avoid overfitting. ANN is trained to minimise loss function, measured in terms of the mean square error (equation (6.34)).

In the present analysis, we will use ANN with 3 hidden layers having Sigmoid function (equation (6.31)) as activation function for hidden layers and identity function as activation function for input and output layers. The depth of hidden layers, H, is kept same for all the hidden layers.

8.6 Validation of MOR

We use the mesh as described in section 8.4 for the reference domain $\hat{\omega}$. The range of physical parameters is given in the table 8.3. In the context of ANN, 70% of the total data provided by the full order model is used for training while remaining 30% of the data is used for validation. The accuracy of MOR is quantified by relative error and projection error as defined by equation (6.35) and equation (6.36) respectively.

Parameter	Minimum value	Maximum value
t_0	0.4	0.6
t_1	0.4	0.6
t_2	0.4	0.6
D_0	0.55	0.75
D_1	0.35	0.55

Table 8.3: Parameter ranges used for MOR training and testing

8.6.1 Thermal model

The reduced basis space for the thermal model is constructed by computing solution fields at randomly selected 400 parameters. The eigenvalue decay is shown in the figure 8.4a. Figure 8.4b shows the relative error for the POD-ANN approach for different number of high-fidelity solutions $n_{tr} = N_t^T$ and depth of hidden layers H of ANN. The online time for POD-ANN approach is $2.7e - 4s$. While the time taken during online phase is same as the linear model, the time taken for FOM computation increases significantly as compared to the linear model due to the Newton's method used for solving nonlinear system of equations. Finally, we show the comparison between FOM solution and POD-ANN solution (Figure 8.5) computed at parameter:

$$\Xi = \{0.45, 0.58, 0.47, 0.63, 0.52\} \ .$$

The numerical results show that POD-ANN approach is able to learn solution fields involving complexities such as nonlinearity. Also, time taken by POD-ANN approach during
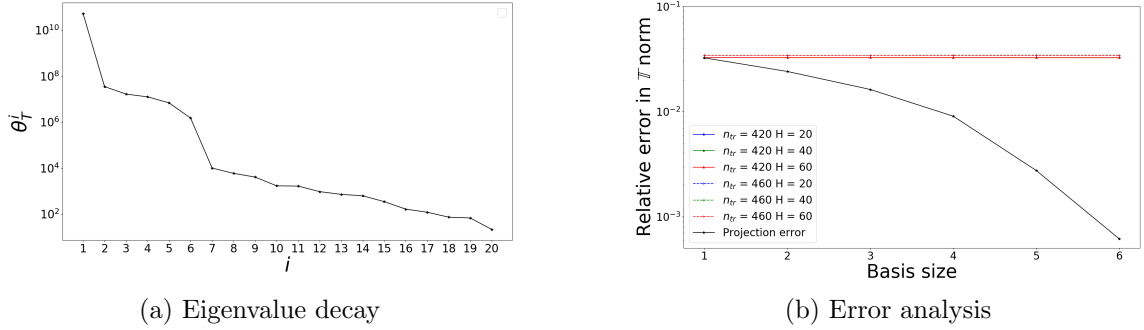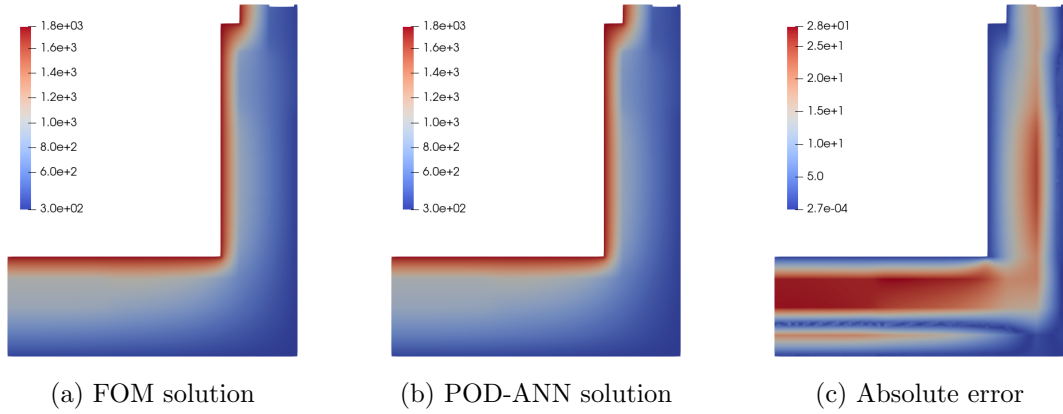
(a) Eigenvalue decay

(b) Error analysis

Figure 8.4: Thermal model: Eigenvalue decay and error analysis

(a) FOM solution   (b) POD-ANN solution   (c) Absolute error

Figure 8.5: Thermal model: comparison between the temperature (in K) computed by FOM and by the POD-ANN methods $\Xi = \{0.45, 0.58, 0.47, 0.63, 0.52\}$. We consider 6 POD modes. For POD-ANN, we set $n_{tr} = 420$ and $H = 40$.

online phase remains almost constant for linear model as well as nonlinear model.

8.6.2   Thermomechanical model

The reduced basis space for the thermomechanical model is constructed by computing solution fields at randomly selected 700 parameters. Figure 8.6a shows the eigenvalue decay. The relative error for the POD-ANN approach for different number of high-fidelity solutions $n_{tr} = N_t^M$ and depth of hidden layers H of ANN is shown in the figure 8.6b. The online time for POD-ANN approach is $3.2e - 4s$. The comparison between FOM solution and POD-ANN solution computed at parameter,

$$\Xi = \{0.45, 0.58, 0.47, 0.63, 0.52\} \ ,$$

is shown in figure 8.7. As evident from the numerical results, POD-ANN approach is computationally efficient and sufficiently acurate.
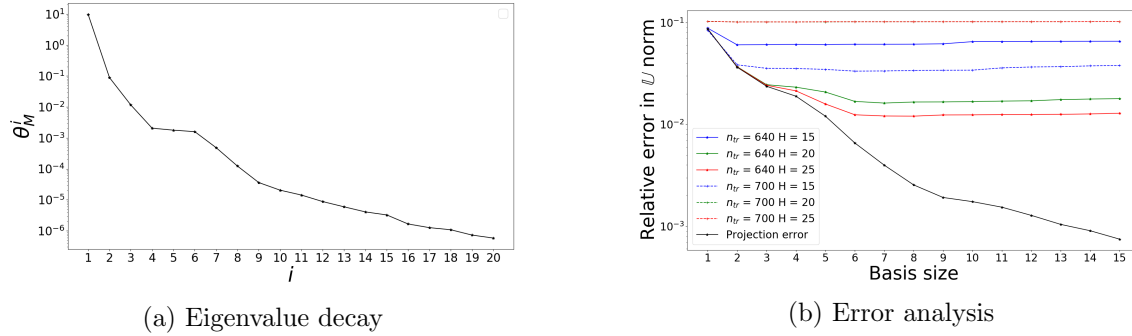

(a) Eigenvalue decay

(b) Error analysis

Figure 8.6: Thermomechanical model: Eigenvalue decay and error analysis

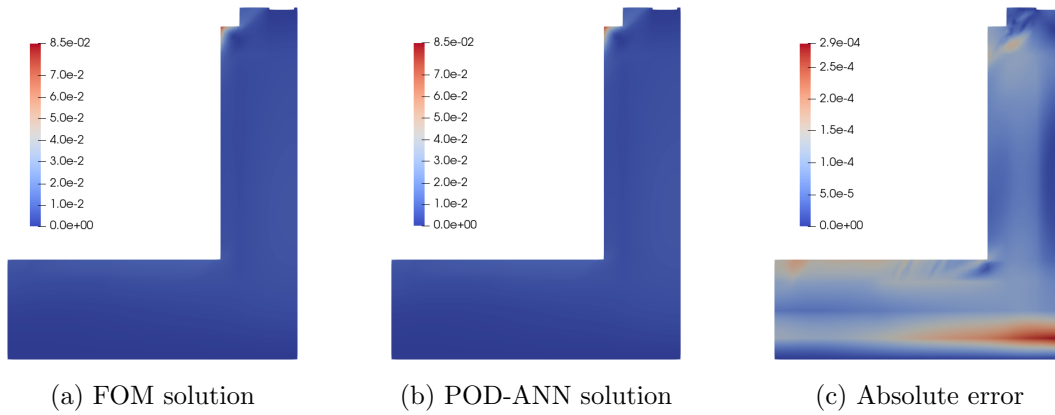(a) FOM solution

(b) POD-ANN solution

(c) Absolute error

Figure 8.7: Thermomechanical model: comparison between the displacement (in m) computed by FOM and by the POD-ANN methods $\Xi = \{0.45, 0.58, 0.47, 0.63, 0.52\}$. We consider 15 POD modes. For POD-ANN, we set $n_{tr} = 640$ and $H = 25$.

We first computed the solution field using finite element method by solving finite element formulation. Then, we introduced relevant geometric parameters. To approximate the solution field quickly under the variation of parameters, we used POD-ANN method as quick and accurate model order reduction approach for the complex thermomechanical model.

Conclusions and perspectives

In this thesis, full and reduced parameterized modelling of thermomechanical phenomena arising in blast furnace hearth has been investigated.

In first part of this work, a linear isotropic homogeneous thermomechanical model was considered. Further, axisymmetric hypothesis was introduced with corresponding weak formulation and finite element formulation. However, since this finite element formulation needs to be solved repeatedly for geometric and material parameters, model order reduction was used to accelarate the computations. We discussed projection based POD-Galerkin approach and data-driven non-intrusive POD-ANN approach. As demonstrated through the numerical tests, model order reduction can approximate the temperature field and the displacement field computed by solving finite element method efficiently with "affordable" compromise in accuracy.

In second part of the thesis, we have introduced more complexities:

- Presence of different materials: Blast furnace hearth is made up of different materials due to technical design requirements. Presence of different materials require imposition of proper interface conditions at the interface between different material zones.

- Temperature dependence of material properties: Normally, material properties are measured at few discrete temperature points. In order to approximate the continuous dependence of material properties on temperature, we used piecewise spline interpolation to approximate material properties at intermediate temperatures.

- Orthotropy: Ceramic cup is made up of periodic assembly of bricks and mortar. We identified an equivalent orthotropic material by incorporating the homogenization technique described in [7] and the equivalent material obtained therein.

In addition, axisymmetric hypothesis was applied to the thermomechanical model involving above complexities. Corresponding weak formulation and finite element formulation were introduced to numerically compute temperature and displacement fields. We again introduced geometric parametrization and POD-ANN based model order reduction approach for this complex model.
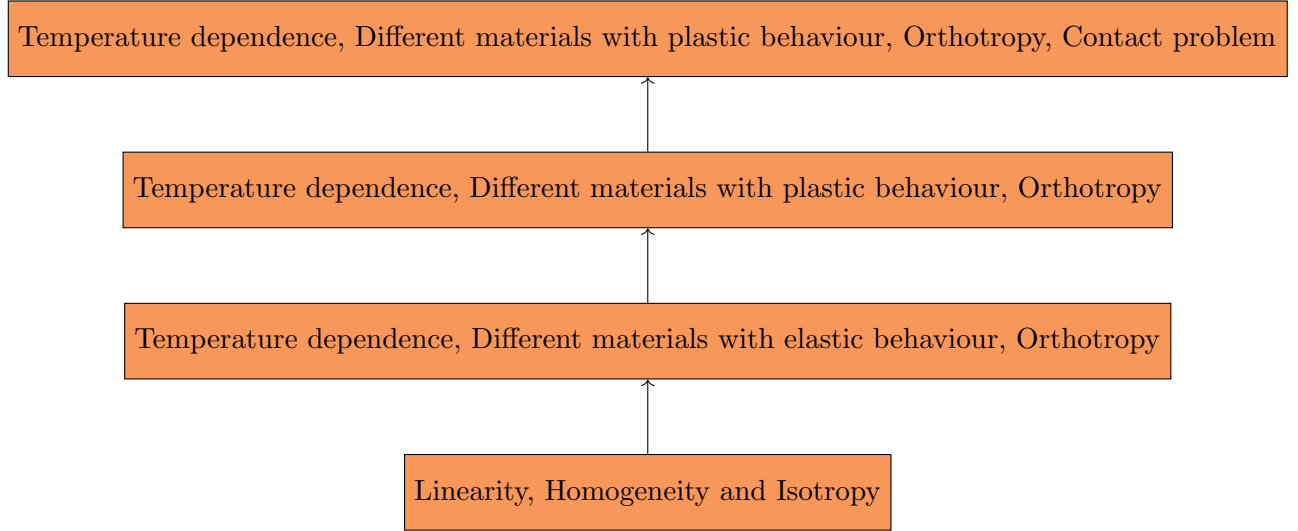
Figure A: Hierarchy for thermomechanical modelling

As described, we took hierarchical approach for thermomechanical modelling (Figure A). In particular, we consider the first two levels; indeed, thermomechanical model as relevant to blast furnace hearth involves further complexities such as non-linear elastic and plastic behaviour as well as contact between different blocks [24, 55]. Development and solution of thermomechanical model involving all these complexities and the application of model order reduction techniques to such complex problem will be a good direction for future work.

In terms of deep learning based model order reduction of parametric partial differential equation, we see multiple possibilities for future development:

- A better sampling algorithm: In the case of model order reduction of parametric partial differential equations, random sampling may neglect crucial parameters within the parameter space. As pertaining to data-driven deep learning methods, such random sampling leads to computation of more snapshots to extract relevant information for training of ANN. Better sampling procedures [20, 53] can alleviate the computational burden by creating good training set from relatively smaller number snapshots based on carefully selected parameters.

- Operator learning: Traditionally, ANN has been used to approximate mapping between two finite dimensional spaces. However, ANN can also be used to learn operators. Operator learning approaches have shown better generalization capabilities, easier training of ANN and error behaviour independent of the resolution of the data [58, 59, 60]. Considering these advantages, it is important to identify opportunities to extend operator learning to model order reduction techniques.

- Improved loss function: One of the primary example of deep learning approach incorporating knowledge of the governing partial differential equations into the loss function is the Physics Informed Deep Learning [27, 76]. Another alternative could be to compute gradient from the data representing solution field and use the computed gradient in the loss function of ANN.

- Multi-fidelity: In case, the computational budget does not allow computing many high-fidelity solutions, low-fidelity models can approximate the high-fidelity solution quickly with affordable compromise in accuracy. In other words, the training set for ANN can be augmented by replacing costly high-fidelity model with faster low-fidelity model.

In summary, thermomechanical modelling for blast furnace hearth and deep learning based model order reduction approaches have considerable potential for further developments. We expect the developments presented in this work could provide clear perspectives for the direction of future work.

Bibliography

[1] S. ALI, F. BALLARIN, AND G. ROZZA, *Stabilized reduced basis methods for parametrized steady stokes and navier–stokes equations*, Computers & Mathematics with Applications, 80 (2020), pp. 2399–2416.

[2] M. S. ALNÆS, J. BLECHTA, J. HAKE, A. JOHANSSON, B. KEHLET, A. LOGG, C. RICHARDSON, J. RING, M. E. ROGNES, AND G. N. WELLS, *The fenics project version 1.5*, Archive of Numerical Software, 3 (2015).

[3] D. AMSALLEM, J. CORTIAL, K. CARLBERG, AND C. FARHAT, *A method for interpolating on manifolds structural dynamics reduced-order models*, International Journal for Numerical Methods in Engineering, 80 (2009), pp. 1241–1258.

[4] E. BADER, M. KÄRCHER, M. GREPL, AND K. VEROY, *Certified reduced basis methods for parametrized distributed elliptic optimal control problems with control constraints*, SIAM Journal on Scientific Computing, 38 (2016), pp. A3921–A3946.

[5] M. BANNENBERG, A. CICCAZZO, AND M. GÜNTHER, *Coupling of model order reduction and multirate techniques for coupled dynamical systems*, Applied Mathematics Letters, 112 (2021), p. 106780.

[6] M. BANNENBERG, A. CICCAZZO, AND M. GÜNTHER, *Reduced order multirate schemes for coupled differential-algebraic systems*, Applied Numerical Mathematics, 168 (2021), pp. 104–114.

[7] P. BARRAL, M. FANJUL, L. PÉREZ-PÉREZ, P. QUINTELA, AND M. SÁNCHEZ, *Equivalent thermo-mechanical model for ceramic cups*, Proceedings of the 139 European Study Group with Industry, (2018), pp. 83–101, `www.math-in.net/139esgi/sites/math-in.net.139esgi/files/139ESGI_proceedings.pdf`.

[8] P. BARRAL, M. C. NAYA-RIVEIRO, AND P. QUINTELA, *Existence and uniqueness of a thermoelastic problem with variable parameters*, European Journal of Applied Mathematics, 26 (2015), p. 497–520.

[9] P. BARRAL, M. C. NAYA-RIVEIRO, AND P. QUINTELA, *Regularity of a thermoelastic problem with variable parameters*, European Journal of Applied Mathematics, 27 (2016), p. 213–232.

[10] P. BARRAL, B. NICOLÁS, AND P. QUINTELA, *Numerical simulation of the shear stress produced by the hot metal jet on the blast furnace runner*, Computers & Mathematics with Applications, 102 (2021), pp. 146–159.

[11] P. BARRAL, L. PÉREZ-PÉREZ, AND P. QUINTELA, *Numerical simulation of the transient heat transfer in a blast furnace main trough during its complete campaign cycle*, International Journal of Thermal Sciences, 173 (2022), p. 107349.

[12] P. BARRAL, P. QUINTELA, AND M. T. SÁNCHEZ, *Mechanical behaviour in dc alloys casting processes*, Archives of Computational Methods in Engineering volume, 21 (2014), pp. 91–125.

[13] M. BARRAULT, Y. MADAY, N. C. NGUYEN, AND A. T. PATERA, *An 'empirical interpolation' method: application to efficient reduced-basis discretization of partial differential equations*, Comptes Rendus Mathematique, 339 (2004), pp. 667–672.

[14] P. BENNER, S. GUGERCIN, AND K. WILLCOX, *A survey of projection-based model reduction methods for parametric dynamical systems*, SIAM Review, 57 (2015), pp. 483–531.

[15] P. BENNER, R. HERZOG, N. LANG, I. RIEDEL, AND J. SAAK, *Comparison of model order reduction methods for optimal sensor placement for thermo-elastic models*, Engineering Optimization, 51 (2019), pp. 465–483.

[16] P. BENNER, M. OHLBERGER, A. PATERA, G. ROZZA, AND K. URBAN, *A survey of projection-based model reduction methods for parametric dynamical systems*, SIAM Review, 57 (2015), pp. 483–531.

[17] P. BENNER, W. SCHILDERS, S. GRIVET-TALOCIA, A. QUARTERONI, G. ROZZA, AND L. M. SILVEIRA, eds., *Model Order Reduction*, De Gruyter, 2020.

[18] A. BERMÚDEZ DE CASTRO, *Continuum thermomechanics. progress in mathematical physics*, Meccanica, 41 (2006), pp. 697–698.

[19] A. BINDER, O. JADHAV, AND V. MEHRMANN, *Error analysis of a model order reduction framework for financial risk analysis*, 2021, https://arxiv.org/abs/2110.00774.

[20] A. BINDER, O. JADHAV, AND V. MEHRMANN, *Model order reduction for the simulation of parametric interest rate models in financial risk analysis*, Journal of Mathematics in Industry, 11 (2021).

[21] D. Boffi, F. Brezzi, L. F. Demkowicz, R. G. Durán, R. S. Falk, and M. Fortin, *Mixed Finite Elements, Compatibility Conditions, and Applications*, Springer, Berlin, Heidelberg, 1 ed., 2006.

[22] M. Bougataya, A. Lakhssassi, Y. Savaria, and D. Massicotte, *Thermo-mechanical stress analysis of vlsi devices by partially coupled finite element method*, vol. 1, 06 2004, pp. 509– 513 Vol.1.

[23] S. Brenner and R. Scott, *The Mathematical Theory of Finite Element Methods*, Springer, New York, NY, 3 ed., 2008.

[24] J. Brulin, A. Rekik, E. Blond, L. Josserand, A. Gasser, and F. Roulet, *Thermomechanical modelling of a blast furnace hearth*, UNITECR'11, (2011). hal-00651546.

[25] I. Cameron, M. Sukhram, K. Lefebvre, and W. Davenport, *Blast furnace ironmaking : Analysis, control, and optimization*, Elsevier, 2019.

[26] G. Carere, M. Strazzullo, F. Ballarin, G. Rozza, and R. Stevenson, *A weighted pod-reduction approach for parametrized pde-constrained optimal control problems with random inputs and applications to environmental sciences*, 2021, `https://arxiv.org/abs/2103.00632`.

[27] W. Chen, Q. Wang, J. S. Hesthaven, and C. Zhang, *Physics-informed machine learning for reduced-order modeling of nonlinear problems*, Journal of Computational Physics, 446 (2021), p. 110666.

[28] P. Ciarlet, *The Finite Element Method for Elliptic Problems*, Elsevier Science, 1978.

[29] G. Cybenko, *Approximation by superpositions of a sigmoidal function*, 2 (1989), pp. 303–314.

[30] N. Demo, M. Strazzullo, and G. Rozza, *An extended physics informed neural network for preliminary analysis of parametric optimal control problems*, 2021, `https://arxiv.org/abs/2110.13530`.

[31] N. Demo, M. Strazzullo, and G. Rozza, *An extended physics informed neural network for preliminary analysis of parametric optimal control problems*, 2021, `https://arxiv.org/abs/2110.13530`.

[32] N. Demo, M. Tezzele, A. Mola, and G. Rozza, *Hull shape design optimization with parameter space and model reductions, and self-learning mesh morphing*, Journal of Marine Science and Engineering, 9 (2021).

[33] N. Demo, M. Tezzele, and G. Rozza, *A non-intrusive approach for the reconstruction of pod modal coefficients through active subspaces*, Comptes Rendus Mécanique, 347 (2019), pp. 873–881. Data-Based Engineering Science and Technology.

[34] H. B. Demuth, M. H. Beale, O. D. Jesús, and M. T. Hagan, *Neural network design*, Cambridge University Press, 2014.

[35] FEniCS, `www.fenicsproject.org`. Accessed: 04-December-2021.

[36] F. Fritzen, *Lecture notes : Introduction to model order reduction of mechanical systems*, University of Stuttgart, (Winter term 2016-2017).

[37] M. Geerdes, R. Chaigneau, and O. Lingiardi, *Modern Blast Furnace Ironmaking: An Introduction (Fourth Edition, 2020)*, IOS Press, 2020.

[38] M. Girfoglio, A. Quaini, and G. Rozza, *Fluid-structure interaction simulations with a les filtering approach in solids4foam*, 2021, `https://arxiv.org/abs/2102.08011`.

[39] M. Gouge, P. Michaleris, E. Denlinger, and J. Irwin, *The Finite Element Method for the Thermo-Mechanical Modeling of Additive Manufacturing Processes*, 01 2018, pp. 19–38.

[40] M. Gurtin, *An Introduction to Continuum Mechanics*, Academic Press, 1981.

[41] N. Guérin, A. Thorin, F. Thouverez, M. Legrand, and P. Almeida, *Thermomechanical model reduction for efficient simulations of rotor-stator contact interaction*, Journal of Engineering for Gas Turbines and Power, 141 (2018).

[42] B. Haasdonk, *Reduced Basis Methods for Parametrized PDEs—A Tutorial Introduction for Stationary and Instationary Problems*, 2017, ch. 2, pp. 65–136.

[43] S. Haykin, *Neural Networks and Learning Machines*, no. v. 10 in Neural networks and learning machines, Prentice Hall, 2009.

[44] P. Hernández-Becerro, D. Spescha, and K. Wegener, *Model order reduction of thermo-mechanical models with parametric convective boundary conditions: focus on machine tools*, Computational Mechanics, 67 (2021), pp. 167–184.

[45] J. Hesthaven and S. Ubbiali, *Non-intrusive reduced order modeling of nonlinear problems using neural networks*, Journal of Computational Physics, 363 (2018), pp. 55–78.

[46] J. S. HESTHAVEN, G. ROZZA, AND B. STAMM, *Certified Reduced Basis Methods for Parametrized Partial Differential Equations*, SpringerBriefs in Mathematics, Springer International Publishing, 2015.

[47] S. HIJAZI, S. ALI, G. STABILE, F. BALLARIN, AND G. ROZZA, *The Effort of Increasing Reynolds Number in Projection-Based Reduced Order Methods: From Laminar to Turbulent Flows*, Springer International Publishing, Cham, 2020, pp. 245–264.

[48] I. HLAVÁČEK, *Korn's inequality uniform with respect to a class of axisymmetric bodies*, Aplikace Matematiky, 34 (1989).

[49] I. HLAVÁČEK, *Shape optimization of elastic axisymmetric bodies*, Aplikace matematiky, 34 (1989), pp. 225–245.

[50] K. C. HOANG AND T.-Y. KIM, *Fast and accurate two-field reduced basis approximation for parametrized thermoelasticity problems*, Finite Elements in Analysis and Design, 141 (2017), pp. 96–118.

[51] K. HORNIK, M. STINCHCOMBE, AND H. WHITE, *Multilayer feedforward networks are universal approximators*, Neural Networks, 2 (1989), pp. 359–366.

[52] D. HUYNH AND A. PATERA, *Reduced basis approximation and a posteriori error estimation for stress intensity factors*, International Journal for Numerical Methods in Engineering, 72 (2007), pp. 1219–1259.

[53] F. KASOLIS AND M. CLEMENS, *Maximum entropy snapshot sampling for reduced basis generation*, 2020, https://arxiv.org/abs/2005.01280.

[54] M. KHAMLICH, F. PICHI, AND G. ROZZA, *Model order reduction for bifurcating phenomena in fluid-structure interaction problems*, 2021, https://arxiv.org/abs/2110.06297.

[55] N. KIKUCHI AND J. T. ODEN, *Contact Problems in Elasticity*, Society for Industrial and Applied Mathematics, 1988.

[56] D. P. KINGMA AND J. BA, *Adam: A method for stochastic optimization, 3rd International Conference on Learning Representations (ICLR)*, 2015, https://arxiv.org/abs/1412.6980.

[57] H. LI, *Finite element analysis for the axisymmetric laplace operator on polygonal domains*, J. Computational Applied Mathematics, 235 (2011), pp. 5155–5176.

[58] Z. LI, N. KOVACHKI, K. AZIZZADENESHELI, B. LIU, K. BHATTACHARYA, A. STUART, AND A. ANANDKUMAR, *Neural operator: Graph kernel network for partial differential equations*, 2020, https://arxiv.org/abs/2003.03485.

[59] Z. LI, N. KOVACHKI, K. AZIZZADENESHELI, B. LIU, K. BHATTACHARYA, A. STU-
     ART, AND A. ANANDKUMAR, *Fourier neural operator for parametric partial differ-
     ential equations*, 2021, https://arxiv.org/abs/2010.08895.

[60] L. LU, P. JIN, G. PANG, Z. ZHANG, AND G. E. KARNIADAKIS, *Learning nonlinear
     operators via deeponet based on the universal approximation theorem of operators*,
     Nature Machine Intelligence, 3 (2021), p. 218–229.

[61] M. MARTINOLLI, J. BIASETTI, S. ZONCA, L. POLVERELLI, AND C. VERGARA,
     *Extended finite element method for fluid-structure interaction in wave membrane
     blood pump*, International Journal for Numerical Methods in Biomedical Engineering,
     37 (2021), p. e3467.

[62] V. MEHRMANN AND T. STYKEL, *Balanced truncation model reduction for large-
     scale systems in descriptor form*, in Dimension Reduction of Large-Scale Systems,
     P. Benner, D. C. Sorensen, and V. Mehrmann, eds., Springer Berlin Heidelberg,
     2005, pp. 83–115.

[63] L. MENEGHETTI, N. DEMO, AND G. ROZZA, *A dimensionality reduction approach
     for convolutional neural networks*, 2021, https://arxiv.org/abs/2110.09163.

[64] U. E. MORELLI, P. BARRAL, P. QUINTELA, G. ROZZA, AND G. STABILE, *A
     numerical approach for heat flux estimation in thin slabs continuous casting molds
     using data assimilation*, International Journal for Numerical Methods in Engineering,
     122 (2021), pp. 4541–4574.

[65] J. NECAS, *Les Methodes Directes en Theorie Des Equations Elliptiques Jindrich
     Necas*, Masson, 1967.

[66] M. NONINO, F. BALLARIN, AND G. ROZZA, *A monolithic and a partitioned, reduced
     basis method for fluid–structure interaction problems*, Fluids, 6 (2021).

[67] D. PAPAPICCO, N. DEMO, M. GIRFOGLIO, G. STABILE, AND G. ROZZA, *The neu-
     ral network shifted-proper orthogonal decomposition: A machine learning approach
     for non-linear reduction of hyperbolic equations*, Computer Methods in Applied Me-
     chanics and Engineering, 392 (2022), p. 114687.

[68] A. PASZKE, S. GROSS, F. MASSA, A. LERER, J. BRADBURY, G. CHANAN,
     T. KILLEEN, Z. LIN, N. GIMELSHEIN, L. ANTIGA, A. DESMAISON, A. KOPF,
     E. YANG, Z. DEVITO, M. RAISON, A. TEJANI, S. CHILAMKURTHY, B. STEINER,
     L. FANG, J. BAI, AND S. CHINTALA, *Pytorch: An imperative style, high-performance
     deep learning library*, in Advances in Neural Information Processing Systems 32,
     H. Wallach, H. Larochelle, A. Beygelzimer, F. d'Alché-Buc, E. Fox, and R. Garnett,
     eds., Curran Associates, Inc., 2019, pp. 8024–8035.

[69] F. PICHI, F. BALLARIN, G. ROZZA, AND J. S. HESTHAVEN, *An artificial neural network approach to bifurcating phenomena in computational fluid dynamics*, 2021, `https://arxiv.org/abs/2109.10765`.

[70] F. PICHI, F. BALLARIN, G. ROZZA, AND J. S. HESTHAVEN, *An artificial neural network approach to bifurcating phenomena in computational fluid dynamics*, 2021, `https://arxiv.org/abs/2109.10765`.

[71] PYTORCH, `www.pytorch.org`. Accessed: 04-December-2021.

[72] A. QUARTERONI, *Numerical Models for Differential Problems*, Springer, Milano, 1 ed., 2009.

[73] A. QUARTERONI, A. MANZONI, AND F. NEGRI, *Reduced Basis Methods for Partial Differential Equations*, no. v. 1 in La Matematica per il 3+2, Springer International Publishing, 2016.

[74] A. QUARTERONI, R. SACCO, AND F. SALERI, *Numerical Mathematics*, Springer-Verlag Berlin Heidelberg, 2007.

[75] A. QUARTERONI, F. SALERI, AND P. GERVASIO, *Scientific Computing with MATLAB and Octave*, Springer, Berlin, Heidelberg, 4 ed., 2014.

[76] M. RAISSI, P. PERDIKARIS, AND G. KARNIADAKIS, *Physics-informed neural networks: A deep learning framework for solving forward and inverse problems involving nonlinear partial differential equations*, Journal of Computational Physics, 378 (2019), pp. 686–707.

[77] M. RAISSI, A. YAZDANI, AND G. E. KARNIADAKIS, *Hidden fluid mechanics: Learning velocity and pressure fields from flow visualizations*, Science, 367 (2020), pp. 1026–1030.

[78] R. RAMLAU AND B. STADLER, *An augmented wavelet reconstructor for atmospheric tomography*, 2020, `https://arxiv.org/abs/2011.06842`.

[79] RBNICS, `www.rbnicsproject.org`. Accessed: 04-December-2021.

[80] R. ROJAS, *Neural Networks: A Systematic Introduction*, Springer-Verlag, 1996.

[81] G. ROZZA, M. HESS, G. STABILE, M. TEZZELE, AND F. BALLARIN, *Basic ideas and tools for projection-based model reduction of parametric partial differential equations*, De Gruyter, 2020, pp. 1–47.

[82] G. ROZZA, D. HUYNH, AND A. PATERA, *Reduced basis approximation and a posteriori error estimation for affinely parametrized elliptic coercive partial differential equations*, Archives of Computational Methods in Engineering, 15 (2007).

[83] O. San, R. Maulik, and M. Ahmed, *An artificial neural network framework for reduced order modeling of transient flows*, Communications in Nonlinear Science and Numerical Simulation, 77 (2019), pp. 271–287.

[84] W. Schilders, *Introduction to Model Order Reduction*, Springer Berlin Heidelberg, Berlin, Heidelberg, 2008, pp. 3–32.

[85] W. H. A. Schilders and A. Lutowska, *A Novel Approach to Model Order Reduction for Coupled Multiphysics Problems*, Springer International Publishing, Cham, 2014, pp. 1–49.

[86] N. V. Shah, M. Girfoglio, P. Quintela, G. Rozza, A. Lengomin, F. Ballarin, and P. Barral, *Finite element based model order reduction for parametrized one-way coupled steady state linear thermomechanical problems*, Submitted, `https://arxiv.org/abs/2111.08534`.

[87] N. V. Shah, M. Girfoglio, and G. Rozza, *Thermomechanical modelling for industrial applications*, Submitted, `https://arxiv.org/abs/2108.13366`.

[88] P. Siena, M. Girfoglio, and G. Rozza, *Fast and accurate numerical simulations for the study of coronary artery bypass grafts by artificial neural network*, 2022, `https://arxiv.org/abs/2201.01804`.

[89] A. Singh, K. Narasimhan, and R. Singh, *Finite element analysis of thermomechanical behavior and residual stresses in cold flowformed ti6al4v alloy*, The International Journal of Advanced Manufacturing Technology, 103 (2019), p. 1257–1277.

[90] T. Sinha, K. Sikka, and R. Lall, *Artificial neural networks and bayesian techniques for flip-chip package thermo-mechanical analysis, 2021 IEEE 71st Electronic Components and Technology Conference (ECTC)*, 2021, pp. 1442–1449.

[91] G. Stabile, S. Hijazi, A. Mola, S. Lorenzi, and G. Rozza, *Pod-galerkin reduced order methods for cfd using finite volume discretisation: vortex shedding around a circular cylinder*, Communications in Applied and Industrial Mathematics, 8 (2017), pp. 210–236.

[92] B. Stadler, R. Biasi, M. Manetti, and R. Ramlau, *Real-time implementation of an iterative solver for atmospheric tomography*, 2020, `https://arxiv.org/abs/2009.00946`.

[93] M. Strazzullo, F. Ballarin, R. Mosetti, and G. Rozza, *Model reduction for parametrized optimal control problems in environmental marine sciences and engineering*, SIAM Journal on Scientific Computing, 40 (2018), pp. B1055–B1079.

[94] M. STRAZZULLO, F. BALLARIN, AND G. ROZZA, *Pod–galerkin model order reduction for parametrized time dependent linear quadratic optimal control problems in saddle point formulation*, Journal of Scientific Computing, 83 (2020).

[95] M. STRAZZULLO, F. BALLARIN, AND G. ROZZA, *Pod-galerkin model order reduction for parametrized nonlinear time dependent optimal flow control: an application to shallow water equations*, 2021, `https://arxiv.org/abs/2003.09695`.

[96] M. STRAZZULLO, Z. ZAINIB, F. BALLARIN, AND G. ROZZA, *Reduced order methods for parametrized non-linear and time dependent optimal flow control problems, towards applications in biomedical and environmental sciences*, in Numerical Mathematics and Advanced Applications ENUMATH 2019, F. J. Vermolen and C. Vuik, eds., Cham, 2021, Springer International Publishing, pp. 841–850.

[97] M. SWARTLING, B. SUNDELIN, A. TILLIANDER, AND P. G. JÖNSSON, *Heat transfer modelling of a blast furnace hearth*, steel research international, 81 (2010), pp. 186–196.

[98] M. TEZZELE, F. BALLARIN, AND G. ROZZA, *Combined Parameter and Model Reduction of Cardiovascular Problems by Means of Active Subspaces and POD-Galerkin Methods*, Springer International Publishing, Cham, 2018, pp. 185–207.

[99] M. TEZZELE, F. SALMOIRAGHI, AND A. MOLA, *Dimension reduction in heterogeneous parametric spaces with application to naval engineering shape design problems*, Advanced Modeling and Simulation in Engineering Sciences, 5 (2018).

[100] A. VIZZACCARO, A. GIVOIS, P. LONGOBARDI, Y. SHEN, J.-F. DEÜ, L. SALLES, C. TOUZÉ, AND O. THOMAS, *Non-intrusive reduced order modelling for the dynamics of geometrically nonlinear flat structures using three-dimensional finite elements*, Computational Mechanics, 66 (2020), p. 1293–1319.

[101] S. VÁZQUEZ-FERNÁNDEZ, A. GARCÍA-LENGOMÍN PIEIGA, C. LAUSÍN-GÓNZALEZ, AND P. QUINTELA, *Mathematical modelling and numerical simulation of the heat transfer in a trough of a blast furnace*, International Journal of Thermal Sciences, 137 (2019), pp. 365 – 374.

[102] Q. WANG, J. S. HESTHAVEN, AND D. RAY, *Non-intrusive reduced order modeling of unsteady flows using artificial neural networks with application to a combustion problem*, Journal of Computational Physics, 384 (2019), pp. 289–307.

[103] M. ZANCANARO, M. MROSEK, G. STABILE, C. OTHMER, AND G. ROZZA, *Hybrid neural network reduced order modelling for turbulent flows with geometric parameters*, 2021, `https://arxiv.org/abs/2107.09591`.

[104] G. ZHANG, B. EDDY PATUWO, AND M. Y. HU, *Forecasting with artificial neural networks:: The state of the art*, International Journal of Forecasting, 14 (1998), pp. 35–62.

[105] S. ZHANG AND C. OSKAY, *Reduced order variational multiscale enrichment method for thermo-mechanical problems*, Computational Mechanics, 59 (2017), p. 887–907.

[106] O. C. ZIENKIEWICZ, R. L. TAYLOR, AND J. Z. ZHU, *The Finite Element Method: Its Basis and Fundamentals, Sixth Edition*, Butterworth-Heinemann, 6 ed., 05 2005.